



APPROVED FOR PUBLIC RELEASE, DISTRIBUTION UNLIMITED

ALEX(02)-TR-75-02-PART A

(5)

AFOSR - TR-75-1000

SOURCE STUDIES IN THE NEAR- AND FAR-FIELD

SEMI-ANNUAL TECHNICAL REPORT NO. 5-PART A

1 MAY 1975 TO 30 NOVEMBER 1975

Prepared by
Lawrence S. Turnbull, David Sun, James C. Batts,
and Frode Ringdal

TEXAS INSTRUMENTS INCORPORATED
Equipment Group
Post Office Box 6015
Dallas, Texas 75222

Contract No. F44620-73-C-0055
Amount of Contract: \$393,369
Beginning 23 April 1973
Ending 31 August 1976

DDC
RECEIVED
SEP 13 1976
B

Prepared for
AIR FORCE OFFICE OF SCIENTIFIC RESEARCH

Sponsored by
ADVANCED RESEARCH PROJECTS AGENCY
Nuclear Monitoring Research Office
ARPA Program Code No. F10
ARPA Order No. 1827

30 November 1975

Acknowledgment: This research was supported by the Advanced Research Projects Agency, Nuclear Monitoring Research Office, under Project VELA-UNIFORM, and accomplished under the direction of the Air Force Office of Scientific Research under Contract Number F44620-73-C-0055.

Equipment Group

ADA 029559



APPROVED FOR PUBLIC RELEASE, DISTRIBUTION UNLIMITED

ALEX(02)-TR-75-02-PART A

SOURCE STUDIES IN THE NEAR- AND FAR-FIELD

SEMI-ANNUAL TECHNICAL REPORT NO. 5-PART A

1 MAY 1975 TO 30 NOVEMBER 1975

Prepared by
Lawrence S. Turnbull, David Sun, James C. Battis,
and Frode Ringdal

TEXAS INSTRUMENTS INCORPORATED
Equipment Group
Post Office Box 6015
Dallas, Texas 75222

Contract No. F44620-73-C-0055
Amount of Contract: \$393,369
Beginning 23 April 1973
Ending 31 August 1976

ACCESSION for	
RTIS	White Section <input checked="" type="checkbox"/>
DGC	Blue Section <input type="checkbox"/>
UNANNOUNCED	
JUSTIFICATION	
BY	
DISTRIBUTION/AVAILABILITY CODES	
DIS.	AVAIL. and/or SPECIAL
A	

Prepared for
AIR FORCE OFFICE OF SCIENTIFIC RESEARCH

Sponsored by
ADVANCED RESEARCH PROJECTS AGENCY
Nuclear Monitoring Research Office
ARPA Program Code No. F10
ARPA Order No. 1827

30 November 1975

Acknowledgment: This research was supported by the Advanced Research Projects Agency, Nuclear Monitoring Research Office, under Project VELA-UNIFORM, and accomplished under the direction of the Air Force Office of Scientific Research under Contract Number F44620-73-C-0055.

Equipment Group

ABSTRACT

Several continuing investigations of the seismic source using near- and far-field data are discussed. We completed our analysis of near-field acceleration data recorded at Bear Valley, California, by examining two small events which occurred on 7 February 1974 and 6 July 1974. The February event, using only spectral analysis, was found to have a moment of 3×10^{21} dyne-cm with an equivalent circular dislocation radius of 0.18 km². Both spectral and time domain waveform fitting techniques were applied to the July event. The solutions using each method were in reasonable agreement, with a seismic moment in the range of 2 to 4×10^{21} dyne-cm over an equivalent dislocation radius of about 0.1 to 0.3 km².

Using far-field surface wave data, two central California area earthquakes (22 June 1973 and 28 November 1974) were re-examined using two new earth models which were determined by McEvilly (1975) for the north-east and southwest side of the San Andreas fault. Several far-field solutions for the source mechanism were obtained by using various combinations of stations and earth models, including use of both structures at once for the first time. However, for the central California event of 28 November 1974, the mechanism which agreed closely with that obtained by other means used only those stations on the west side of the fault, with the southwest structure used in the spectral fit.

Theoretical first higher mode surface wave spectra were generated for a double couple source in a layered half space. Both Gutenberg-Bullen and Hamilton-Healy earth models were used. As with fundamental mode spectra, 'holes' were found almost exclusively for vertical strike-slip faults. Higher mode spectral levels in the 3 to 9 second period range were

found to be comparable with 15 to 50 second period fundamental mode spectra. Also, from the excitation of the earth models, greater amplitude higher mode signals from shallow events should occur from high velocity crustal source regions.

Preliminary results have been obtained for five large events which were a part of the Sinkiang, China earthquake swarm of August 1974. Both simple spectral and spectral ratio fitting methods were employed. The far-field solutions showed a consistent trend for these five events of shallow focal depth.

Finally, we concluded our examination of the scatter of the earthquake population in the $M_s - m_b$ discriminant. Focusing on the body-wave magnitude estimate instead of the surface wave magnitude as in previous studies, we applied the maximum likelihood method of Ringdal (1975) in an attempt to improve the accuracy of the PDE bodywave magnitudes. Although the scatter of the population did not change significantly, the slope of the data set decreased approximately 0.25.

ACKNOWLEDGMENTS

Mr. James Battis produced the analysis and wrote the text for Section II. Dr. David Sun generated major parts of Section III, including the computer program which utilizes two different earth models in fitting far-field spectra.

Section IV was a joint project with Frode Ringdal while this author visited NORSAR, and this section was written by Frode.

Mrs. Cherylann Saunders typed all of the text, prepared the majority of the figures and all of the tables.

Lawrence S. Turnbull, Jr.

TABLE OF CONTENTS

SECTION	TITLE	PAGE
	ABSTRACT	iii
	ACKNOWLEDGMENTS	v
I.	INTRODUCTION	I-1
II.	ANALYSIS OF TWO SMALL BEAR VALLEY EVENTS	II-1
	A. INTRODUCTION	II-1
	B. EVALUATION OF SOURCE PARAMETERS	II-5
	C. THE FEBRUARY 7, 1974 EARTHQUAKE	II-8
	D. THE JULY 6, 1974 EARTH- QUAKE	II-14
	E. DISCUSSION OF RESULTS	II-21
III.	FAR-FIELD SOURCE STUDIES	III-1
	A. INTRODUCTION	III-1
	B. CONTINUED EVALUATION OF THE FAR-FIELD SOURCE MECHANISM FOR TWO CALIFORNIA EARTHQUAKES	III-1
	C. CONTINUED EXAMINATION OF THE THEORETICAL HIGHER MODE SPECTRA	III-9
	D. ANALYSIS OF THE SINKIANG, CHINA EARTHQUAKE SWARM OF AUGUST 1974	III-10

TABLE OF CONTENTS
(continued)

SECTION	TITLE	PAGE
IV.	THE $M_s - m_b$ RELATIONSHIP	IV-1
V.	REFERENCES	V-1
	APPENDIX A	A-1
	APPENDIX B	B-1
	APPENDIX C	C-1

LIST OF FIGURES

FIGURE	TITLE	PAGE
II-1	MAP OF BEAR VALLEY ACCELEROMETER ARRAY SHOWING EPICENTERS OF THE FEBRUARY 7, 1974 AND JULY 6, 1974 EARTHQUAKES	II-4
II-2	ACCELEROGRAMS FROM STATION 2 OF THE FEBRUARY 7, 1974 EARTHQUAKE	II-9
II-3	DERIVED VELOCITY TRACES FROM STA- TION 2 OF THE FEBRUARY 7, 1974 EARTHQUAKE	II-10
II-4	NORMALIZED ACCELERATION S-WAVE ENERGY DENSITY SPECTRUM OF N45E COMPONENT OF STATION 2; EARTHQUAKE OF FEBRUARY 7, 1974	II-11
II-5	NORMALIZED VELOCITY S-WAVE ENERGY DENSITY SPECTRUM OF N45E COMPONENT OF STATION 2; EARTHQUAKE OF FEBRUARY 7, 1974	II-12
II-6	NORMALIZED DISPLACEMENT S-WAVE ENERGY DENSITY SPECTRUM OF N45E COMPONENT OF STATION 2; EARTH- QUAKE OF FEBRUARY 7, 1974	II-13
II-7	ACCELEROGRAMS FROM STATION 3 FOR THE JULY 6, 1974 EARTHQUAKE	II-16
II-8	DERIVED VELOCITY TRACES FROM STATION 3 FOR THE JULY 6, 1974 EARTHQUAKE	II-17
II-9	ACCELEROGRAMS FROM STATION 7 FOR THE JULY 6, 1974 EARTHQUAKE	II-18
II-10	DERIVED VELOCITY TRACES FROM STATION 7 FOR THE JULY 6, 1974 EARTHQUAKE	II-19

LIST OF FIGURES
(continued)

FIGURE	TITLE	PAGE
II-11	NORMALIZED ACCELERATION S-WAVE ENERGY DENSITY SPECTRUM FOR N45E COMPONENT OF STATION 8; EARTHQUAKE OF JULY 6, 1974	II-23
II-12	NORMALIZED VELOCITY S-WAVE ENERGY DENSITY SPECTRUM FOR N45E COMPONENT OF STATION 8; EARTHQUAKE OF JULY 6, 1974	II-24
II-13	NORMALIZED DISPLACEMENT S-WAVE ENERGY DENSITY SPECTRUM FOR N45E COMPONENT OF STATION 8; EARTHQUAKE OF JULY 6, 1974	II-25
II-14	OBSERVED LOCAL MAGNITUDES VERSUS NEAR-FIELD SPECTRAL SEISMIC MOMENTS	II-27
III-1	TRAVEL PATHS TO THE AVAILABLE STATIONS FOR THE JUNE 22, 1973 EARTHQUAKE	III-5
III-2	TRAVEL PATHS TO THE AVAILABLE STATIONS FOR THE NOVEMBER 28, 1974 EARTHQUAKE	III-6
III-3	LOCATION OF SINKIANG, CHINA SWARM OF AUGUST, 1974	III-11
III-4	THE NUMBER AND MAGNITUDE CHRONOLOGY OF THE RECORDED EVENTS OF THE SINKIANG EARTHQUAKE SWARM OF AUGUST 1974	III-12
IV-1	EXPECTED BIAS OF CONVENTIONAL MAGNITUDE \bar{m} RELATIVE TO TRUE MAGNITUDE μ FOR A HYPOTHETICAL NETWORK AS A FUNCTION OF THE PER- CENTAGE OF DETECTING STATIONS	IV-3
IV-2	NORSAR m_b VERSUS PDE m_b	IV-8

LIST OF FIGURES
(continued)

FIGURE	TITLE	PAGE
IV-3	NORSAR m_b VERSUS PDE MAXIMUM LIKELIHOOD m_b	IV-9
IV-4	PDE m_b VERSUS VLPE M_s	IV-10
IV-5	MAXIMUM LIKELIHOOD PDE m_b VERSUS VLPE M_s	IV-11
A-1	BEAR VALLEY STRUCTURE - NORTHEAST SIDE OF FAULT	A-2
A-2	RAYLEIGH AND LOVE WAVE DISPERSION FOR BEAR VALLEY STRUCTURE (NORTH- EAST SIDE OF FAULT)	A-3
A-3	BEAR VALLEY STRUCTURE - SOUTHWEST SIDE OF FAULT	A-4
A-4	RAYLEIGH AND LOVE WAVE DISPERSION FOR BEAR VALLEY STRUCTURE (SOUTH- WEST SIDE OF FAULT)	A-5
B-1a	FUNDAMENTAL MODE RAYLEIGH WAVE SPECTRA USING THE SOURCE MECHANISM OF THE 22 JUNE 1973 BEAR VALLEY EVENT IN THE NORTHEAST STRUCTURE	B-2
B-1b	FUNDAMENTAL MODE LOVE WAVE SPECTRA USING THE SOURCE MECHANISM OF THE 22 JUNE 1973 BEAR VALLEY EVENT IN THE NORTHEAST STRUCTURE	B-3
B-2a	FUNDAMENTAL MODE RAYLEIGH WAVE SPECTRA USING THE SOURCE MECHANISM OF THE 22 JUNE 1973 BEAR VALLEY EVENT IN THE SOUTHWEST STRUCTURE	B-4
B-2b	FUNDAMENTAL MODE LOVE WAVE SPECTRA USING THE SOURCE MECHANISM OF THE 22 JUNE 1973 BEAR VALLEY EVENT IN THE SOUTHWEST STRUCTURE	B-5

LIST OF FIGURES
(continued)

FIGURE	TITLE	PAGE
B-3a	FUNDAMENTAL MODE RAYLEIGH AND LOVE WAVE RADIATION (T=20 SECONDS) USING THE SOURCE MECHANISM OF THE 22 JUNE 1973 BEAR VALLEY EVENT IN THE NORTHEAST STRUCTURE	B-6
B-3b	FUNDAMENTAL MODE RAYLEIGH AND LOVE WAVE RADIATION (T=30 SECONDS) USING THE SOURCE MECHANISM OF THE 22 JUNE 1973 BEAR VALLEY EVENT IN THE NORTHEAST STRUCTURE	B-7
B-4a	FUNDAMENTAL MODE RAYLEIGH AND LOVE WAVE RADIATION (T=20 SECONDS) USING THE SOURCE MECHANISM OF THE 22 JUNE 1973 BEAR VALLEY EVENT IN THE SOUTHWEST STRUCTURE	B-8
B-4b	FUNDAMENTAL MODE RAYLEIGH AND LOVE WAVE RADIATION (T=30 SECONDS) USING THE SOURCE MECHANISM OF THE 22 JUNE 1973 BEAR VALLEY EVENT IN THE SOUTHWEST STRUCTURE	B-9
B-5a	FUNDAMENTAL MODE RAYLEIGH WAVE SPECTRA USING THE SOURCE MECHANISM OF THE 28 NOVEMBER 1974 CENTRAL CALIFORNIA EVENT IN THE NORTHEAST STRUCTURE	B-10
B-5b	FUNDAMENTAL MODE LOVE WAVE SPECTRA USING THE SOURCE MECHANISM OF THE 28 NOVEMBER 1974 CENTRAL CALIFORNIA EVENT IN THE NORTHEAST STRUCTURE	B-11
B-6a	FUNDAMENTAL MODE RAYLEIGH WAVE SPECTRA USING THE SOURCE MECHANISM OF THE 28 NOVEMBER 1974 CENTRAL CALIFORNIA EVENT IN THE SOUTHWEST STRUCTURE	B-12

LIST OF FIGURES
(continued)

FIGURE	TITLE	PAGE
B-6b	FUNDAMENTAL MODE LOVE WAVE SPECTRA USING THE SOURCE MECHANISM OF THE 28 NOVEMBER 1974 CENTRAL CALIFORNIA EVENT IN THE SOUTHWEST STRUCTURE	B-13
B-7a	FUNDAMENTAL MODE RAYLEIGH AND LOVE WAVE RADIATION (T=20 SECONDS) USING THE SOURCE MECHANISM OF THE 28 NOVEMBER 1974 CENTRAL CALIFORNIA EVENT IN THE NORTHEAST STRUCTURE	B-14
B-7b	FUNDAMENTAL MODE RAYLEIGH AND LOVE WAVE RADIATION (T=30 SECONDS) USING THE SOURCE MECHANISM OF THE 28 NOVEMBER 1974 CENTRAL CALIFORNIA EVENT IN THE NORTHEAST STRUCTURE	B-15
B-8a	FUNDAMENTAL MODE RAYLEIGH AND LOVE WAVE RADIATION (T=20 SECONDS) USING THE SOURCE MECHANISM OF THE 28 NOVEMBER 1974 CENTRAL CALIFORNIA EVENT IN THE SOUTHWEST STRUCTURE	B-16
B-8b	FUNDAMENTAL MODE RAYLEIGH AND LOVE WAVE RADIATION (T=30 SECONDS) USING THE SOURCE MECHANISM OF THE 28 NOVEMBER 1974 CENTRAL CALIFORNIA EVENT IN THE SOUTHWEST STRUCTURE	B-17
C-1a	THEORETICAL FIRST HIGHER MODE RAYLEIGH AND LOVE WAVE SPECTRA FOR THREE SOURCE DEPTHS IN A GUTENBERG-BULLEN EARTH MODEL: Period Range 3 to 15 Seconds, Dip (δ) = Variable, Slip (λ) = 0° , Strike (θ) = 0°	C-2

LIST OF FIGURES
(continued)

FIGURE	TITLE	PAGE
C-1b	THEORETICAL FIRST HIGHER MODE RAYLEIGH AND LOVE WAVE SPECTRA FOR THREE SOURCE DEPTHS IN A GUTENBERG-BULLEN EARTH MODEL: Period Range 3 to 15 Seconds, Dip (δ) = 90°, Slip (λ) = Variable, Strike (θ) = 0°	C-3
C-1c	THEORETICAL FIRST HIGHER MODE RAYLEIGH AND LOVE WAVE SPECTRA FOR THREE SOURCE DEPTHS IN A GUTENBERG-BULLEN EARTH MODEL: Period Range 3 to 15 Seconds, Dip (δ) = 60°, Slip (λ) = Variable, Strike (θ) = 0°	C-4
C-1d	THEORETICAL FIRST HIGHER MODE RAYLEIGH AND LOVE WAVE SPECTRA FOR THREE SOURCE DEPTHS IN A GUTENBERG-BULLEN EARTH MODEL: Period Range 3 to 15 Seconds, Dip (δ) = 90°, Slip (λ) = 0°, Strike (θ) = Variable	C-5
C-2	THEORETICAL FIRST HIGHER MODE RAYLEIGH AND LOVE WAVE SPECTRA FOR THREE SOURCE DEPTHS IN A HAMILTON-HEALY EARTH MODEL: Period Range 3 to 15 Seconds, Dip (δ) = Variable, Slip (λ) = 0°, Strike (θ) = 0°	C-6
C-3	THEORETICAL FIRST HIGHER MODE RAYLEIGH AND LOVE WAVE SPECTRA FOR THREE SOURCE DEPTHS IN A GUTENBERG-BULLEN EARTH MODEL: Period Range 15 to 40 Seconds, Dip (δ) = Variable, Slip (λ) = 0°, Strike (θ) = 0°	C-7

LIST OF TABLES

TABLE	TITLE	PAGE
II-1	BEAR VALLEY VELOCITY MODEL	II-3
II-2	S-WAVE SPECTRAL ESTIMATES OF SOURCE PARAMETERS FEBRUARY 7, 1974 EARTHQUAKE	II-15
II-3	BEAR VALLEY EARTHQUAKE OF JULY 6, 1974 HASKELL SOURCE MODEL SOLUTION	II-22
II-4	S-WAVE SPECTRAL ESTIMATES OF SOURCE PARAMETERS JULY 6, 1974 EARTHQUAKE	II-26
II-5	SEISMIC MOMENTS FOR EACH EVENT AT BEAR VALLEY AS CALCULATED AT EACH STATION	II-29
III-1	BEAR VALLEY REGION STRUCTURE (McEVILLY, 1975)	III-2
III-2	SOURCE PARAMETERS FOR THE TWO CALIFORNIA EVENTS	III-3
III-3	ESTIMATIONS OF SOURCE PARAMETERS FOR THE CENTRAL CALIFORNIA EVENT OBTAINED BY AMPLITUDE SPECTRAL FITTING BASED ON MINIMUM-RESIDUAL CRITERION	III-7
III-4	ESTIMATIONS OF SOURCE PARAMETERS FOR THE CENTRAL CALIFORNIA EVENT OBTAINED BY AMPLITUDE SPECTRAL FITTING BASED ON DISTRIBUTION-OF- MINIMUM-RESIDUAL CRITERION	III-8
IV-1	EVENT PARAMETERS OF EURASIAN DATA BASE	IV-5
IV-2	RELATIONSHIP $M_s - m_b$ FOR VARIOUS COMBINATIONS OF M_s AND m_b MEASUREMENT PROCEDURES	IV-13

SECTION I

INTRODUCTION

In this report, we present a discussion of several continuing investigations of the seismic source from near- and far-field data. We complete our analysis of near-field acceleration data recorded at Bear Valley in Section II. Two rather small events (m_b 's of 3.0 and 3.2) that were recorded in 1974 (7 February and 6 July) were studied using both spectral methods and time domain waveform techniques.

Several studies using far-field surface wave data to determine source parameters are discussed in Section III. Two central California area earthquakes, 22 June 1973 and 28 November 1974, are re-examined using two new earth models by McEvilly (1975) for the northeast and southwest sides of the San Andreas fault. In particular, we examine the problem of fitting far-field surface wave spectra when the source region contains a major discontinuity. In this section, we continue our examination of theoretical first higher mode spectra for characteristics that would reflect source depth and structural dependence, such as 'holes' and amplitude level over a particular frequency range. Also in this section, we present a preliminary analysis of several events that occurred during an earthquake swarm in Sinkiang, China, in August 1974.

Finally, in Section IV, we conclude our examination of the scatter of the earthquake population in the $M_s - m_b$ discriminant. Instead of focusing on the M_s determination as in our previous studies, we apply the maximum likelihood method of Ringdal (1975) in an attempt to improve the accuracy of the PDE bodywave magnitudes for our data base.

SECTION II

ANALYSIS OF TWO SMALL BEAR VALLEY EVENTS

A. INTRODUCTION

Since the occurrence of a magnitude 4.2 earthquake in June of 1973 two additional events having potential for near-zone analysis have been recorded by stations of the University of California accelerometer array located along the Bear Valley segment of the San Andreas Fault. These events were a magnitude 3.0 earthquake which occurred on February 7, 1974 and one of magnitude 3.2 which was recorded on July 6, 1974. While being of significantly lower magnitudes than earthquakes previously studied in the near-field, accelerometer records of relatively high signal-to-noise ratios, probably accounted for by the shallow depths associated with these events, were obtained at a sufficient number of stations to warrant analysis to determine the source characteristics. As with the earlier June earthquake, (Turnbull and Battis, 1974), the intermediate-zone coverage of the July 6 earthquake, resulting in determinations of location and fault plane solution independent of near-field observations, along with the relatively wide azimuthal coverage in the near-field would provide a set of restrictions on any solution resulting from the Haskell moving dislocation source model. For this reason and as a test of the applicability of the Haskell earthquake source approximation to events of very low magnitude, the near-zone analysis concentrated on the July 6, 1974 earthquake.

The University of California Bear Valley accelerometer array is located approximately 30 km southeast of Hollister, California along a seismically active segment of the San Andreas Fault. In the vicinity of the array the main fault zone strikes to the northwest, separating two distinct crustal

structures. To the southwest of the fault lies a region of high velocity granite and metamorphic strata with lower velocity sedimentary rocks predominating in the northeastern block. Detailed crustal studies have been conducted for this region (McEvelly, personal communication, 1974; Aki and Lee, 1975; and Engdahl and Lee, 1975) which have indicated a structure of complex inhomogeneities within the fault zone. As the Haskell moving dislocation source model is a whole space representation, the velocity profile determined by McEvelly, as given in Table II-1, was used to evaluate two sets of 'whole-space' velocities for use with stations on each side of the fault. These velocities were obtained by using a weighted average of the velocity profile from the hypocentral depth to the surface with the weighting factors for each velocity being proportional to the thickness of its respective layer. These weighting factors and the whole-space velocities for each crust block are also given in Table II-1. It should be noted, however, that in the case of spectral evaluation of the source characteristics using Brune's model (1970), it was felt that the velocities of the layer containing the earthquake hypocenter under study were more appropriate for use in analysis.

In Figure II-1, the location of each station in the near-field array, as operational during the recording of the two events studied in this report is shown. Each site is equipped with a three component accelerometer. The dashed line in this figure represents the surface trend of the San Andreas Fault through Bear Valley. In an effort to improve the azimuthal coverage of events occurring close to the near-field array, several modifications in the network configuration have been made since the June 23, 1973 earthquake. Of primary importance is the shift of station 6 from the northeast to the southwestern side of the fault zone. This added a second station located on the higher velocity crustal material to the southwest which aids in evaluation of differences in signal character as a function of the receiver location relative to the fault.

TABLE II-1
BEAR VALLEY VELOCITY MODEL

Depth To Bottom Of Layer (km)	Weighting Factor	Southwest Structure		Northeast Structure	
		V _p (km/sec)	V _s (km/sec)	V _p (km/sec)	V _s (km/sec)
0.6	0.09	4.25	2.46	2.38	1.51
2.5	0.29	5.2	3.0	3.04	1.76
5.5	0.45	6.34	3.66	5.88	3.30
10.0	0.17	5.96	3.45	4.84	2.80
Whole Space Model		5.76	3.32	4.56	2.60

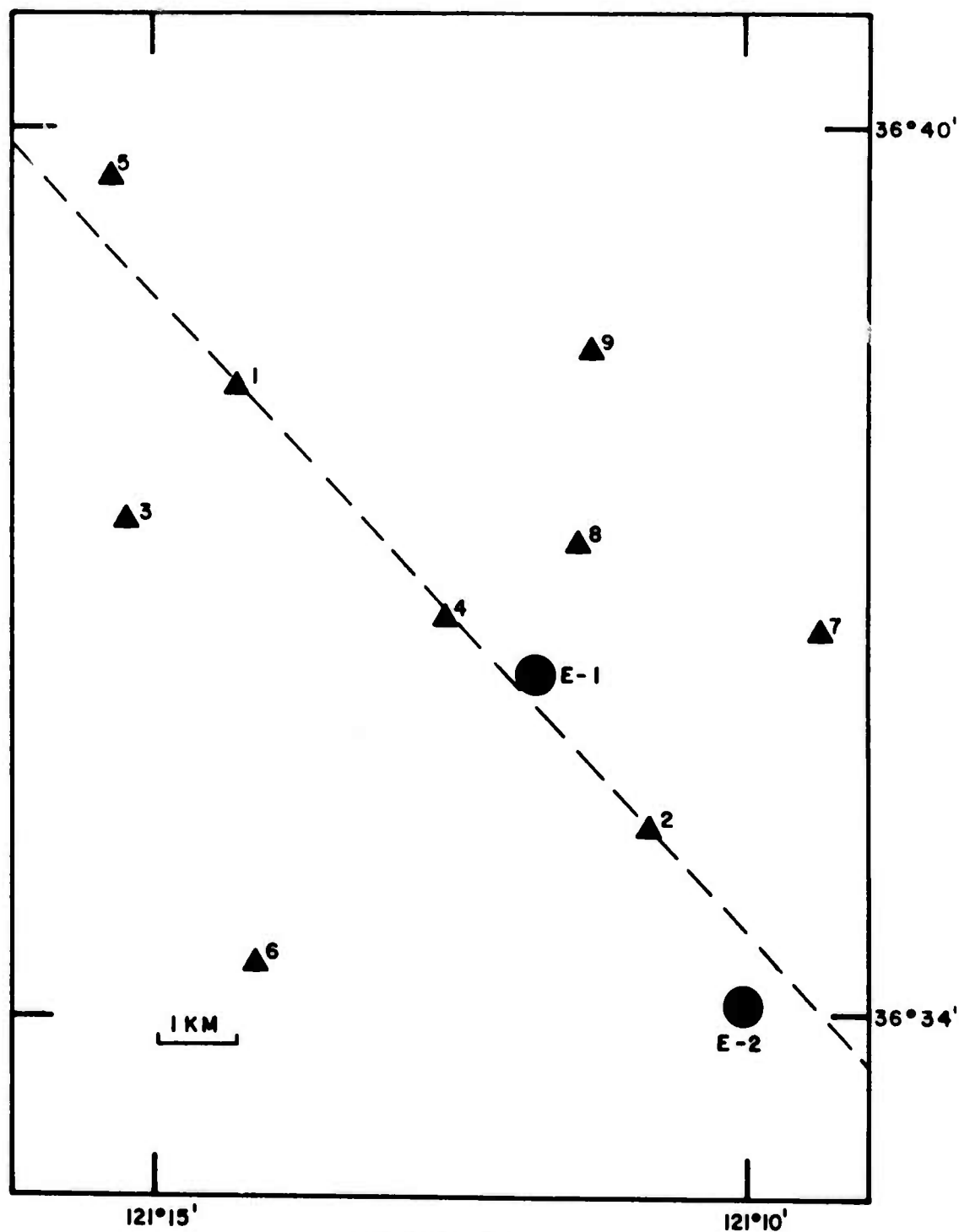


FIGURE II-1

MAP OF BEAR VALLEY ACCELEROMETER ARRAY SHOWING
EPICENTERS OF THE FEBRUARY 7, 1974 (E-1) AND
JULY 6, 1974 (E-2) EARTHQUAKES

For this report the source parameters of both the February and the July earthquakes were determined using spectral techniques. In addition, for reasons stated earlier, time domain waveform fitting was used with the July event. In the following sections the methods used in the analysis and the results of the analysis of each event is presented and the implications of these results are discussed in relation to an earlier examination of the June 22, 1973 Bear Valley event (Turnbull and Battis, 1974).

B. EVALUATION OF SOURCE PARAMETERS

The techniques used to evaluate source parameters from near-zone data have been covered in detail by earlier reports (Turnbull and Battis, 1974; Turnbull, et al., 1975). However, to facilitate the understanding of the results presented here, a brief discussion of the two methods used in this report are given below.

Using Brune's source model (1970) it is possible to estimate the seismic moment, M_0 , and a measure of the area of faulting, r , the equivalent circular dislocation radius, from the displacement amplitude spectrum of a given record of an earthquake. The equations giving these relationships are:

$$M_0 = 4\pi\rho\beta^3 R \Omega_0 \quad (\text{II-1})$$

and

$$r = \left(\frac{7\pi}{4}\right)^{1/2} \beta / (2\pi f_c) \quad (\text{II-2})$$

where ρ is the material density, β the propagation velocity of the type of bodywave dominating the time gate used to calculate the spectra, R is the hypocenter to station distance, all supposedly known parameters, and Ω_0 is the low frequency spectral level and f_c is the corner frequency of the

spectra. In addition, other parameters of the source, such as stress drop, can be evaluated from this model.

In this study the acceleration amplitude spectrum of each component is calculated directly from the acceleration data as a preliminary step to evaluation of the associated displacement spectrum. Due to the superior noise suppression qualities of the maximum entropy spectral estimator over the discrete fast fourier transform (Turnbull, et al., 1975) the maximum entropy method is used for this step. The acceleration amplitude spectrum is then converted to a displacement spectrum by two subsequent divisions of the spectra by $(2\pi f)$. At this point all necessary information for the evaluation of the corner frequency and low frequency level for a given component is available.

The first division of the acceleration amplitude spectrum yields the velocity amplitude spectrum. The corner frequency of the displacement spectrum is the frequency of the peak value of the velocity amplitude spectrum. As noise in the acceleration spectrum will usually cause the extreme low frequency velocity amplitudes to blow up, these frequencies are neglected in evaluation of f_c . Given the value of f_c the low frequency level is then calculated as the average displacement spectral amplitude between the point at which the low frequency spectrum deviates from a slope of $(2\pi f)^{-2}$ and the corner frequency.

To obtain the values used for evaluation of source parameters the information from the components of each site must be combined. In the case of Ω_0 this is done by resolving the individual component low frequency levels. In the case of corner frequency the intermediate value is selected. This would seem to be more rational than simple averaging as the latter may result in a value of f_c which could not be supported by the spectra. As was stated earlier, these values are then used in the equations of Brune's model to obtain estimates of the source parameters.

The second method of source characteristic evaluation used in this report is Haskell's moving dislocation model (Haskell, 1969). In this process the time domain acceleration traces are numerically integrated to yield velocity waveforms for each component of a station. As the Haskell model is a whole space representation, the complex structure of the P- and S-waves packets can not be simulated by this model. Thus, by some means a single period of the P- or S-wave must be isolated for each station to be used in the fitting process.

Using external information such as hypocenter locations and fault plane solutions to provide an initial case, theoretical waveforms for unit transverse and longitudinal dislocations of the fault plane are calculated for each station. At this point adjustments to fault length and width, rise time, and rupture velocity are made to produce theoretical pulse durations approximating those of the empirical waveforms. Again, restrictions such as spectral estimates of fault area are used to constrain the parameters. Following these adjustments least squared error combination of the two dislocations are calculated for fitting each station separately and as a group. The fault plane parameters of dip and strike are then perturbed to locate the minimum residual solution for each station and for all stations together. Once this set of solutions is determined the theoretical waveforms for each solution at every station is calculated. At this point a qualitative judgement on the 'goodness of fit' is made to determine which solution is accepted.

It should be noted that the least squares error combination for all stations taken as a whole may not necessarily be the best solution. This situation can result from such things as uncertainties in determining which pulses to fit for some of the stations or interference patterns effecting the empirical amplitudes. Under these circumstances the observer may select one of the solutions based on a single station as being a superior fit to the empirical waveforms.

C. THE FEBRUARY 7, 1974 EARTHQUAKE

On February 7, 1974 an earthquake of local magnitude 3.0 occurred along the San Andreas Fault in Bear Valley, California and was recorded by three stations of the University of California accelerometer array. The epicenter of this event was located approximately 1.5 kms southeast of Station 4 of the array (McEvilly and Johnson, 1974). The location of this epicenter is shown in Figure 11-1 by the closed circle labeled E-1. The depth of the event was calculated to be 5.28 kms. Considering possible location errors and variations in the fault surface with depth it would appear that this event occurred on the main fault surface of the San Andreas Fault.

Probably due to the low magnitude of the earthquake, only the records of the three stations closest to the epicenter, Sites 2, 4, and 8, were of satisfactory quality for analysis. As an example of the records produced by this event the acceleration and derived velocity traces from Station 2 are displayed in Figures 11-2 and 11-3. It is apparent that the S-wave portion of the signal is dominated by a much higher frequency signal than in previously studied earthquakes (Turnbull and Battis, 1973; Turnbull and Battis, 1974). However, while the S-wave packet of the velocity waveforms examined heretofore tended to be dominated by a single pulse, it can be seen in Figure 11-3 this is not true for the February earthquake. As the isolation of a dominant pulse is essential to the successful application of the Haskell model it was decided to use only spectral methods to ascertain the earthquake source parameters of this event.

The acceleration, velocity and displacement normalized energy density spectra of the S-wave estimated by the maximum entropy method for the N45E component of Station 2 are shown in Figures 11-4 through 11-6. A highpass filter with a corner frequency of 0.8 Hz was applied to the acceleration data prior to evaluation of the spectra. In this case a spectral corner frequency of 6.0 Hz can be seen and the low frequency spectral level was

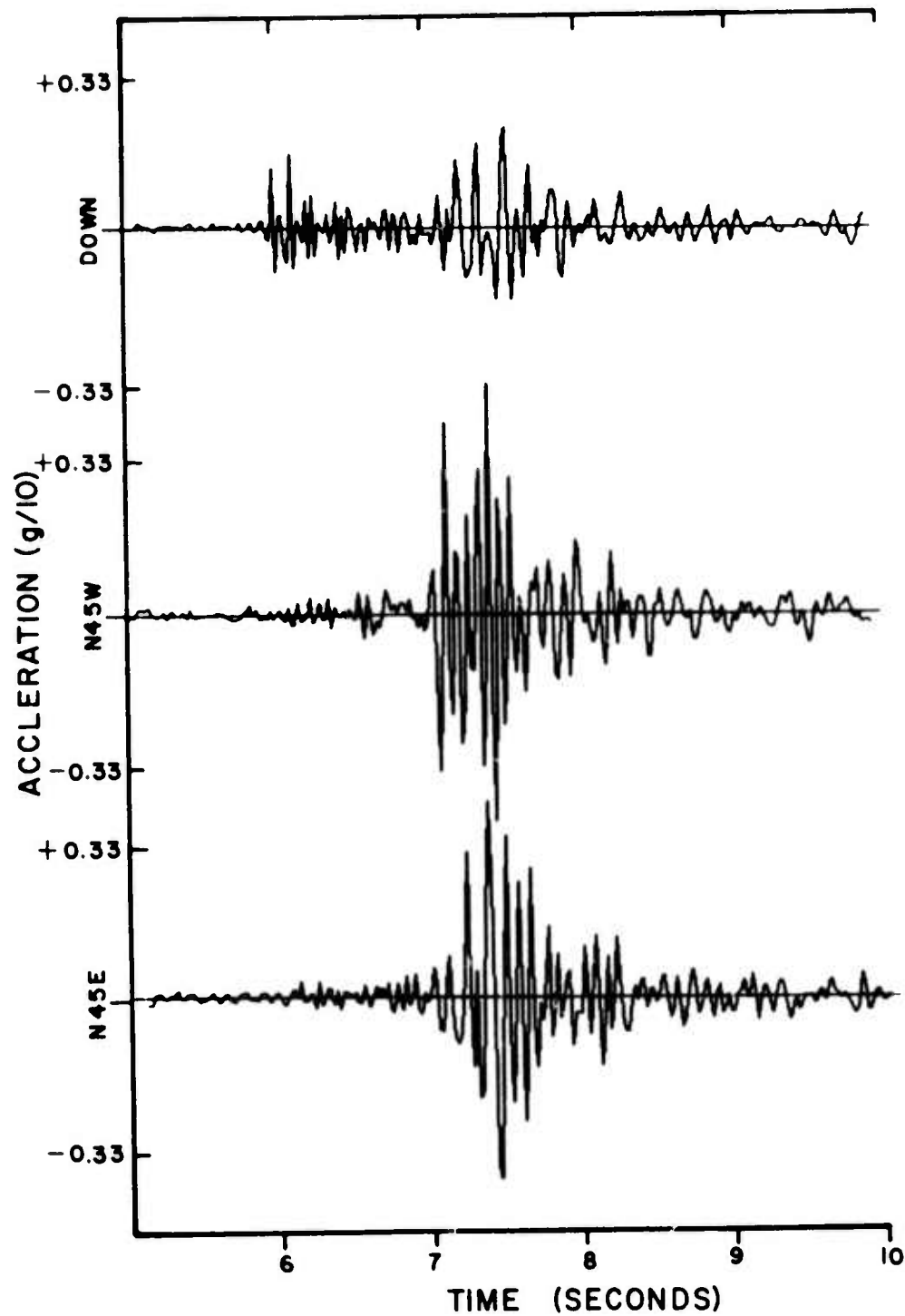


FIGURE II-2
ACCELEROGRAMS FROM STATION 2 OF THE
FEBRUARY 7, 1974 EARTHQUAKE

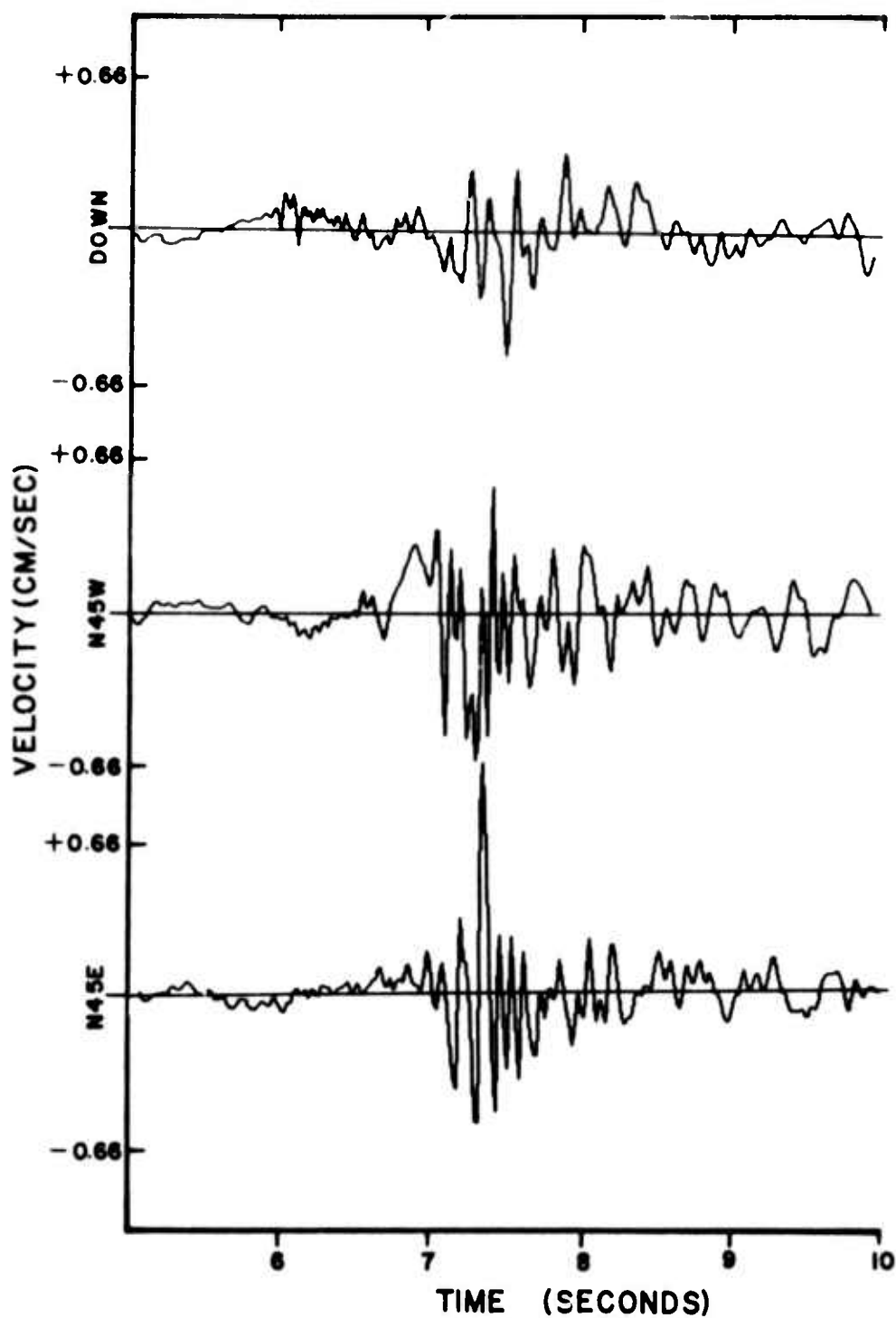


FIGURE II-3
DERIVED VELOCITY TRACES FROM STATION 2 OF
THE FEBRUARY 7, 1974 EARTHQUAKE

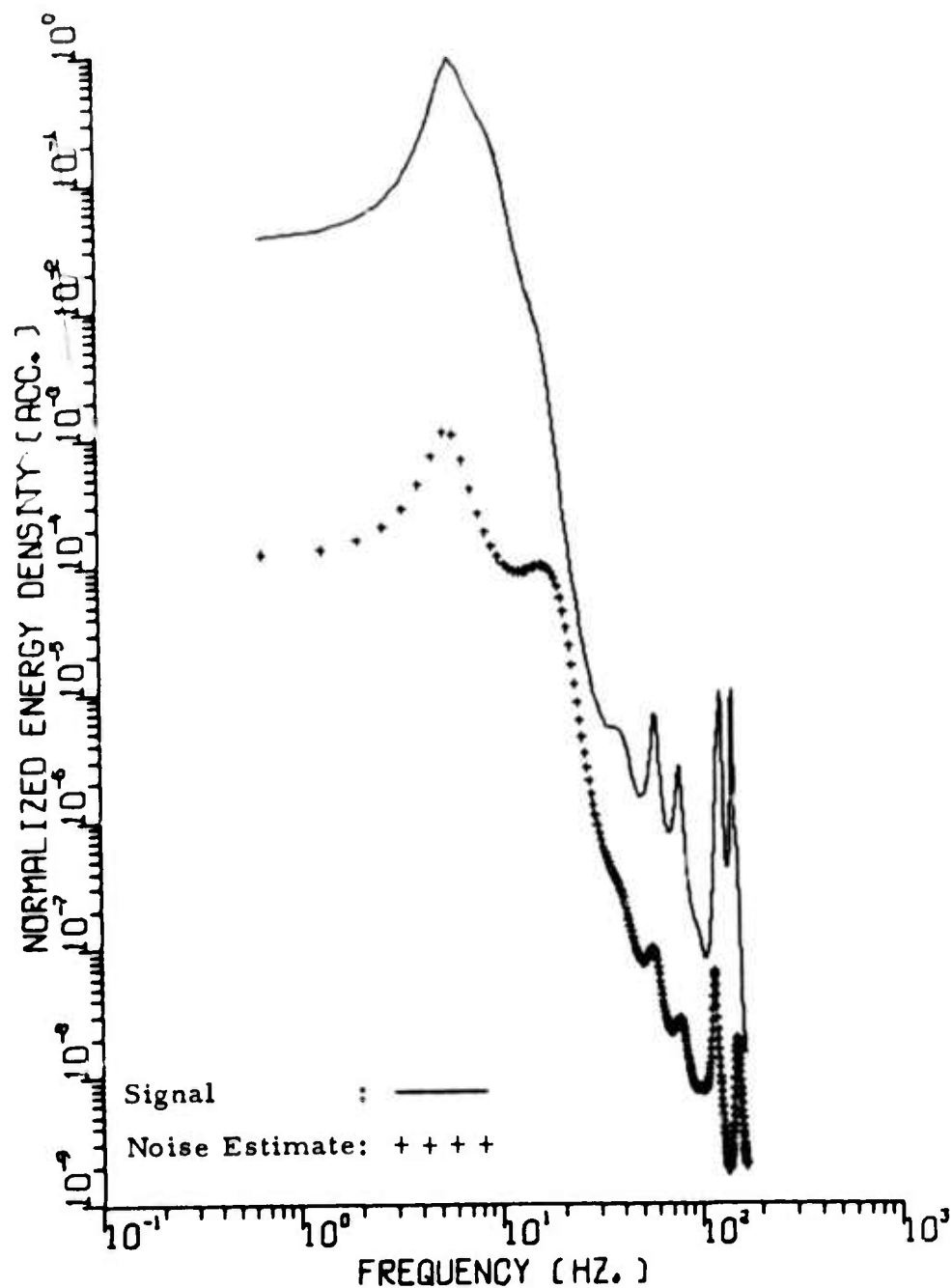
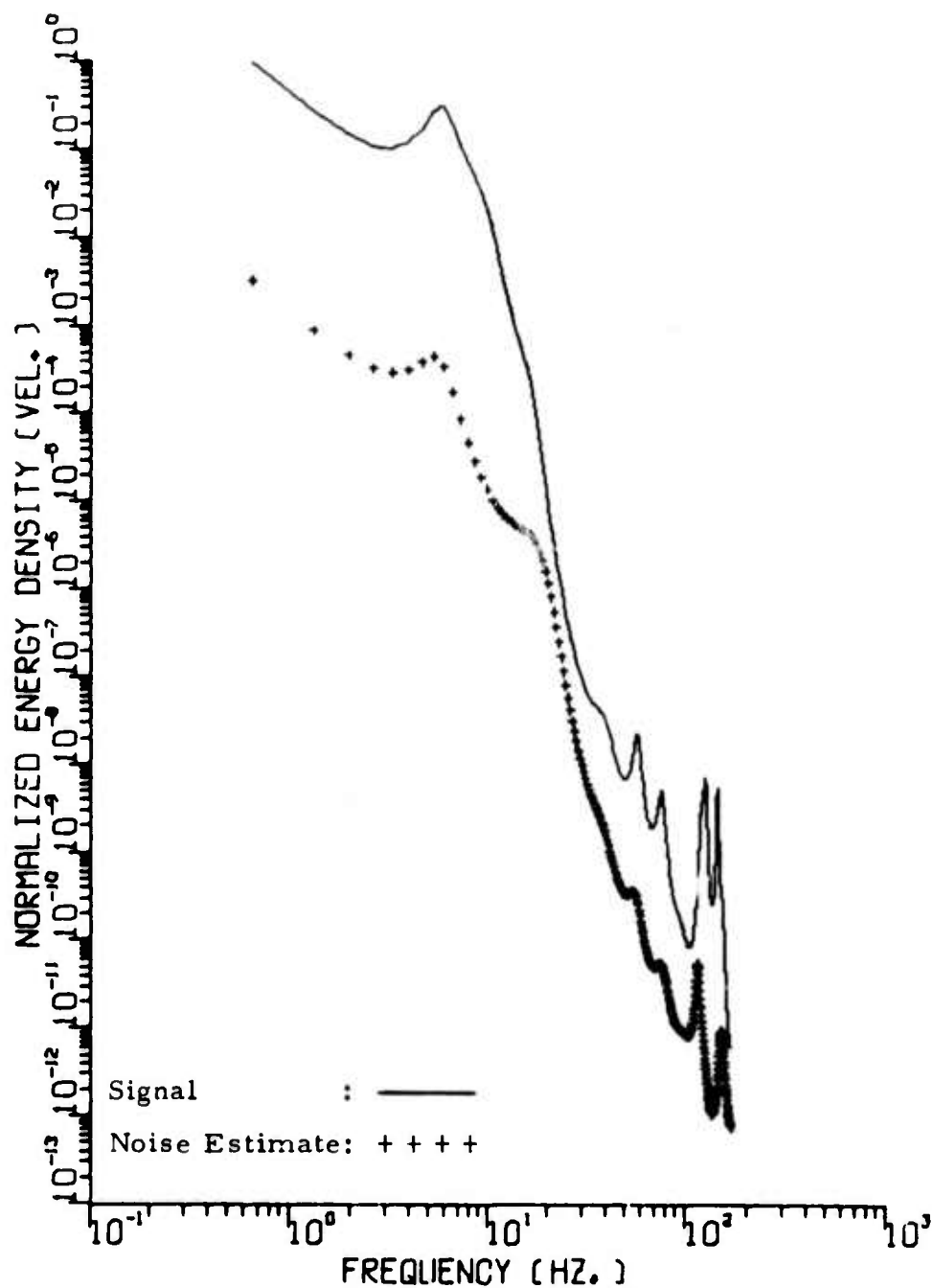


FIGURE II-4

NORMALIZED ACCELERATION S-WAVE ENERGY DENSITY
SPECTRUM OF N45E COMPONENT OF STATION 2;
EARTHQUAKE OF FEBRUARY 7, 1974



2/7/74 - STAT 2 COMP N45E / NOISE ESTIMATION COMP N45E

FIGURE II-5

NORMALIZED VELOCITY S-WAVE ENERGY DENSITY
SPECTRUM OF N45E COMPONENT OF STATION 2;
EARTHQUAKE OF FEBRUARY 7, 1974



2/7/74 - STAT 2 COMP N45E / NOISE ESTIMATION COMP N45E

FIGURE II-6

NORMALIZED DISPLACEMENT S-WAVE ENERGY DENSITY
SPECTRUM OF N45E COMPONENT OF STATION 2;
EARTHQUAKE OF FEBRUARY 7, 1974

calculated as 5.44×10^{-2} cm·sec. Similar spectra were calculated for each of the other components recording the event.

The results of this analysis and the implied source characteristics are given in Table II-2. As would be expected for an event of this low magnitude, the seismic moments and dislocation radii are of low values. However, as this analysis does not consider factors such as attenuation, the corner frequencies given are lower bounds and thus the dislocation radii could be even smaller. However, attenuation should have only slight effect on Ω_0 and thus the estimated values of M_0 are probably valid.

D. THE JULY 6, 1974 EARTHQUAKE

The July 6, 1974 earthquake was recorded by six stations of the Bear Valley accelerometer array. In addition this magnitude 3.2 earthquake was also recorded in the intermediate field which provided a hypocentral location and a fault plane solution for this event. The epicenter of this event is shown in Figure II-1 by the circle labeled E-2 (McEvelly and Johnson, 1974). A depth of 6.57 kms was determined for the hypocenter. Both the Haskell model and spectral estimates of the source characteristics were made for this event. The time domain process will be discussed first.

The accelerometer stations recording the event were Stations 2 and 4 which lie directly on the surface trace of the San Andreas, 3 and 6 which lie to the southeast of the fault and Sites 7 and 8 which are located on the lower velocity northeastern crustal block. The acceleration waveforms recorded at the various stations are of a highly complex nature and it is again difficult to pick what might be considered a dominant pulse for use in time domain waveform fitting in the velocity traces of most sites. As an example, the acceleration and velocity waves recorded at Stations 3, Figures II-7 and II-8, and 7, Figures II-9 and II-10, respectively are shown. In both cases the high variability of signal content from component to component make selection of a dominant pulse difficult.

TABLE II-2
S-WAVE SPECTRAL ESTIMATES OF SOURCE PARAMETERS
FEBRUARY 7, 1974 EARTHQUAKE

Station	Component	f_c (Hz)	Ω_o (cm · sec $\times 10^{-2}$)	r (km)	M_o (dyne · cm $\times 10^{21}$)
2	N45E	6.0	0.544		
	N45W	9.3	0.198		
	Vertical	6.67	0.117		
	Total Spectra	6.67	0.591	0.18	3.96
4	N45E	8.67	0.0326		
	N45W	9.33	0.0480		
	Vertical	9.33	0.0470		
	Total Spectra	9.33	0.0747	0.13	0.47
8	N45E	6.0	0.306		
	N45W	6.0	0.363		
	Vertical	6.0	0.119		
	Total Spectra	6.0	0.489	0.21	3.16

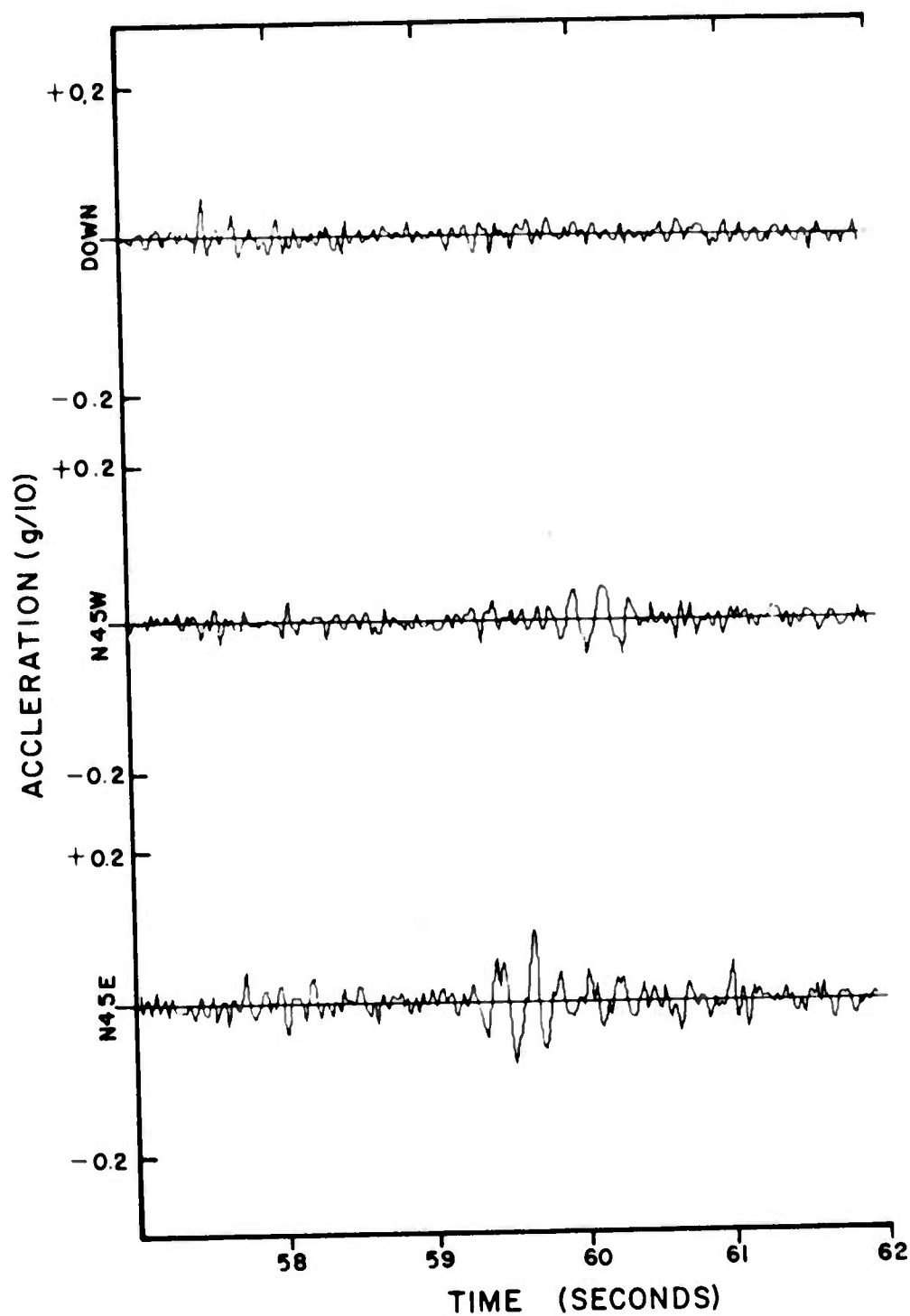


FIGURE II-7
ACCELEROGRAMS FROM STATION 3 FOR THE
JULY 6, 1974 EARTHQUAKE

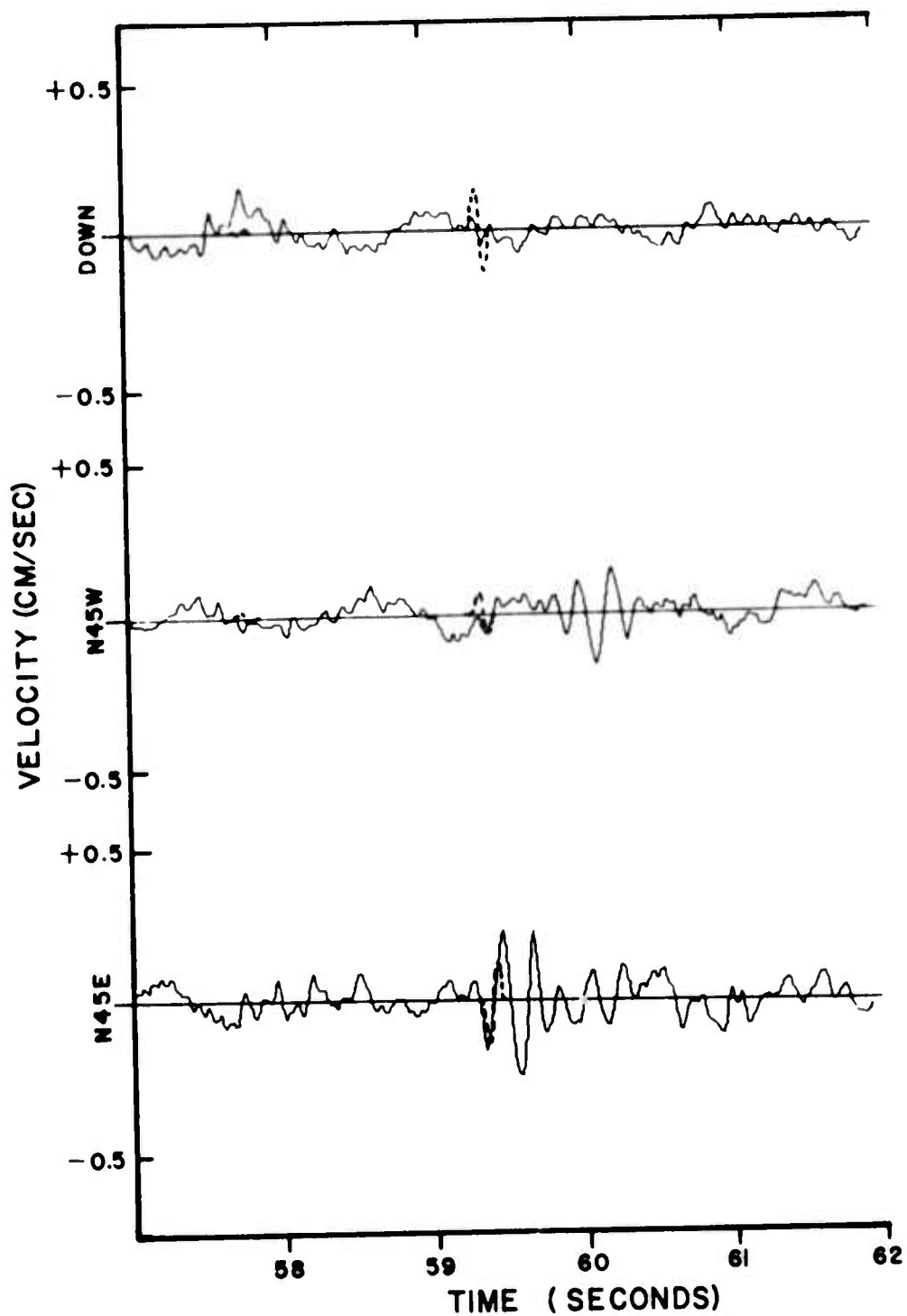


FIGURE II-8

DERIVED VELOCITY TRACES FROM STATION 3
FOR THE JULY 6, 1974 EARTHQUAKE
(DASHED LINE REPRESENTS HASKELL MODEL SOLUTION)

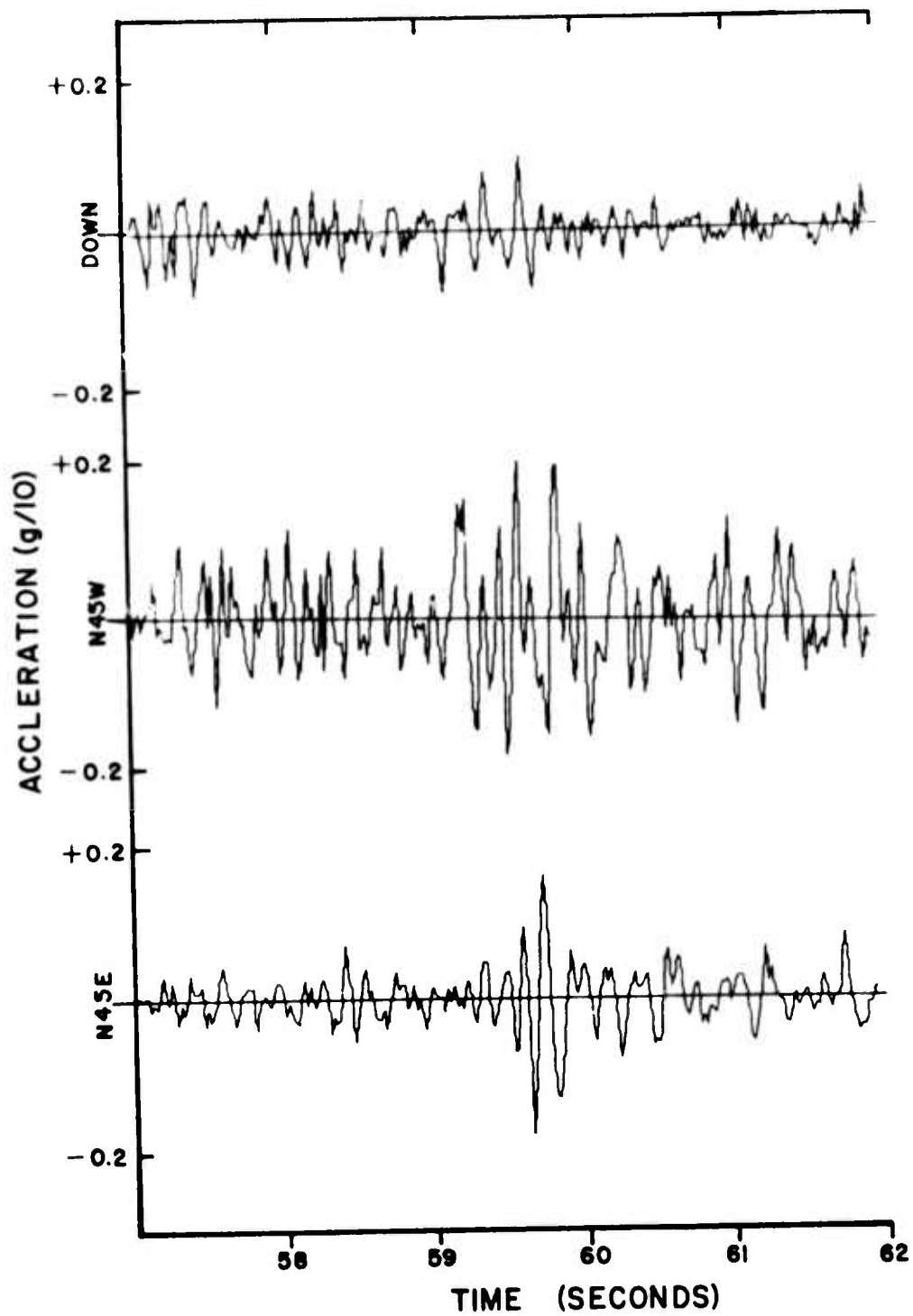


FIGURE II-9

ACCELEROGRAMS FROM STATION 7 FOR THE
JULY 6, 1974 EARTHQUAKE

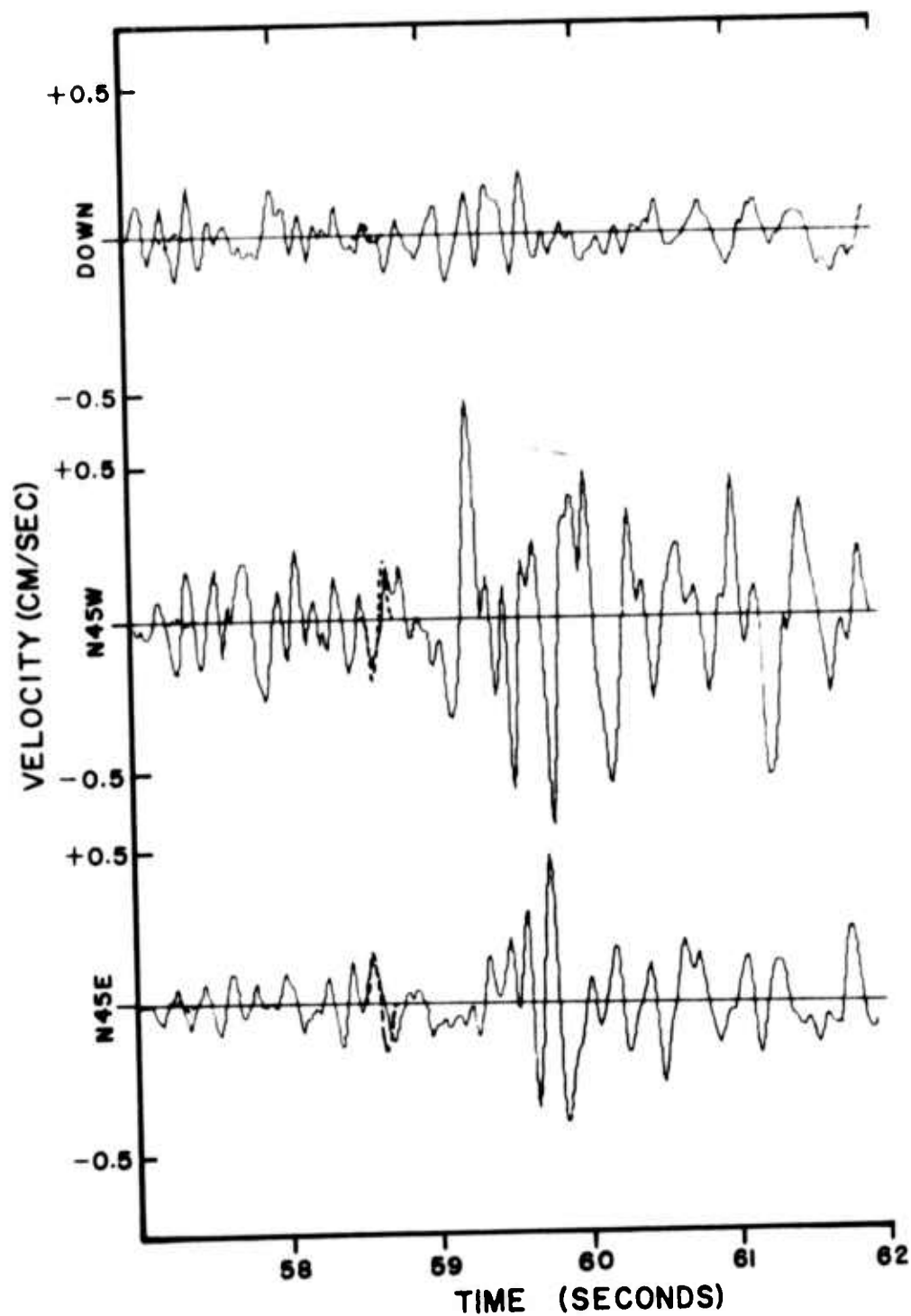


FIGURE II-10

DERIVED VELOCITY TRACES FROM STATION 7
FOR THE JULY 6, 1974 EARTHQUAKE
(DASHED LINE REPRESENTS HASKELL MODEL SOLUTION)

To overcome the difficulty, the whole space velocities calculated previously were used to determine approximate P- and S-wave arrival times. The velocity of the crustal block on which the station was located was used for each station. For Stations 2 and 4, those lying directly on the fault trace, times based on each model and an average velocity were used. As most stations recorded a strong P-arrival on at least one component, it was apparent that errors of as much as one second existed in these calculations. For this reason the dominant pulse used for fitting with the Haskell model was selected by using the S-P times to locate the approximate S-arrival time and then picking the nearest apparent dominant pulse.

As previously explained, once the pulses to be used in the fitting process are selected, unit dislocation waveforms for each station are calculated using as many external restrictions as possible. In this case the hypocentral location and a fault plane solution have been determined for the source from intermediate field data (McEvelly and Johnson, 1974). The fault plane solution defined a fault striking N40W and nearly vertical in dip. However, this was taken as the strike direction solely because it parallels the San Andreas surface trace in the vicinity of the epicenter. The auxiliary plane of N50E could also define the fault and thus both planes were used to produce theoretical waveforms by Haskell's source model.

Using least squared error fitting on the amplitudes of the selected pulses from all stations simultaneously and separately, the initial source structures were perturbed to produce 7 solutions defined by the minimum residual over all test cases for each set of fittings. Each solution was then used to produce theoretical waveforms at every station which were judged for overall 'goodness of fit'. Of these solutions for the July earthquake the one determined by waveform fitting at Site 6 separately was selected. At best, the quality of this fit can be considered marginal, in general being poorer than the fits shown in Figures II-8 and II-10 for Stations 3 and 7, respectively.

From Figures II-8 and II-10 it would appear that the modeled pulse duration is less than the observed indicating error in the calculated fault length, rise time or rupture velocity. At other stations the theoretical duration is closer to the observed value. However, this may indicate that these parameters are in error to some degree. The source parameters are given in Table II-3. That the Haskell model could not produce a satisfactory solution at all stations is probably the result of several problems which will be discussed later in this report.

In addition to the time domain modeling of the earthquake source, spectral estimates of the source characteristics were also made for this event. As is apparent on consideration of the empirical velocity waveforms in Figures II-8 and II-10 the spectra calculated for each station are highly variable and no single set of spectra could be considered typical of this event. However, the S-wave spectra of the N45E component at Station 8 are shown in Figures II-11 to II-13. The corner frequency, f_c , for this component is somewhat lower than for other stations but appears as a well defined peak in the velocity spectra at about 4 Hz. The results for all stations are shown in Table II-4. As with the February earthquake the relatively high corner frequency, indicating small fault area, and low seismic moments calculated for this event are as expected from a low local magnitude earthquake.

E. DISCUSSION OF RESULTS

While the general levels of seismic moments calculated for both the February and July earthquakes are reasonable when compared to the seismic moments and local magnitudes of other events studied from the near-zone, as shown in Figure II-14, it is apparent that a high level of variation in spectrally determined seismic moment exists between stations of the near-field array for each event. While this is in part accounted for by variations in the seismic source radiation patterns, a comparison of results studied in

TABLE II-3
BEAR VALLEY EARTHQUAKE OF JULY 6, 1974
HASKELL SOURCE MODEL SOLUTION

Epicenter	:	36°34.1'N	
Depth	:	121°10.1'W	
Velocities	:	Southwest Crustal Stations:	$V_p = 5.76 \text{ km/sec}$ $V_s = 3.32 \text{ km/sec}$
		Northeast Crustal Stations:	$V_p = 4.56 \text{ km/sec}$ $V_s = 2.60 \text{ km/sec}$
Strike Angle	:	N40W	
Dip Angle	:	80° to NE	
Fault Dimensions:		Length = 0.18 km Width = 0.18 km	
Rise Time	:	0.02 sec	
Rupture Velocity	:	2.5 km/sec	
Dislocations	:	Strike-Slip: 6.24 cm Dip-Slip : 5.84 cm	
Seismic Moment	:	$8.3 \times 10^{20} \text{ dyne cm}$	

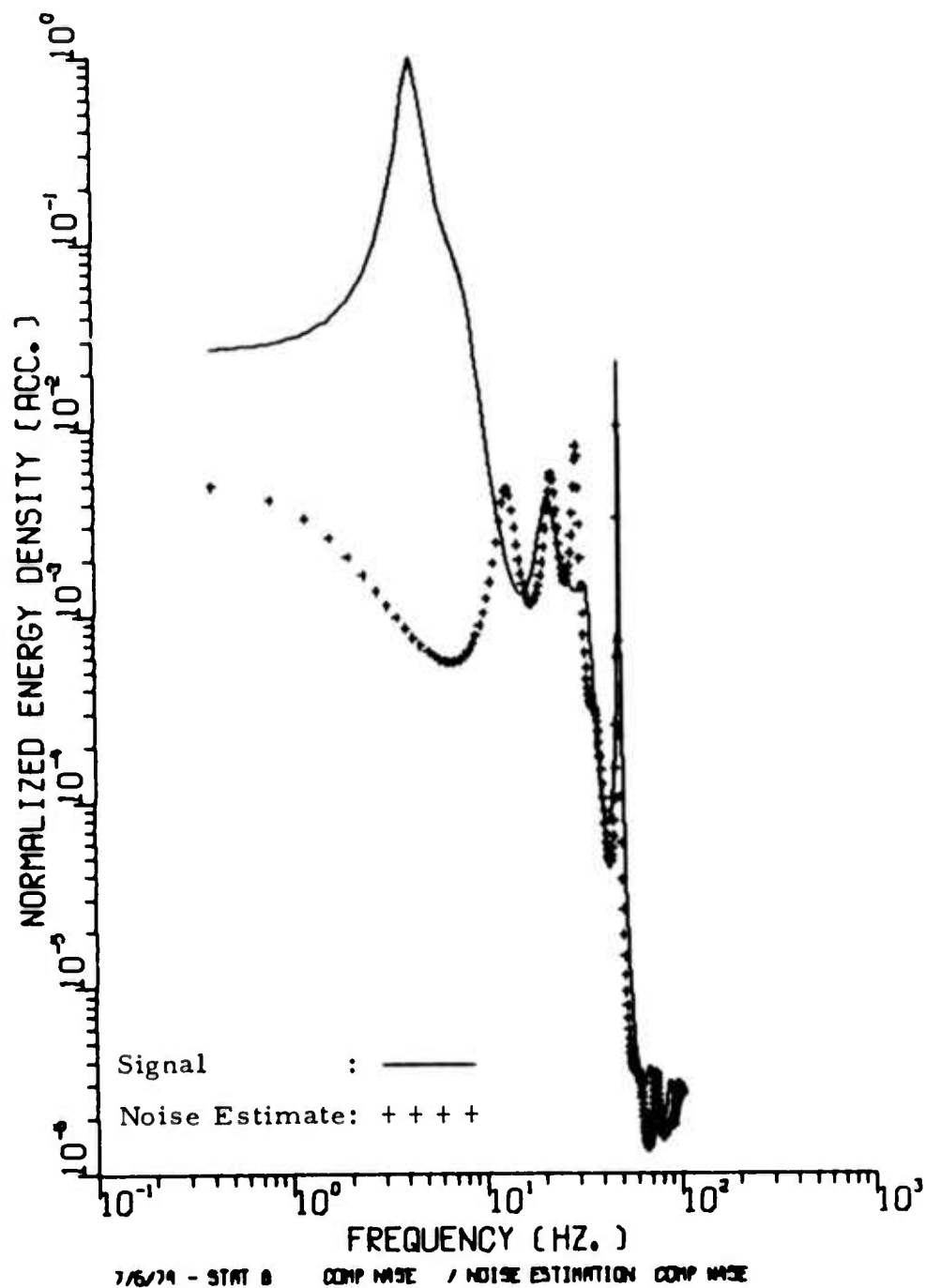
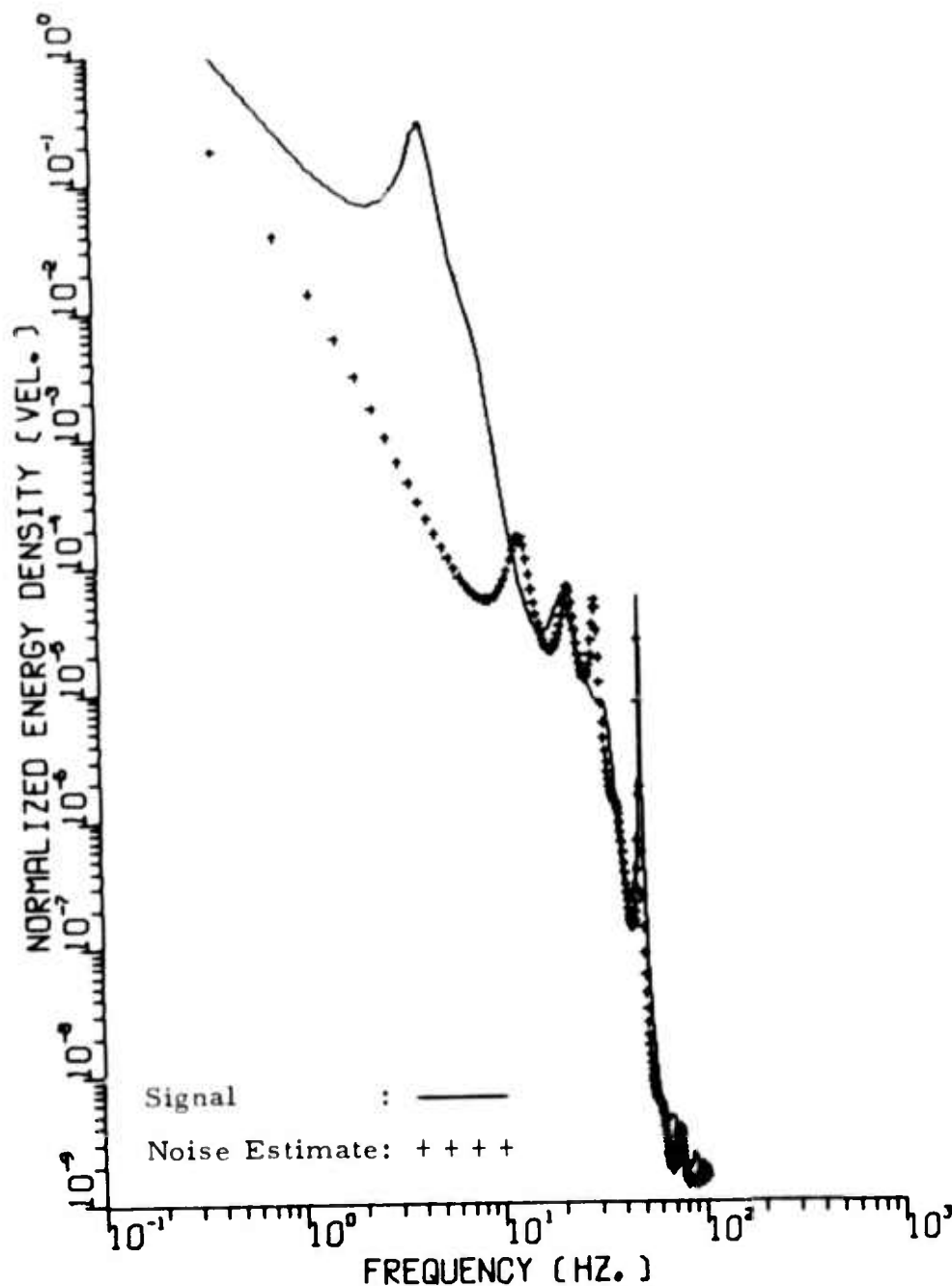


FIGURE II-11

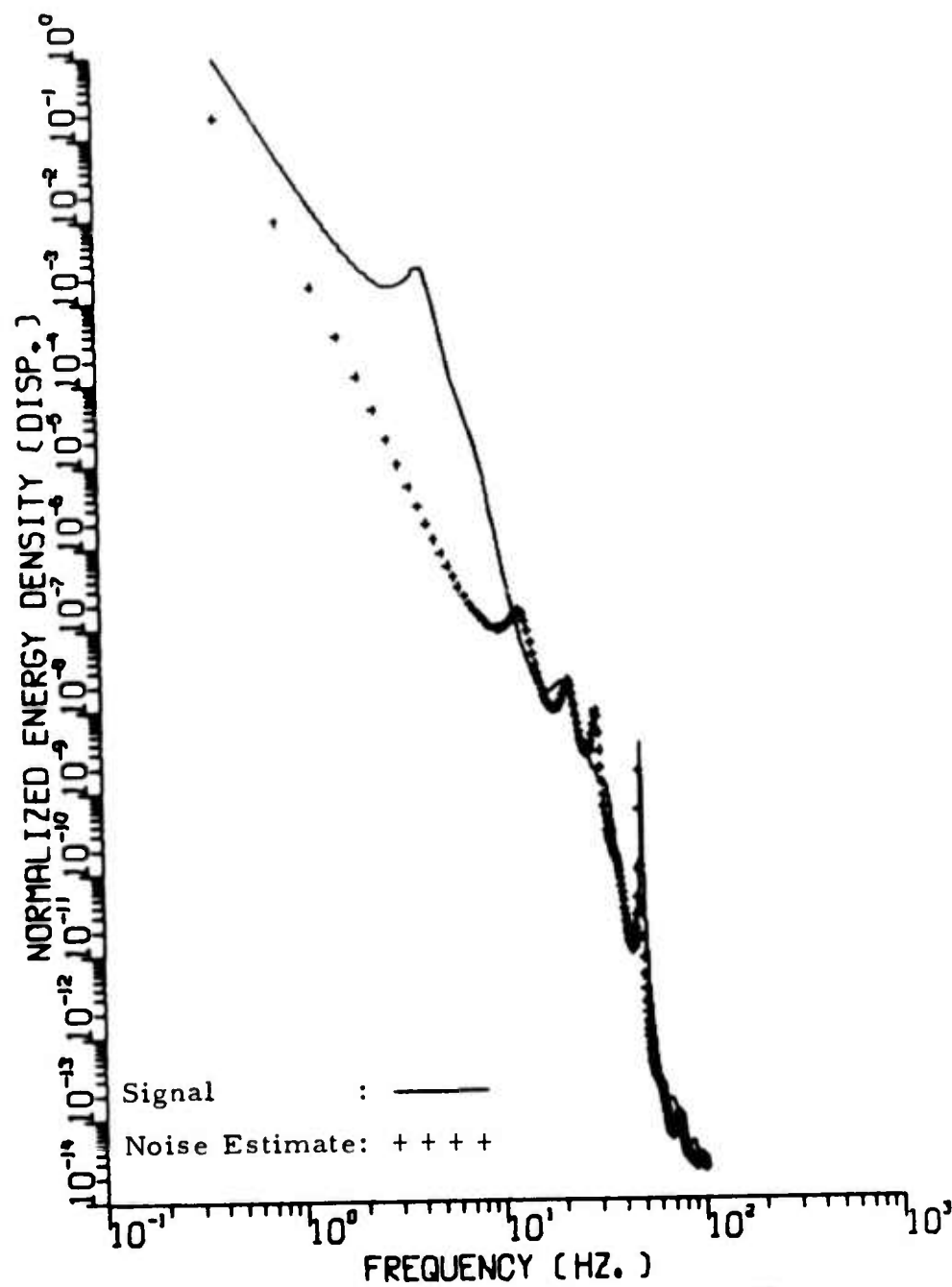
NORMALIZED ACCELERATION S-WAVE ENERGY DENSITY
SPECTRUM FOR N45E COMPONENT OF STATION 8;
EARTHQUAKE OF JULY 6, 1974



7/6/74 - STAT 8 COMP MADE / NOISE ESTIMATION COMP MADE

FIGURE II-12

NORMALIZED VELOCITY S-WAVE ENERGY DENSITY
SPECTRUM FOR N45E COMPONENT OF STATION 8;
EARTHQUAKE OF JULY 6, 1974



7/6/74 - STAT 8 COMP WAVE / NOISE ESTIMATION COMP WAVE

FIGURE II-13

NORMALIZED DISPLACEMENT S-WAVE ENERGY DENSITY
SPECTRUM FOR N45E COMPONENT OF STATION 8;
EARTHQUAKE OF JULY 6, 1974

TABLE II-4
S-WAVE SPECTRAL ESTIMATES OF SOURCE PARAMETERS
JULY 6, 1974 EARTHQUAKE

Station	Component	f_c (Hz)	Ω_0 (cm \cdot sec $\times 10^{-2}$)	r (km)	M_0 (dyne \cdot cm $\times 10^{21}$)
2	N45E	8.4	0.25	0.17	4.4
	N45W	6.0	0.41		
	Vertical	7.6	0.06		
	Total Spectra	7.6	0.48		
3	N45E	4.0	0.24	0.29	4.4
	N45W	4.4	0.12		
	Vertical	?	0.01		
	Total Spectra	4.4	0.27		
4	N45E	5.6	0.12	0.23	2.1
	N45W	6.4	0.09		
	Vertical	5.2	0.08		
	Total Spectra	5.6	0.17		
6	N45E	11.2	0.02	0.20	1.2
	N45W	6.4	0.06		
	Vertical	4.8	0.08		
	Total Spectra	6.4	0.10		
7	N45E	5.4	0.20	0.24	3.1
	N45W	8.4	0.13		
	Vertical	5.2	0.13		
	Total Spectra	5.4	0.27		
8	N45E	4.4	0.62	0.29	9.0
	N45W	4.0	0.37		
	Vertical	6.8	0.06		
	Total Spectra	4.4	0.72		

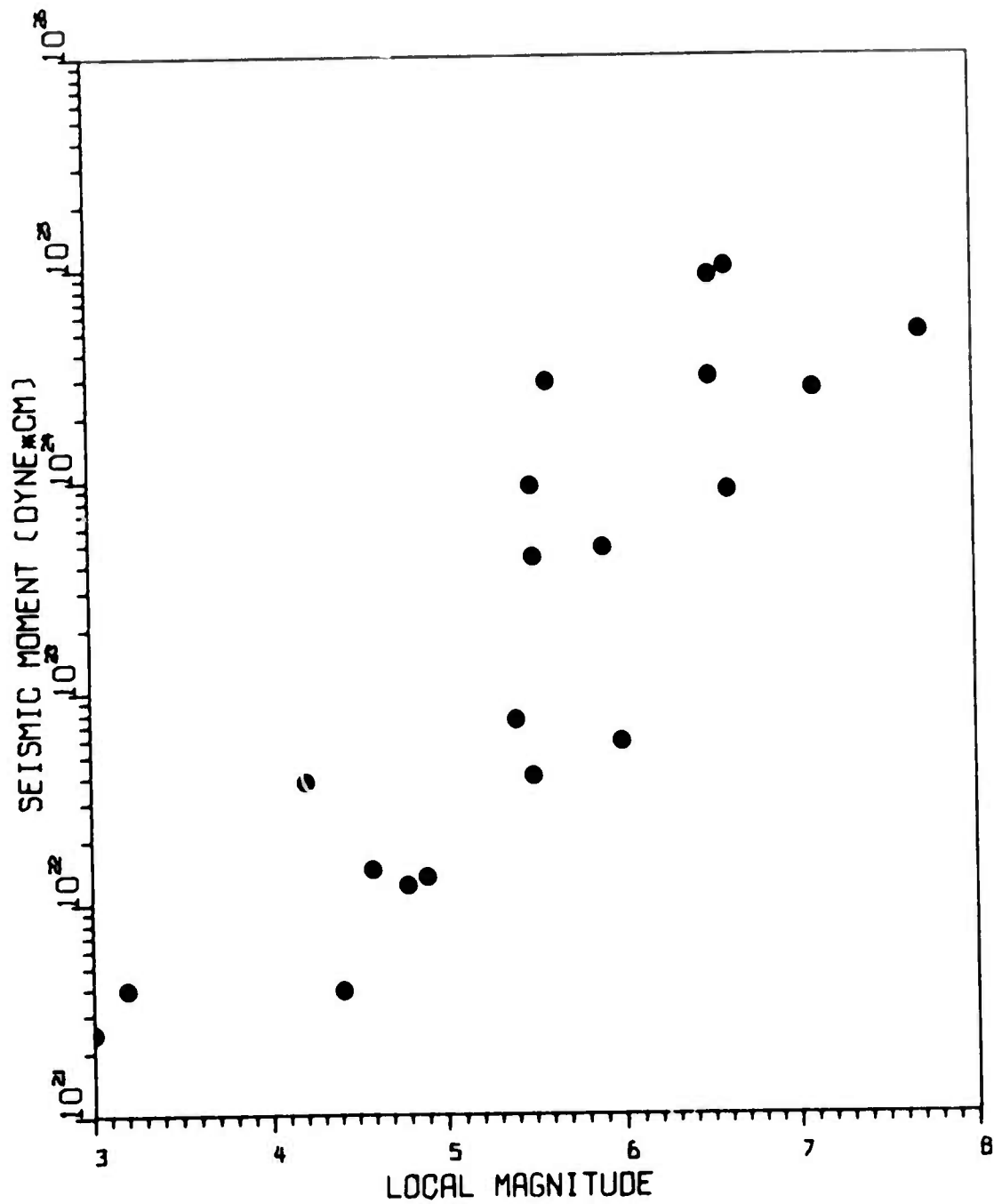


FIGURE II-14
OBSERVED LOCAL MAGNITUDES VERSUS NEAR-FIELD
SPECTRAL SEISMIC MOMENTS

this report and of the June 22, 1973 Bear Valley earthquake (Turnbull, et al., 1975; Turnbull et al., 1974b) indicate that the transmission and site effects may be more important in causing these variations.

In Table II-5 the seismic moments calculated by spectral means for the three Bear Valley earthquakes are shown for each station recording an event. It would appear from this data that the seismic moment found at each site is dependent on location of the site. The average moment for Stations 7 and 8, which are located to the northeast of the San Andreas Fault, tend to be higher than for Stations 2 and 4 which lie on the fault and Stations 3 and 6, which lie to the southwest, seem to have the lowest moments. McEvilly and Johnson (1974) have found a similar correlation between seismic moment for a given event and site location. Based on their data they find a factor of between 3 and 4 difference between stations to the southwest and to the northeast of the fault with the stations on the fault having a seismic moment intermediate between these stations. In addition, however, it would appear from Table II-5 that even for stations on the same structure significant variations occur. This can be seen in the consistent lower moment estimate at Station 4 as compared to Station 2.

Systematic variations in the acceleration amplitudes, as indicated by the variations in seismic moment, can explain the difficulty of the Haskell model to fit the July 6, 1974 earthquake. First, using multiple station fitting, it is apparent that one is attempting to find the fault whose radiation pattern can model the empirical amplitude pattern. However, if the empirical data is significantly altered by means external to the source, as appears to be the case at Bear Valley, then it is highly unlikely that a source model can reproduce these effects with a 'reasonable' earthquake source. Secondly, the complexities of the structure produce anomalous phases which reduce the dominance of any single pulse in the empirical wavetrain. Under these conditions it is highly unlikely that the same arrival will be selected at

TABLE II-5
SEISMIC MOMENTS FOR EACH EVENT AT BEAR VALLEY
AS CALCULATED AT EACH STATION

	6/22/73	2/7/74	7/6/74
Station 2	1.8×10^{22}	4.0×10^{21}	4.4×10^{21}
Station 3	--	--	4.4×10^{21}
Station 4	6.5×10^{21}	4.7×10^{20}	2.1×10^{21}
Station 6	--	--	1.2×10^{21}
Station 7	5.4×10^{22}	--	3.1×10^{21}
Station 8	7.5×10^{22}	3.2×10^{21}	9×10^{21}

all stations used in the fitting process. This in turn results in incorrect phase and amplitude relations between the stations making a 'good fit' within such restrictions as the fault plane solution nearly impossible. Thus, it can be concluded that the failure of the Haskell model in this case is not failure of the source model but rather of its inability to cope with transmission effects.

It is also possible that these transmission or site effects can explain the apparent disagreement of seismic moments calculated for the June 22, 1973 earthquake from near, intermediate, and far-field data. Using Haskell's model a seismic moment of 1.2×10^{23} dyne.cm was calculated for this event. However, moments of much lower magnitude were found in the intermediate and far-field. Smith (1973) calculated an intermediate zone moment of 2×10^{22} dyne.cm while the best far-field estimates ranged between 0.7 and 2×10^{22} dyne.cm (D. Sun, personal communication, 1975). If one assumes that the variations of amplitude result from site amplifications for stations on the fault and to the northeast of it, then using McEvelly and Johnson's correction factor, the recorded amplitudes of Stations 7 and 8 should be reduced by a factor of about 3.5. Reducing these amplitudes will reduce the modeled dislocations and seismic moment an equal amount. Thus a seismic moment of 3.4×10^{22} dyne.cm would be obtained, in much better agreement with the intermediate and far-field results for this earthquake.

SECTION III

FAR-FIELD SOURCE STUDIES

A. INTRODUCTION

For the past several months, the examination of far-field spectra for source characteristics has been conducted along several lines of investigation. The investigation of two California earthquakes (22 June 1973 and 28 November 1974) using far-field surface wave data has been extended from the last study (Turnbull, et al., 1975). In Subsection B, we discuss the effect a new source region structure (McEvelly, 1975) would have on the source mechanism solution. The investigation of theoretical higher mode spectra has also been continued, with comprehensive spectral displays produced and analyzed for two different representative earth structures in Subsection C. Finally, in Subsection D, we present preliminary results on the investigation of a swarm of earthquakes that occurred in Sinkiang, China in 1974.

B. CONTINUED EVALUATION OF THE FAR-FIELD SOURCE MECHANISM FOR TWO CALIFORNIA EARTHQUAKES

In previous work (Turnbull, et al., 1975), it was felt that one of the limitations to the far-field solutions for these events was knowledge of the source region structure. From a field survey conducted by McEvelly (1975), we were able to obtain better structure estimates for both sides of the San Andreas fault in the Bear Valley region. This structure is listed in Table III-1, with the dispersion curves for both sides of the fault displayed in Appendix A. The major difference between the structure on each side of the fault, of course, is the higher velocity layers in the structure on the southwest side.

TABLE III-1
BEAR VALLEY REGION STRUCTURE (McEVILLY, 1975)

Depth h	Layer Thickness Δh	Northeast Side of Fault			Southwest Side of Fault		
		ρ	V_p	V_s	ρ	V_p	V_s
0.6	0.6	2.0	2.38	1.51	2.7	4.25	2.46
2.5	1.9	2.1	3.04	1.76	2.7	5.2	3.0
5.5	3.0	2.7	5.88	3.30	2.74	6.34	3.66
10.0	4.5	2.75	4.84	2.80	2.74	5.96	3.45
15.5	5.5	2.75	4.98	2.88	2.8	6.94	4.0
19.3	3.8	2.8	6.02	3.48	2.8	6.67	3.86
21.0	1.7	2.9	6.55	3.79	3.0	6.55	3.78
25.0	4.0	3.0	6.86	3.97	3.0	6.55	3.78
50.0	25.0	3.32	8.2	4.65	3.32	8.2	4.65
<div style="display: flex; justify-content: space-between; align-items: center;"> ↓ Merge With Gutenberg-Bullen Earth Model ↓ </div>							

Another way to determine the impact the structural differences have on the observed spectra is to generate theoretical spectra using a source imbedded in these structures. Using the bodywave source mechanisms for these two events, spectral variation with respect to depth and radiation patterns of a particular depth were generated. The two source mechanisms are listed below in Table III-2.

TABLE III-2
SOURCE PARAMETERS FOR THE TWO CALIFORNIA EVENTS

Event Description	Depth - h (km)	Dip - δ (deg)	Slip - λ (deg)	Strike - θ N (deg) E
Bear Valley 6-22-73	10.25	70	30	135
Central California 11-28-74	4	90	0	35

These spectra and radiation patterns are displayed for both events in Appendix B. The major conclusions that can be drawn from comparisons between the two structural responses are:

- From the displays of Rayleigh and Love wave amplitude spectra as a function of depth we see that, for the appropriate source depth, and for both events, the spectral levels for the northeast structure are approximately an order of magnitude higher than those levels generated by the southwest side.
- From the Rayleigh and Love wave radiation patterns for both events generated at 20 seconds period, we see that the patterns have shapes that are structure dependent as well as having different spectral levels.

With these structural properties firmly in mind, we attempted to 'fit' the observed spectra in the same manner as in previous analysis of these events (Turnbull, et al., 1975). The stations available for the Bear Valley event of 22 June 1973 are displayed in Figure III-1, with the Rayleigh wave traces used from OGD and ALQ, and the Love wave trace from LASA. In the spectral fitting process, no absolute minimum residual was observed, but a solution was obtained by picking the local minimum residual. Because the stations lie to the east of the fault, the northeast structure was used. The solution was found to be close to the bodywave mechanism, with a depth of 6 km, dip of 80° , slip of 0° , strike of $N175^{\circ}E$, and a seismic moment of 0.9×10^{22} dyne-cm. This moment is about an order of magnitude less than that obtained by fitting near-field acceleration data, and approximately the same as that obtained previously using the Helmberger structure.

Analysis of the central California event of 28 November 1974 presented a more complex situation. The stations available are displayed in Figure III-2, with the Rayleigh wave traces used from NORSAR, TLO, ALPA, ZLP, and KIP, and the Love wave trace from LASA. With stations on both sides of the fault, a problem arises as to which source region structure is appropriate. An exhaustive approach was applied to this situation, with solutions obtained by using the northeast model only, the southwest model only, and for the first time, a combination of the two structures. The solutions obtained for the different combinations of stations and structures based on the minimum residual criteria and the distribution of minimum residual criteria are given in Tables III-3 and III-4, respectively. All of the solutions yield a similar source mechanism; a vertical strike-slip fault with a strike direction of $N45^{\circ}E$. This agrees very well with the bodywave solution. However, except for the solution obtained by fitting the three stations in the west with the southwest model, all of the focal depth estimates were too deep.

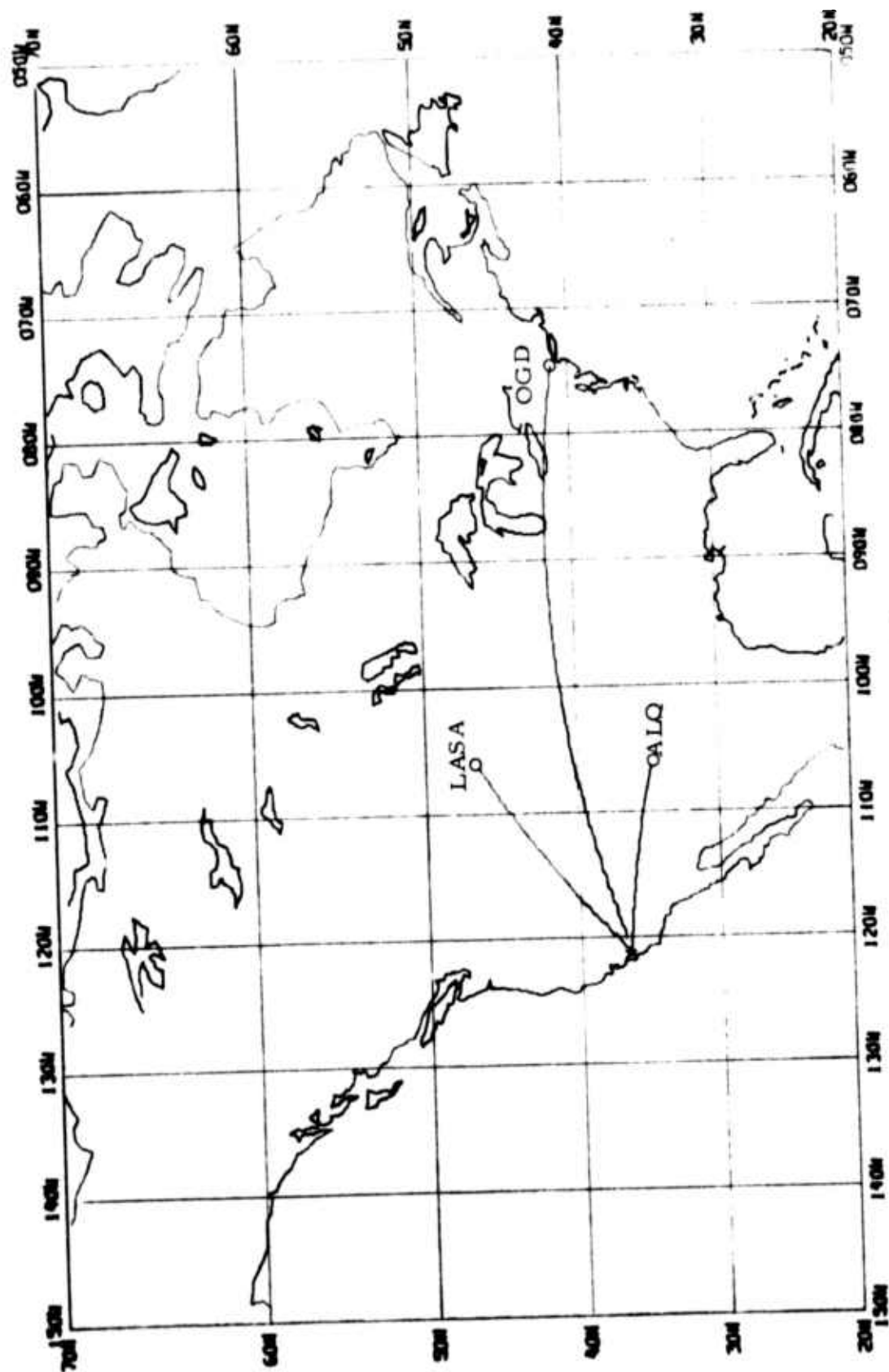


FIGURE III-1
TRAVEL PATHS TO THE AVAILABLE STATIONS FOR THE
JUNE 22, 1973 EARTHQUAKE

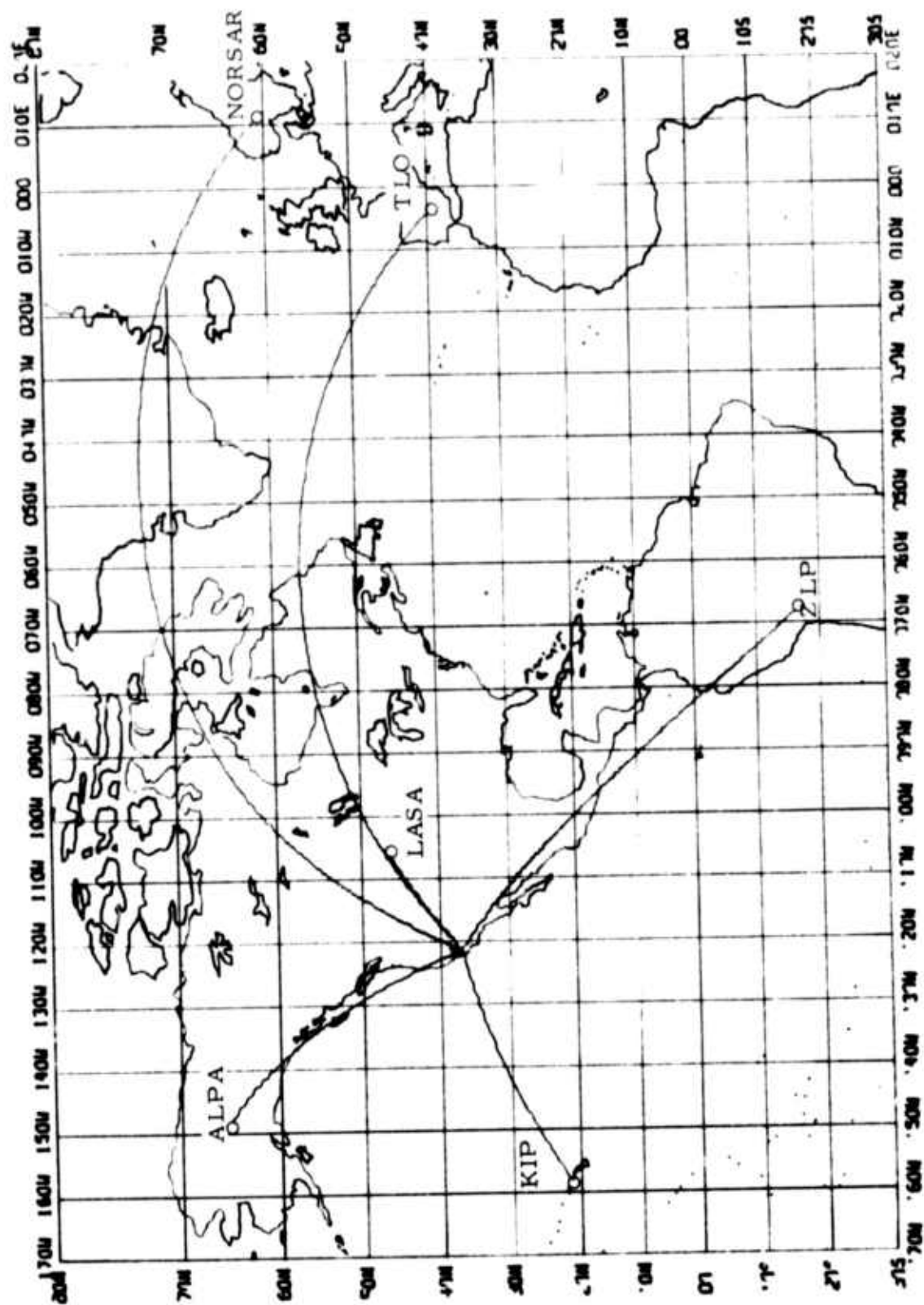


FIGURE III-2
TRAVEL PATHS TO THE AVAILABLE STATIONS FOR THE
NOVEMBER 28, 1974 EARTHQUAKE

TABLE III-3
ESTIMATIONS OF SOURCE PARAMETERS FOR THE CENTRAL CALIFORNIA
EVENT OBTAINED BY AMPLITUDE SPECTRAL FITTING BASED ON
MINIMUM-RESIDUAL CRITERION

Structure	Stations Used	Optimal Solution					Moment 10 ²⁵ dyne-cm
		Depth h (km)	Dip angle δ (degrees)	Slip Angle λ (degrees)	Strike N θ° E		
Southwest Only	ALPA ZLP KIP	6	80	30	135	0.530 x 10 ⁻¹	
Southwest Only	ALPA LASA NORSAR	37.5	90	0	40 130	0.232	
Southwest Only	All Stations	37.5	80	0	45	0.226	
Northeast Only	LASA NORSAR TLO	27.5	80	0	125	0.111	
Northeast Only	ALPA LASA NORSAR	27.5	80	0	60	0.113	
Northeast Only	All Stations	27.5	90	0	40 130	0.104	
Both	All Stations	27.5	80	0	60	0.115	

TABLE III-4
ESTIMATIONS OF SOURCE PARAMETERS FOR THE CENTRAL CALIFORNIA
EVENT OBTAINED BY AMPLITUDE SPECTRAL FITTING BASED ON
DISTRIBUTION-OF-MINIMUM-RESIDUAL CRITERION

Structure	Stations Used	Source Parameters							
		Depth h (km)		Dip Angle δ°		Slip Angle λ°		Strike $N\theta^\circ E$	
		Probable Range	% Con- fidence	Probable Range	% Con- fidence	Probable Range	% Con- fidence	Probable Range	% Con- fidence
Southwest Only	ALPA ZLP KIP	4.5-10.25	78	60-90	79	-30, 0, 30	78	15- 45 110-140	38 48
Southwest Only	ALPA LASA NORSAR	32.5-42.0	89	80-90	100	0	100	35- 50 125-140	48 48
Southwest Only	All Stations	32.5-42.0	70	80-90	100	0	100	40- 50 130-140	51 32
Northeast Only	LASA NORSAR TLO	23.0-37.5	89	70-90	84	0	75	25- 55 115-145	45 44
Northeast Only	ALPA LASA NORSAR	23.0-37.5	78	80-90	98	0	100	55- 65 145-155	54 46
Northeast Only	All Stations	23.0-37.5	88	80-90	79	0	100	30- 60 120-150	42 42
Both	All Stations	23.0-37.5	79	80-90	89	0	100	55- 65 145-155	46 46

From the above analysis, we have reached the following conclusions:

- Fitting the surface wave spectra with one earth model using stations on both sides of the fault neglects the effect of the medium discontinuity. One possible way to correct for this discontinuity would be to make the appropriate travel path correction. This problem will be examined in future studies.
- Fitting the surface wave spectra with two earth models would seem to be a reasonable approach, if we consider the effect of the discontinuity as a difference in the source excitation. One problem in this approach is, however, that the combination of the two earth models for simulating both sides of the fault actually neglects the possible physical complexity of the source due to the discontinuity.
- At the present time, we have no solution to the above problems. Since the location of this event is definitely on the west side of the San Andreas fault, the far-field solution obtained by using the three stations to the west of the fault with the southwest earth model should be considered a good estimate.

C. CONTINUED EXAMINATION OF THE THEORETICAL HIGHER MODE SPECTRA

Continuing with our examination of theoretical first higher mode Rayleigh and Love wave spectra, double couple sources were placed at three representative depths (4, 30, and 50 km) in a Gutenberg-Bullen earth model and a Hamilton-Healy earth model. Variations of the spectra with respect to dip, slip, and strike were examined (see Appendix C). We can summarize the properties of this spectra as follows:

- Regardless of the structure, the only consistent 'holes' in the spectra occur for Rayleigh waves generated by a vertical strike-slip source mechanism. In particular, for the Gutenberg-Bullen structure, two 'holes' appeared for this source mechanism placed 30 km deep at 9 and 20 seconds period.
- The level of first higher mode spectra is approximately an order of magnitude less than that of the fundamental mode spectra over the same frequency range (15 to 40 seconds period). The higher mode spectra over the 3 to 15 second period range is, however, approximately the same level as the fundamental mode 15 to 40 second spectra.
- For the Gutenberg-Bullen structure, the first higher mode spectra drops off rapidly for periods greater than 9 seconds, especially for Love waves. This drop-off is even more severe for the Hamilton-Healy structure, starting at 6 seconds period. This is a direct result of the lower velocity material in the upper crust of the Hamilton-Healy model. Therefore, we should expect to observe higher modes with greater regularity from thick high velocity source region crustal structures using presently installed instrumentation.

D. ANALYSIS OF THE SINKIANG, CHINA EARTHQUAKE SWARM OF AUGUST 1974

During most of the month of August and the early part of September 1974, a major earthquake swarm of over 300 recorded events occurred in Sinkiang, China. The location of the swarm is shown by the boxed area in Figure III-3. (This map was part of an earlier study by Turnbull, et al., 1974a). The number and magnitude of these events as a function of date is shown in Figure III-4.

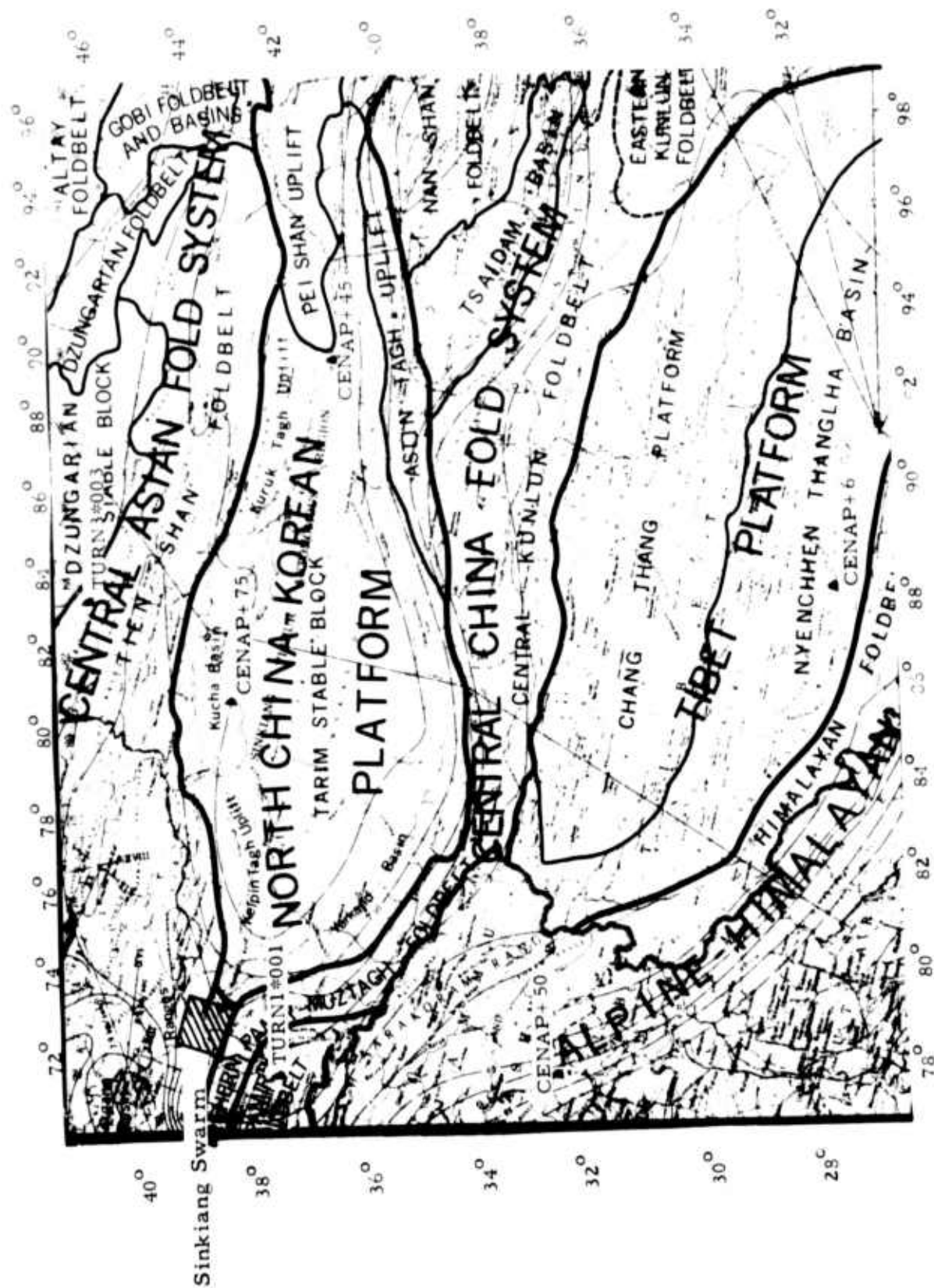


FIGURE III-3

LOCATION OF SINKIANG, CHINA SWARM OF AUGUST, 1974 - (BOXED AREA)

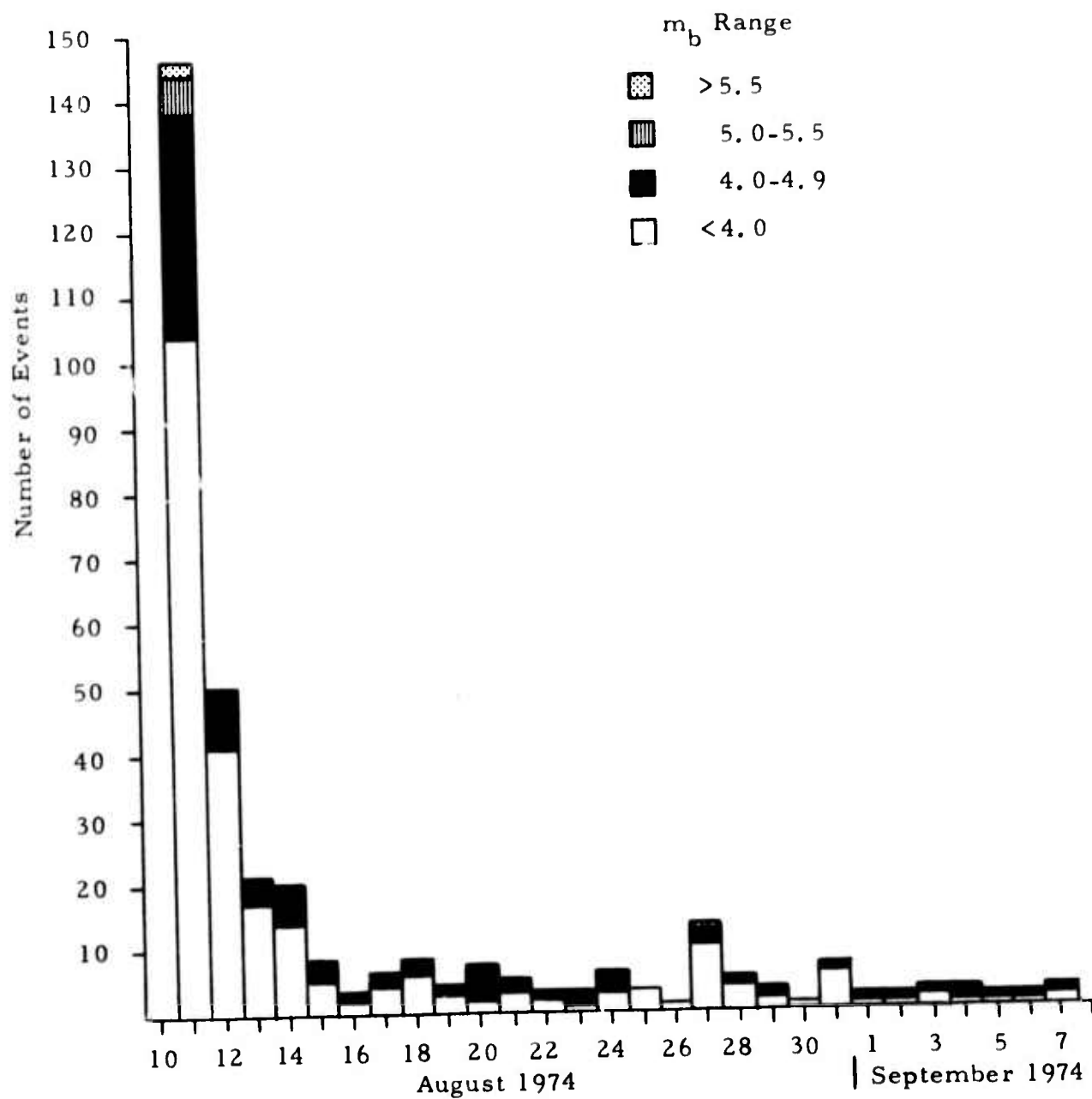


FIGURE III-4
THE NUMBER AND MAGNITUDE CHRONOLOGY OF THE
RECORDED EVENTS OF THE SINKIANG EARTHQUAKE
SWARM OF AUGUST 1974

This swarm was chosen for intensive analysis because of the following reasons:

- The opportunity to analyze a large number of events from a small region - investigate the repeatability of source mechanism from event to event and local tectonics.
- The possibility of using a master event or events with spectral ratios to measure path effects.
- The opportunity to determine effective attenuation by eliminating radiation pattern effects (knowing the source mechanism) and by two station path corrections (in the instances where they occur).

Preliminary analysis of five of these events have consistently yielded shallow source depths in the 4 to 10 km range. The source mechanism details, though, have not followed a particular trend at this point of the study. A more detailed analysis of this swarm will be presented in the next report.

SECTION IV

THE $M_s - m_b$ RELATIONSHIP

In previous work by Turnbull et al. (1974b, 1975) the $M_s - m_b$ discriminant was investigated with the objective of reducing the scatter of the earthquake population. Several methods were tried to achieve such a reduction; all of them designed to modify in various ways the M_s determinations at individual single stations of the VLPE network, and assess the impact on network magnitude measurements. However, no significant reduction of the $M_s - m_b$ scatter was observed.

In this report we focus upon the m_b determination, and apply the maximum likelihood method of Ringdal (1975) in an attempt to improve the accuracy of the PDE bodywave magnitudes for our data base. The basic idea is that PDE magnitudes of small events tend to be biased high, because only a few stations (with particularly favorable radiation patterns) report such events, and network magnitudes are therefore obtained by averaging over a set of stations that is not representative of the whole network. By taking into account the estimated noise levels at the non-detecting stations, this magnitude bias can partly be compensated for. Our model is as follows:

- For large events, the typical number of PDE stations that report a bodywave magnitude is assumed to be at least N_0 (where N_0 is a number to be estimated)
- For a given event, the number N of stations that actually report a magnitude is compared to N_0 . If $N \geq N_0$, it is assumed that essentially all PDE stations detected the event. If $N < N_0$, we assume that, for each of $(N_0 - N)$ stations, the magnitude was less than a certain threshold value m .

- The threshold values m at each station are assumed to be independently sampled from a normal distribution $m \sim N(m_o, \sigma_o^2)$
- The world-wide magnitude values of the event are assumed to follow a normal distribution $N(\mu, \sigma_S^2)$; where the parameter μ denotes the true magnitude of the event.

The likelihood function (Ringdal, 1975) becomes; for

$N < N_o$:

$$L(\mu) = \prod_{i=1}^N \frac{1}{\sigma_S} \cdot \phi \left(\frac{m_i - \mu}{\sigma_S} \right) \cdot \left[\Phi \left(\frac{m_o - \mu}{\sqrt{\sigma_S^2 + \sigma_o^2}} \right) \right]^{N_o - N} \quad (IV-1)$$

where the m_i denote the magnitude measured at the detecting stations, and where ϕ and Φ are the standard normal density and distribution functions, respectively. An estimate of μ is then obtained by numerical maximization of (IV-1).

In order to do this, it is necessary to have available realistic estimates of the parameters $\sigma_S, m_o, \sigma_o, N_o$; besides the observed quantities N and $\{m_i; i = 1, \dots, N\}$. Studies by Evernden (1969) of the noise levels of some of the better WWSSN stations seem to indicate values of $m_o = 5.0$ and $\sigma_o = 0.2$ as realistic estimates. Veith and Clawson (1972) found $\sigma_S = 0.4$ to be representative of the WWSSN network. From studies of PDE bulletins, we have found a value of $N_o = 25$ as a reasonable estimate of the number of stations expected to report magnitudes of large Eurasian events.

Figure IV-1 shows the theoretical bias $(\bar{m} - \mu)$ between the average magnitude \bar{m} (over the N detecting stations) and the true magnitude μ as a function of the ratio N/N_o and for various values of $(\bar{m} - m_o)$. Equation (IV-1) has been used to compute these bias values. Note that the only assumed parameter values in Figure IV-1 are $\sigma_S = 0.4$ and $\sigma_o = 0.2$;

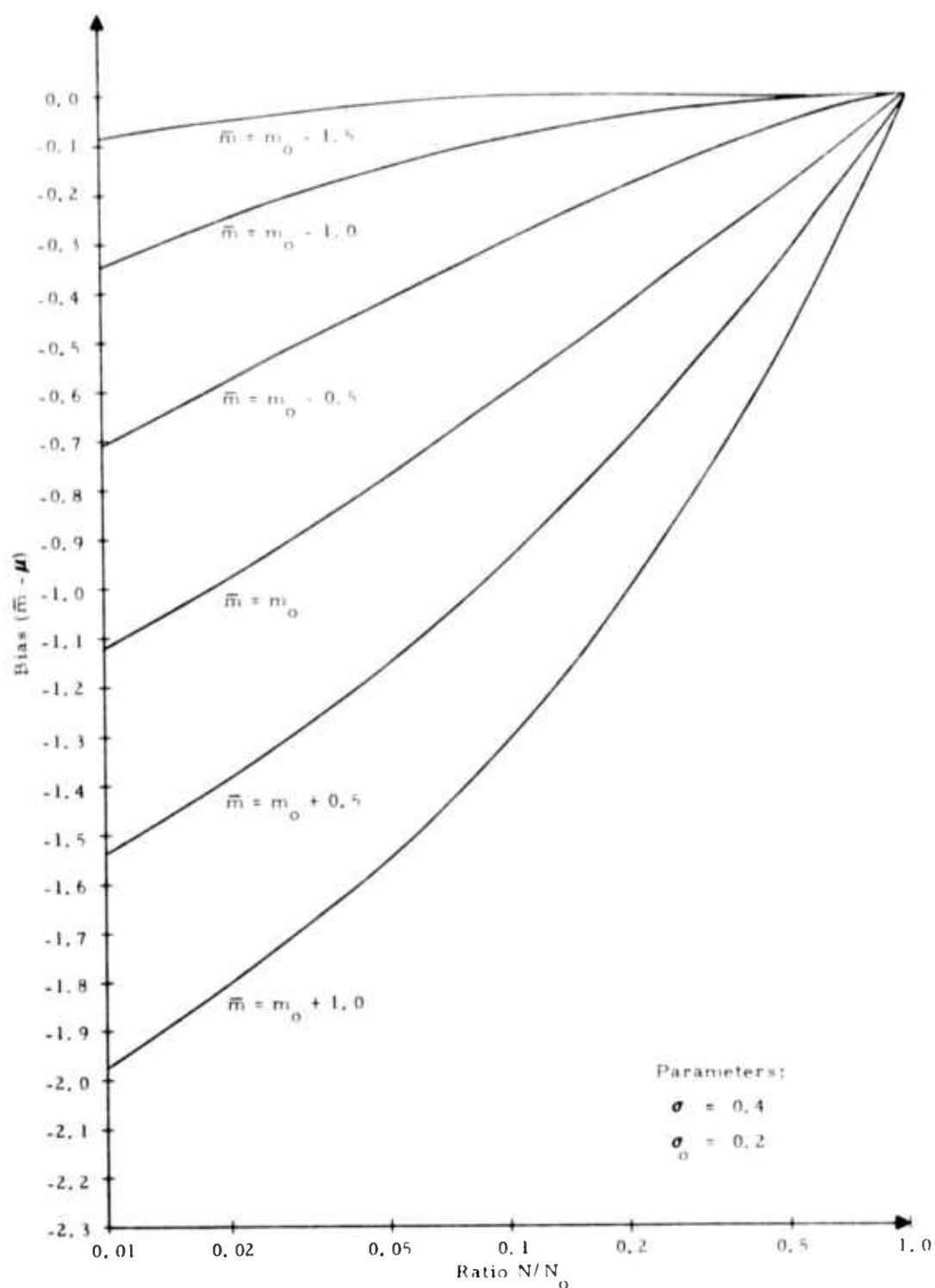


FIGURE IV-1
 EXPECTED BIAS OF CONVENTIONAL MAGNITUDE \bar{m} RELATIVE
 TO TRUE MAGNITUDE μ FOR A HYPOTHETICAL NETWORK AS
 A FUNCTION OF THE PERCENTAGE OF DETECTING STATIONS

hence the graphs can also be applied to networks with different parameter values N_0 and m_0 than used here.

Table IV-1 lists the events in the data set along with certain event parameters. Among those are the NORSAR and PDE reported m_b values; the number N of PDE station magnitudes available, and the maximum likelihood PDE magnitudes from the preceding model. Figures IV-2 and IV-3 plot NORSAR magnitudes versus PDE standard m_b and PDE maximum likelihood (M-L) m_b , respectively. It is seen that the latter case produces a linear trend with a slope close to 1.00, while Figure IV-2 exhibits the network magnitude bias effect for small events, and produces a more horizontal slope of about 0.8. The conclusion is that the maximum likelihood m_b values are more consistent estimates of μ than the standard PDE m_b for our data set.

In order to see if the use of maximum likelihood m_b values would reduce the scatter in the $M_s - m_b$ population, VLPE M_s was plotted against PDE m_b (Figure IV-4) and against PDE(M-L) m_b (Figure IV-5). The straight line of each figure is a least squares orthogonal fit, and the orthogonal standard deviation σ has been computed together with the slope α and intercept β of the estimated functional relationship:

$$M_s = \alpha \cdot m_b + \beta \quad (IV-2)$$

We note that the value of σ does not decrease when PDE m_b 's are replaced by maximum likelihood estimates; on the contrary, a slight increase is found (from 0.238 to 0.262). However, the slope α is much steeper in the first case (1.54 versus 1.23), hence the values of σ are not directly compatible. (For example, an estimation method that assigned identical m_b values to all events would produce a vertical slope with $\sigma = 0$; hence, a low value of σ does not necessarily imply improved estimation techniques.)

TABLE IV-1
EVENT PARAMETERS OF EURASIAN DATA BASE
(PAGE 1 OF 3)

Event Number	Number Of PDE Stations	PDE (M-L) m_p	PDE m_p	NORSAR m_p	VLPE Station - M_s Values											ALPA M_s	NORSAR M_s
					1	2	3	4	5	6	7	8	9	10	11		
31	9	4.7	5.0	4.6	0.0	4.2	5.9	4.1	0.0	4.8	4.1	0.0	0.0	0.0	0.0	3.7	4.3
36	12	4.7	4.9	4.6	0.0	3.9	0.0	3.3	0.0	3.5	4.1	0.0	0.0	0.0	0.0	4.0	4.2
37	2	4.3	4.8	4.3	0.0	4.1	0.0	4.5	0.0	4.3	4.2	0.0	0.0	0.0	0.0	4.3	4.2
39	22	5.2	5.3	5.1	0.0	5.0	0.0	4.9	0.0	5.4	5.1	0.0	0.0	0.0	0.0	4.8	5.2
43	9	4.5	4.7	4.7	0.0	3.2	3.6	3.7	0.0	3.4	0.0	0.0	0.0	0.0	0.0	3.0	3.6
62	1	4.1	4.6	4.6	0.0	4.0	0.0	0.0	0.0	3.8	4.0	0.0	0.0	0.0	0.0	3.6	0.0
73	1	4.4	5.9	4.2	0.0	4.2	3.9	3.8	0.0	4.0	4.1	0.0	0.0	0.0	0.0	4.0	3.9
87	7	4.4	4.6	4.2	0.0	3.4	3.5	3.6	0.0	3.6	3.4	0.0	0.0	0.0	0.0	3.3	3.3
88	14	4.9	5.1	5.0	0.0	3.9	4.4	4.4	0.0	4.5	4.9	0.0	0.0	0.0	0.0	4.3	0.0
89	2	4.1	4.5	4.4	0.0	3.5	4.4	4.3	0.0	4.0	4.3	0.0	0.0	0.0	0.0	4.1	4.1
95	11	4.9	5.2	4.9	0.0	3.9	4.8	0.0	0.0	4.1	3.9	0.0	0.0	0.0	0.0	0.0	0.0
112	28	5.7	5.7	5.7	0.0	4.4	5.1	5.1	0.0	4.8	5.3	0.0	0.0	0.0	0.0	4.8	0.0
123	10	4.5	4.6	3.9	0.0	4.0	3.6	4.1	0.0	3.8	0.0	0.0	0.0	0.0	0.0	3.9	3.9
134	28	5.4	5.4	5.2	0.0	0.0	4.7	0.0	0.0	4.8	5.0	0.0	0.0	0.0	0.0	0.0	0.0
294	23	5.2	5.2	4.6	0.0	4.1	4.5	4.2	0.0	5.0	0.0	0.0	0.0	0.0	0.0	4.6	4.8
341	9	5.0	5.4	5.2	5.1	0.0	0.0	0.0	0.0	5.3	0.0	5.6	4.4	0.0	0.0	3.8	0.0
472	17	5.1	5.2	4.4	3.8	0.0	0.0	4.0	0.0	4.0	0.0	4.1	0.0	0.0	0.0	0.0	4.0
505	22	5.2	5.3	5.2	3.9	0.0	0.0	3.7	4.7	0.0	0.0	4.6	3.3	0.0	0.0	4.1	4.2
605	10	4.9	5.1	4.5	0.0	0.0	0.0	4.3	4.3	0.0	0.0	4.3	0.0	0.0	0.0	0.0	5.0
611	8	4.7	5.0	4.4	0.0	0.0	0.0	4.4	4.2	0.0	0.0	4.2	0.0	0.0	0.0	0.0	0.0

TABLE IV-1
EVENT PARAMETERS OF EURASIAN DATA BASE
(PAGE 2 OF 3)

Event Number	Number Of PDE Stations	PDE (M-L)	PDE m_p	PDE m_p	NORSAR m_p	VLPE Station - M_s Values											ALPA M_s	NORSAR M_s
						1	2	3	4	5	6	7	8	9	10	11		
653	16	5.0	5.2	5.1	4.2	0.0	0.0	0.0	3.9	4.3	0.0	0.0	4.1	0.0	0.0	0.0	4.0	4.2
710	7	4.4	4.5	4.5	0.0	3.9	0.0	0.0	0.0	0.0	4.2	0.0	3.7	3.8	0.0	0.0	3.5	3.8
711	11	5.0	5.4	5.0	0.0	4.6	0.0	0.0	0.0	0.0	4.7	0.0	4.2	0.0	0.0	0.0	4.2	4.7
716	19	5.4	5.5	4.8	0.0	4.6	0.0	0.0	0.0	0.0	5.7	0.0	5.0	4.2	0.0	0.0	4.5	0.0
744	26	5.7	5.7	5.2	5.7	5.6	0.0	0.0	0.0	0.0	5.5	0.0	5.5	5.0	4.9	0.0	4.9	5.9
775	17	5.2	5.4	5.3	0.0	5.2	0.0	0.0	0.0	0.0	4.9	0.0	4.9	5.3	5.4	0.0	5.0	0.0
776	5	4.5	4.8	4.8	0.0	3.8	0.0	0.0	0.0	0.0	3.9	0.0	3.7	3.4	0.0	0.0	3.7	0.0
799	35	6.0	6.0	5.8	0.0	6.0	0.0	0.0	0.0	0.0	0.0	0.0	5.8	5.6	5.8	0.0	5.4	5.7
818	26	5.7	5.7	5.6	4.4	4.5	0.0	0.0	0.0	0.0	0.0	0.0	4.8	4.3	0.0	0.0	0.0	0.0
825	3	4.3	4.7	4.6	4.2	4.4	0.0	0.0	0.0	0.0	0.0	0.0	4.4	3.9	4.1	0.0	0.0	0.0
828	12	5.3	5.7	5.6	5.3	6.1	0.0	0.0	0.0	0.0	0.0	0.0	5.8	5.8	5.8	0.0	5.5	5.8
837	7	4.6	4.9	4.7	3.8	3.1	0.0	0.0	0.0	0.0	0.0	0.0	3.9	3.7	4.0	0.0	3.4	0.0
859	54	5.7	5.7	5.3	5.0	5.4	0.0	0.0	0.0	5.1	5.2	0.0	5.2	5.1	0.0	5.3	5.3	5.2
881	14	5.0	5.2	5.1	0.0	3.6	0.0	0.0	0.0	3.6	3.8	0.0	3.8	0.0	0.0	4.2	3.5	3.8
890	30	5.3	5.3	4.8	0.0	4.8	0.0	0.0	0.0	0.0	5.2	0.0	4.7	5.1	0.0	5.5	4.6	5.1
897	13	4.8	5.0	4.5	0.0	0.0	0.0	0.0	0.0	2.6	4.3	0.0	3.9	4.0	4.0	0.0	3.6	4.1
929	10	4.8	5.1	4.7	0.0	4.2	0.0	0.0	0.0	0.0	4.6	0.0	4.0	0.0	3.9	3.5	0.0	4.5
937	18	5.1	5.2	4.2	0.0	4.3	0.0	0.0	0.0	0.0	4.0	0.0	3.7	0.0	0.0	4.5	3.9	4.0
946	4	4.2	4.3	4.1	0.0	3.3	0.0	0.0	0.0	0.0	0.0	0.0	0.0	0.0	0.0	0.0	3.4	3.4
950	2	4.3	4.9	4.2	0.0	0.0	0.0	0.0	0.0	0.0	4.1	0.0	3.8	4.1	3.9	0.0	0.0	4.0

TABLE IV-1
EVENT PARAMETERS OF EURASIAN DATA BASE
(PAGE 3 OF 3)

Event Number	Number Of PDE Stations	PDE (M-L) m_p	PDE m_p	NORSAR m_p	VLPE Station - M_s Values											ALPA M_s	NORSAR M_s
					1	2	3	4	5	6	7	8	9	10	11		
956	8	4.4	4.5	4.1	0.0	0.0	0.0	0.0	0.0	4.4	0.0	4.5	4.2	4.1	0.0	4.2	4.3
965	8	4.6	4.8	4.6	0.0	0.0	0.0	0.0	0.0	3.9	0.0	4.1	3.5	0.0	3.2	3.5	4.2
966	17	5.1	5.2	4.8	0.0	0.0	0.0	0.0	3.8	4.1	0.0	4.2	0.0	4.3	4.3	4.1	0.0
1039	25	6.1	6.1	6.3	5.5	0.0	0.0	0.0	5.7	5.3	0.0	5.9	5.6	5.0	5.7	5.7	5.5
1065	6	4.4	4.6	4.6	0.0	4.1	0.0	0.0	3.4	4.3	0.0	0.0	3.9	0.0	4.0	0.0	4.3
1080	9	4.6	4.8	4.5	3.9	4.2	0.0	0.0	3.8	4.2	0.0	4.3	0.0	0.0	0.0	3.5	4.5
1083	40	5.7	5.7	5.3	4.8	5.3	0.0	0.0	3.8	5.3	0.0	5.0	5.1	4.3	5.2	4.9	5.3
1085	56	6.1	6.1	5.7	5.4	5.8	0.0	0.0	4.6	5.9	0.0	5.9	5.7	4.8	5.6	5.7	6.0
1132	24	5.5	5.5	5.2	5.5	5.3	0.0	0.0	0.0	5.9	0.0	0.0	0.0	4.8	5.4	0.0	0.0
1166	15	5.0	5.2	5.4	4.2	4.9	0.0	4.7	0.0	0.0	3.3	4.7	0.0	0.0	4.4	4.3	4.7
1172	23	5.4	5.4	5.8	3.4	4.7	0.0	5.0	0.0	4.3	4.5	4.7	0.0	4.2	0.0	5.2	0.0
1180	19	5.2	5.3	5.6	0.0	5.0	0.0	4.8	0.0	4.8	4.7	4.7	0.0	0.0	0.0	4.4	0.0

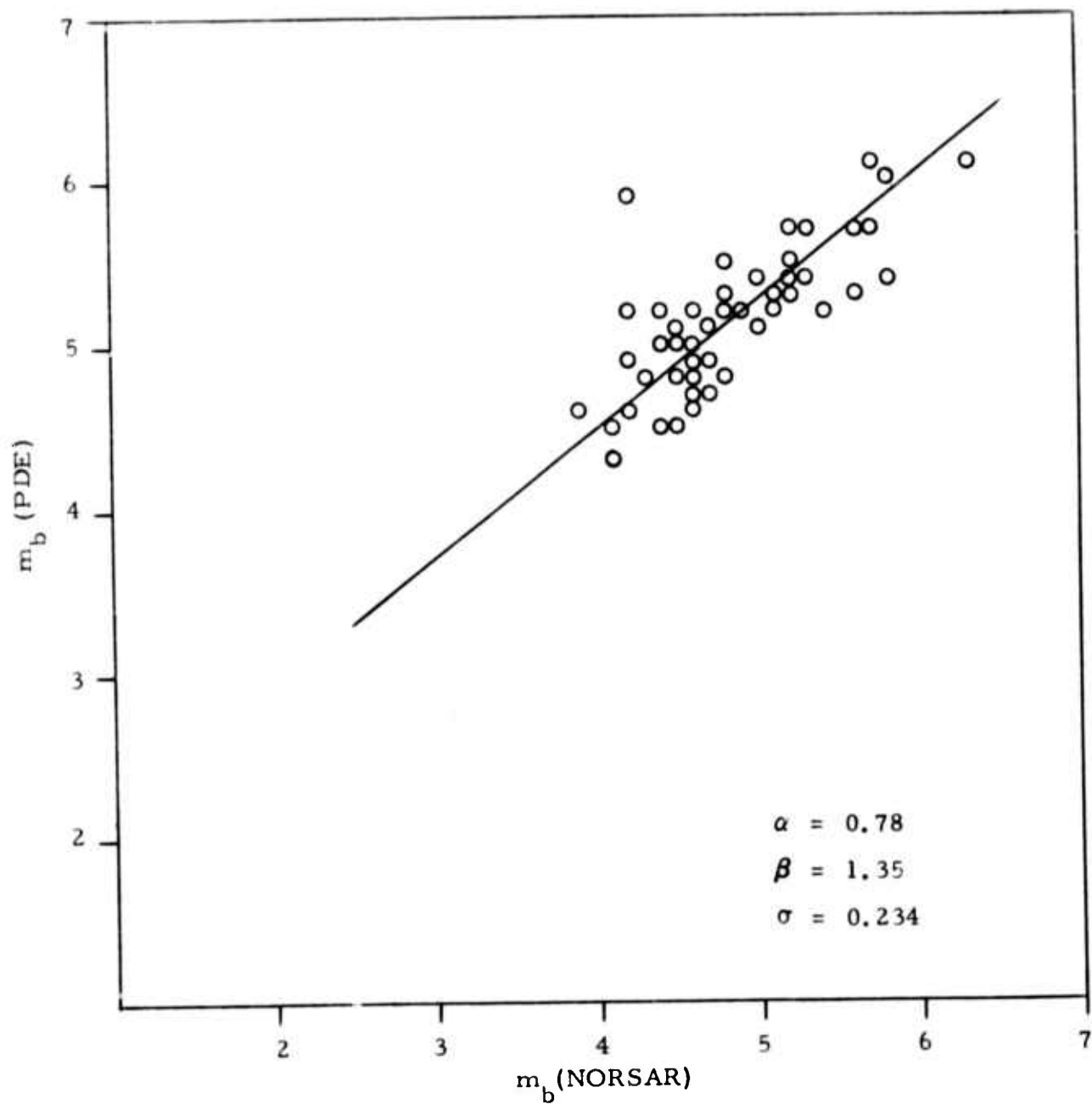


FIGURE IV-2
NORSAR m_b VERSUS PDE m_b

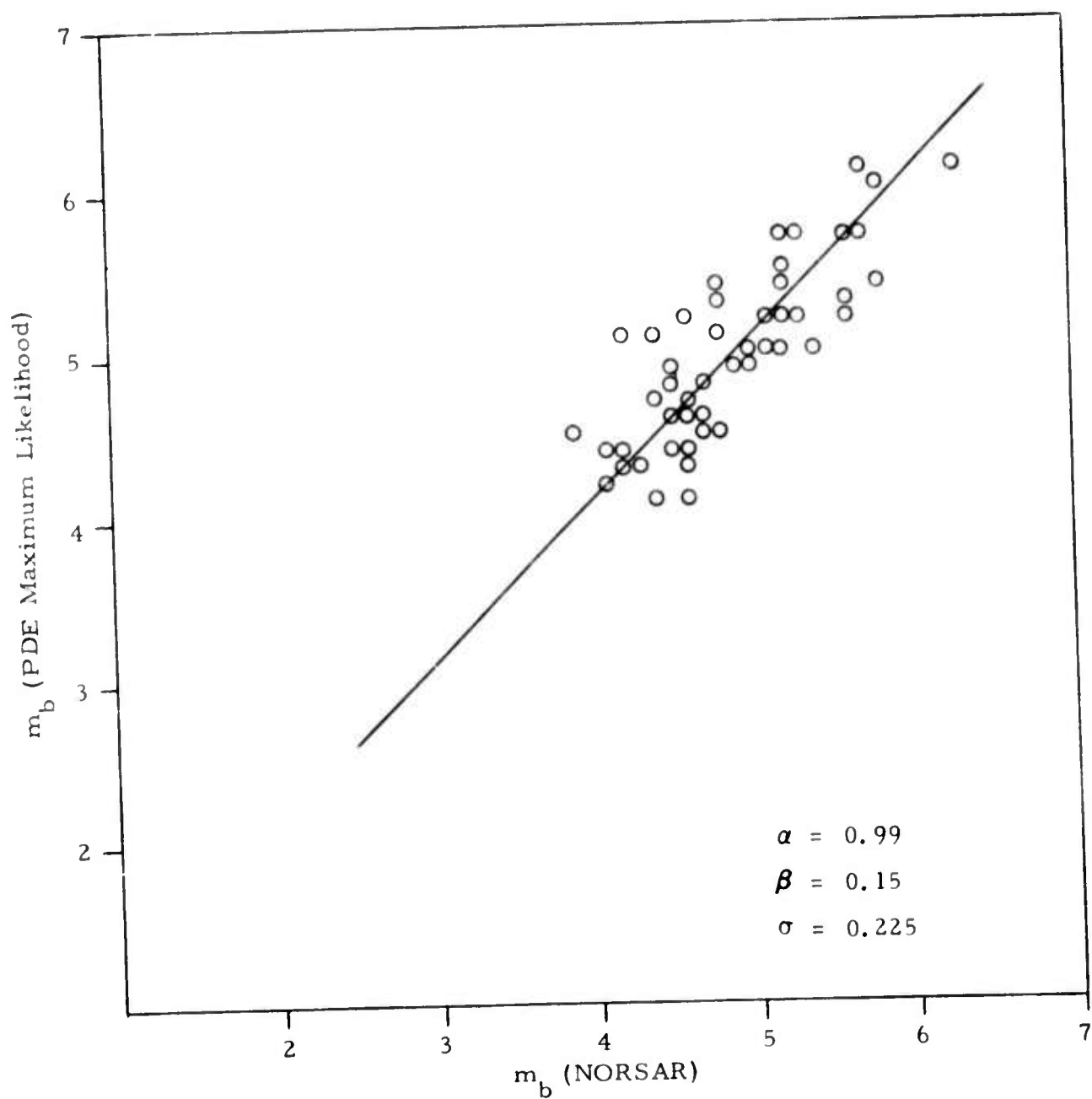


FIGURE IV-3
NOR SAR m_b VERSUS PDE MAXIMUM LIKELIHOOD m_b

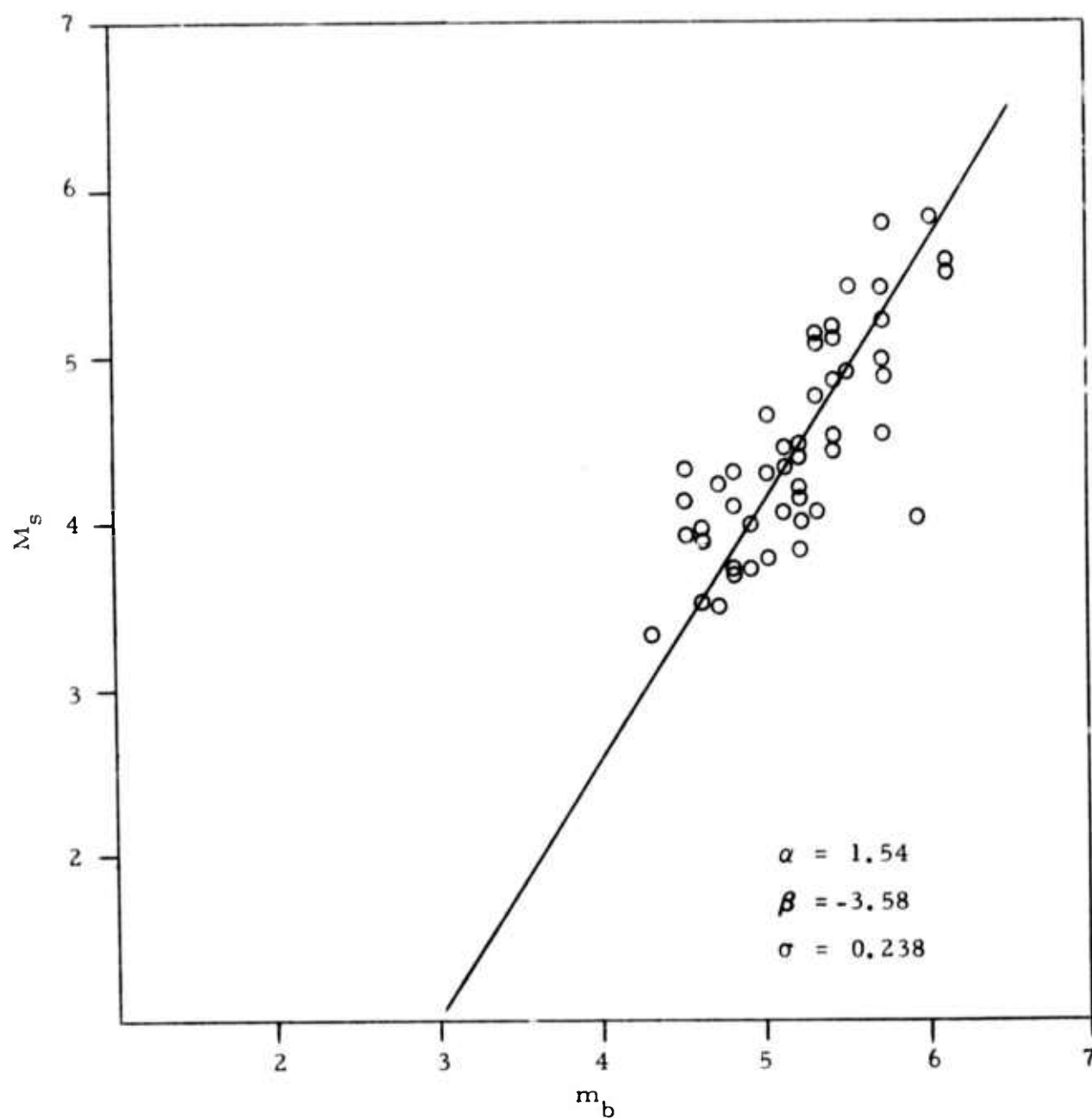


FIGURE IV-4
PDE m_b VERSUS VLPE M_s

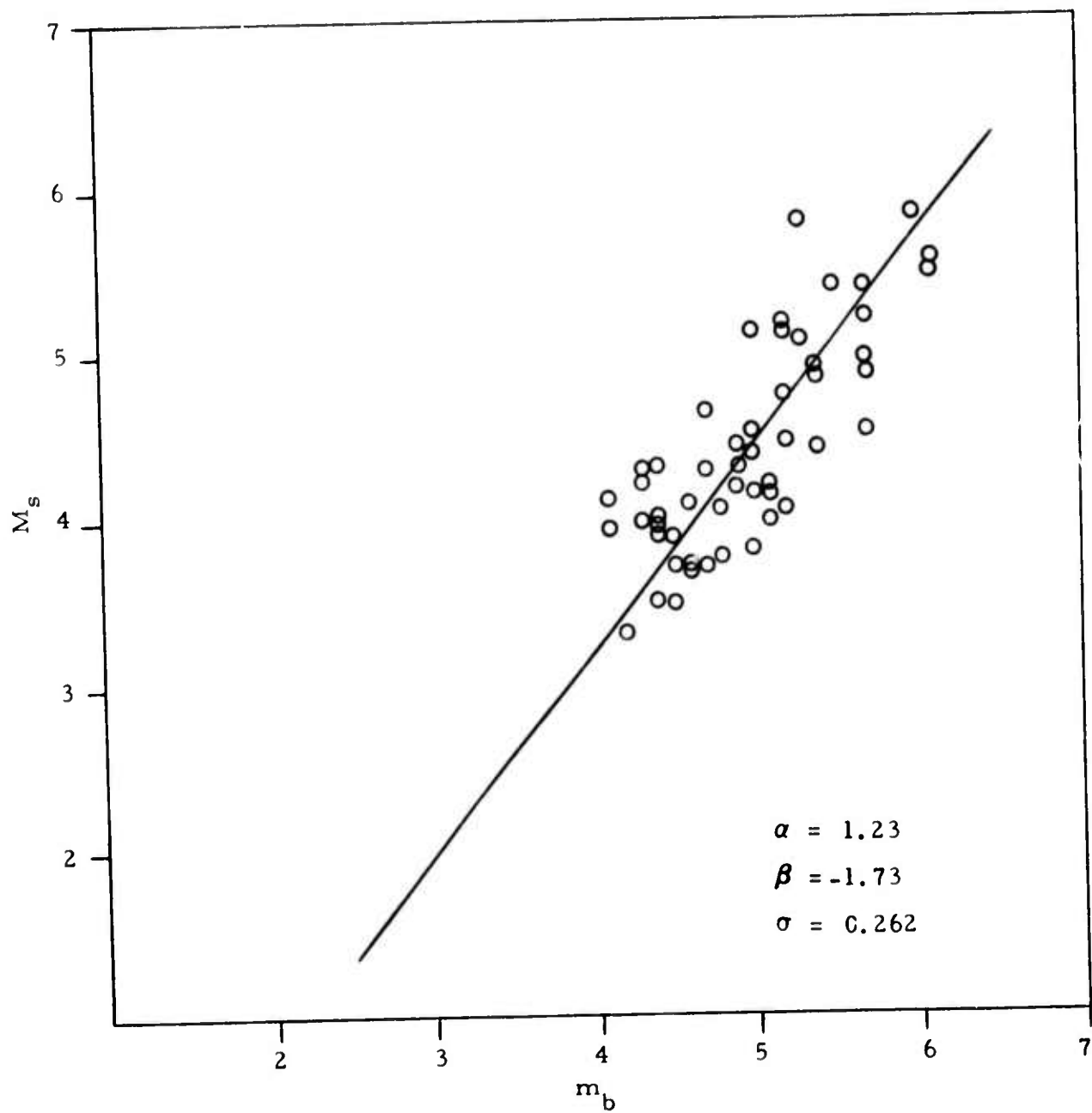


FIGURE IV-5
MAXIMUM LIKELIHOOD PDE m_b VERSUS VLPE M_s

In order to examine more closely the variations of the $M_s - m_b$ slope as a function of estimation techniques of M_s and m_b , a total of nine cases were run based on the given event population. In each case, the M_s values estimated by either VLPE (averaging), ALPA or NORSAR were combined with the m_b values of NORSAR, PDE, and PDE(M-L). The results are summarized in Table IV-2. The following points are noteworthy:

- Four of the runs produce a virtually identical slope ($\alpha \approx 1.37$). These are precisely those four runs that combine 'consistent' M_s and m_b values, i.e., values free of network bias effects. (NORSAR or ALPA M_s versus NORSAR or PDE(M-L) m_b .)
- A consistently high value of the slope (1.66 or 1.64) is found when PDE m_b is plotted against a consistent M_s .
- A consistently low value of α (1.23 or 1.24) results when VLPE M_s is plotted against a consistent m_b .
- When PDE m_b is plotted against VLPE M_s , α is again high, showing that the network bias effects in PDE magnitudes dominate those of VLPE.

Hence, the behavior of the computed slope agrees well with what could be expected from network bias consideration, and it appears that the most accurate linear functional relationship between M_s and m_b for the given data set (ranging in m_b values from about 4.0 to 6.0) has a slope of approximately 1.4.

Considering closer the four cases of consistent slope estimates, it is interesting to note that the value of σ is lower when using PDE(M-L) m_b versus either ALPA or NORSAR M_s compared to when NORSAR m_b is used ($\sigma \approx 0.26$ versus $\sigma \approx 0.31$). It would be interesting to compare PDE(M-L) m_b to the VLPE-ALPA-NORSAR combined network with the network bias reduced

TABLE IV-2
RELATIONSHIP M_s - m_b FOR VARIOUS COMBINATIONS OF
 M_s AND m_b MEASUREMENT PROCEDURES

m_b	M_s	Number Of Points NP	Slope α	Intercept β	σ Orthogonal	σ (M_s/m_b)
PDE	VLPE	52	1.54	-3.58	0.238	0.437
	ALPA	41	1.66	-4.33	0.253	0.490
	NORSAR	35	1.64	-3.95	0.276	0.530
PDE Maximum Likelihood	VLPE	52	1.23	-1.73	0.262	0.415
	ALPA	41	1.37	-2.57	0.257	0.436
	NORSAR	35	1.37	-2.25	0.259	0.439
NORSAR	VLPE	52	1.24	-1.67	0.309	0.492
	ALPA	41	1.37	-2.48	0.321	0.544
	NORSAR	35	1.39	-2.14	0.305	0.522

* The missing data points (NP < 52) are due to lack of available data for NORSAR or ALPA M_s for some events, and not due to nondetection at these stations.

by maximum likelihood processing; however, we have not been able to do this, mostly because of the lack of reliable VLPE data for some stations.

SECTION V
REFERENCES

- Aki, K., and W. H. K. Lee, 1975, Determination of Three Dimensional Velocity Anomalies Under a Seismic Array Using First P-Arrival Times from Local Earthquakes. Part 1 - A Homogeneous Initial Model, paper presented at 47th Annual Eastern Seismological Society of America Meeting, St. Louis, Missouri.
- Brune, J. N., 1970 Tectonic Stress and the Spectra of Seismic Shear Waves, J. Geophysical Research, 75, 4997-5009.
- Engdahl, E. R., and W. H. K. Lee, 1975, Relocation of Local Earthquakes by Seismic Ray Tracing, paper presented at 47th Annual Eastern Seismological Society of America Meeting, St. Louis, Missouri.
- Evernden, J. F., 1969, Precision of Epicenters Obtained by Small Numbers of World-Wide Stations, Bull. Seismological Society of America, 59, 1365-1398.
- Harkrider, D. G., 1964, Surface Waves in Multilayered Elastic Media; I. Rayleigh and Love Waves from Buried Sources in A Multilayered Elastic Half-Space, Bull. Seismological Society of America, 54, 627-679.
- Haskell, N. A., 1969, Elastic Displacements in the Near Field of a Propagating Fault, Bull. Seismological Society of America, 59, 865-908.
- McEvelly, T. V., 1974, Personal Communication.
- McEvelly, T. V., 1975, Personal Communication at Near-Field Study Group Meeting, Orchas Island, Washington.

- McEvilly, T. W., and L. R. Johnson, 1974, Near Field Accelerometer Array, Technical Report No. 4, Grant No. AFOSR-72-2392, University of California, Berkeley, California.
- Ringdal, F., 1975, Maximum Likelihood Estimation of Seismic Event Magnitude From Network Data, Technical Report No. 1, Texas Instruments Report Number ALEX(01)-TR-75-01, Contract Number F08606-75-C-0029, Texas Instruments Incorporated, Dallas, Texas.
- Smith, S. W., 1973, Joint Experiment on the Spectrum of Earthquake Sources-Long Period Instrumentation, Semi-Annual Technical Report No. 3, Grant No. AFOSR 72-2304, University of Washington, Seattle, Washington.
- Sun, D., 1975, Personal Communication.
- Turnbull, Jr., L. S., and J. C. Battis, 1973, Interpretation of Strong-Motion Earthquake Accelerograms Using A Moving Dislocation Model, Semi-Annual Technical Report No. 3, Texas Instruments Report Number ALEX(02)-TR-73-03, Contract Number F44620-72-C-0073, Texas Instruments Incorporated, Dallas, Texas.
- Turnbull, Jr., L. S., and J. C. Battis, 1974, Interpretation of Strong-Motion Earthquake Accelerograms: The Bear Valley Event of 1973, Final Report, Texas Instruments Report Number ALEX(02)-FR-74-01, Contract Number F44620-72-C-0073, Texas Instruments Incorporated, Dallas, Texas.
- Turnbull, Jr., L. S., David Sun, and D. G. Black, 1974a, Determination of Seismic Source Parameters From Long-Period Teleseismic Waves, Semi-Annual Technical Report No. 2- Part A, Texas Instruments Report Number ALEX(02)-TR-74-02-PART A, Contract Number F44620-73-C-0055, Texas Instruments Incorporated, Dallas, Texas.

Turnbull, Jr., L. S., James C. Battis, and David Sun, 1974b, Source Studies in the Near- and Far-Field, Semi-Annual Technical Report No. 3-Part A, Texas Instruments Report Number ALEX(02)-TR-74-03-PART A, Contract Number F44620-73-C-0055, Texas Instruments Incorporated, Dallas, Texas.

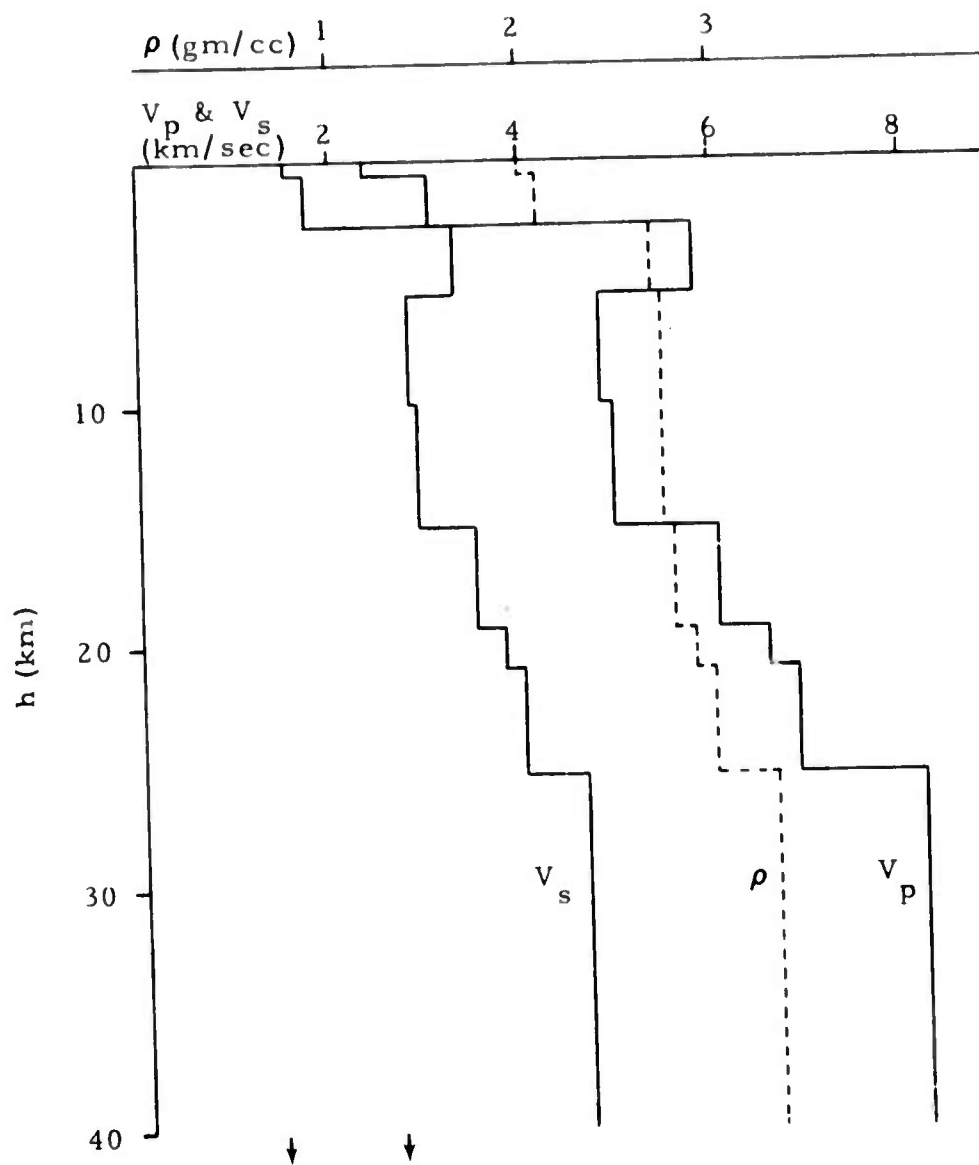
Turnbull, Jr., L. S., James C. Battis, David Sun, and Alan C. Strauss, 1975, Source Studies in the Near- and Far-Field, Semi-Annual Technical Report No. 4-Part A, Texas Instruments Report Number ALEX(02)-TR-75-01-PART A, Contract Number F44620-73-C-0055, Texas Instruments Incorporated, Dallas, Texas.

Veith, K. F., and G. E. Clawson, 1972, Magnitude from Short-Period P-Wave Data, Bulletin Seismological Society of America, 62, 435-452.

APPENDIX A
DISPERSIVE CHARACTERISTICS OF THE
BEAR VALLEY STRUCTURE

Using the velocity profile obtained by McEvilly (1975), dispersion curves were generated for the structures representing both sides of the fault. Figure A-1 shows the velocity-density profile for the northeast side, and the associated Rayleigh and Love wave dispersion curves are displayed in Figure A-2. Similarly, the velocity-density profile and associated dispersion curves are given in Figures A-3 and A-4, respectively.

The major difference between these structures is the higher velocity material on the southwest side of the fault. This is reflected in the dispersion curves, with higher group and phase velocities between 10 and 30 seconds period for the southwest structure.



Same as Gutenberg-Bullen Earth Model

FIGURE A-1
BEAR VALLEY STRUCTURE - NORTHEAST
SIDE OF FAULT

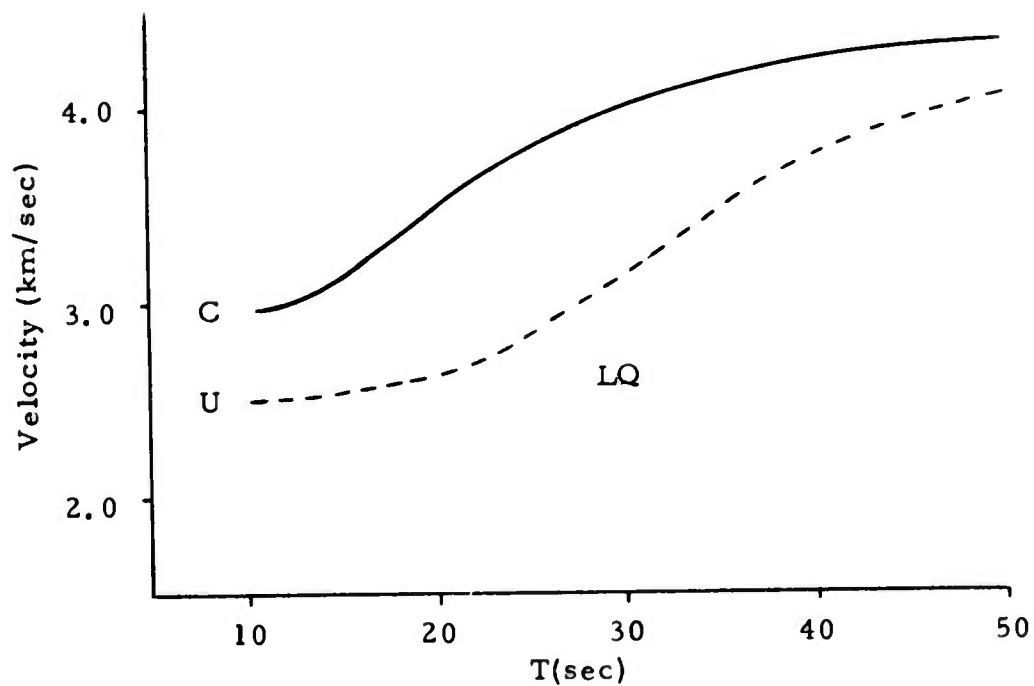
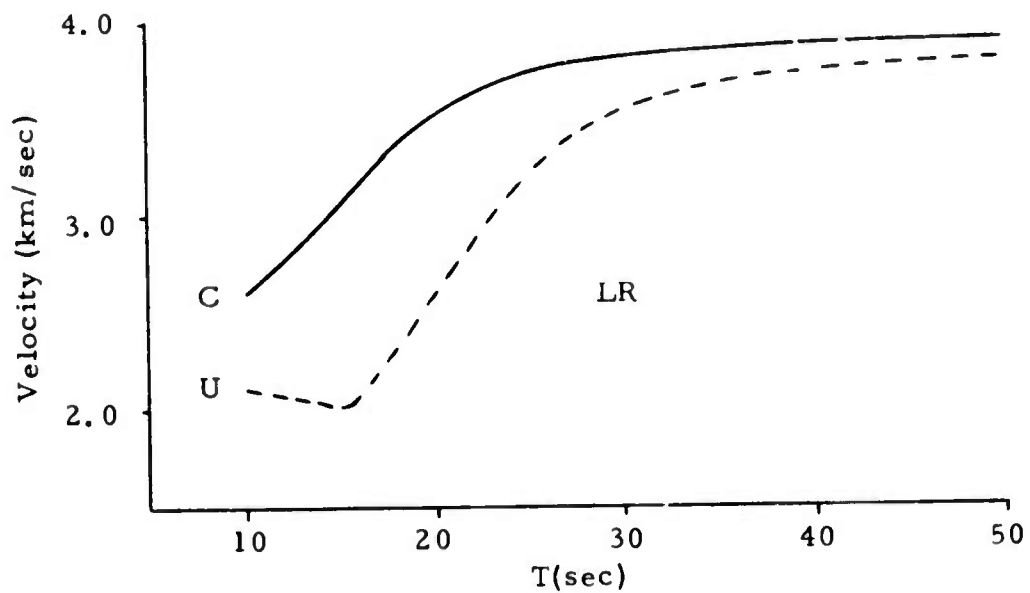
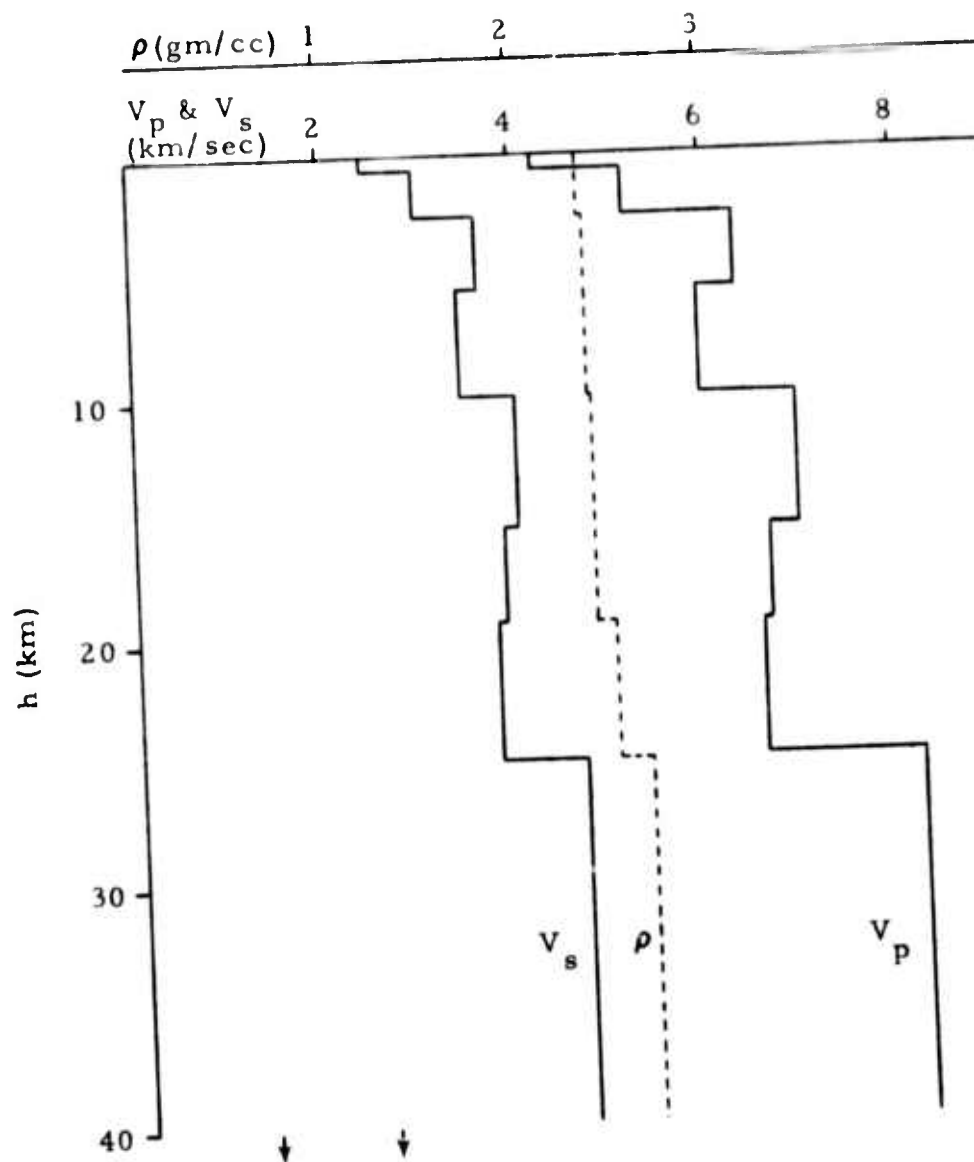


FIGURE A-2
RAYLEIGH AND LOVE WAVE DISPERSION
FOR BEAR VALLEY STRUCTURE
(NORTHEAST SIDE OF FAULT)



Same as Gutenberg-Bullen Earth Model

FIGURE A-3
BEAR VALLEY STRUCTURE - SOUTHWEST
SIDE OF FAULT

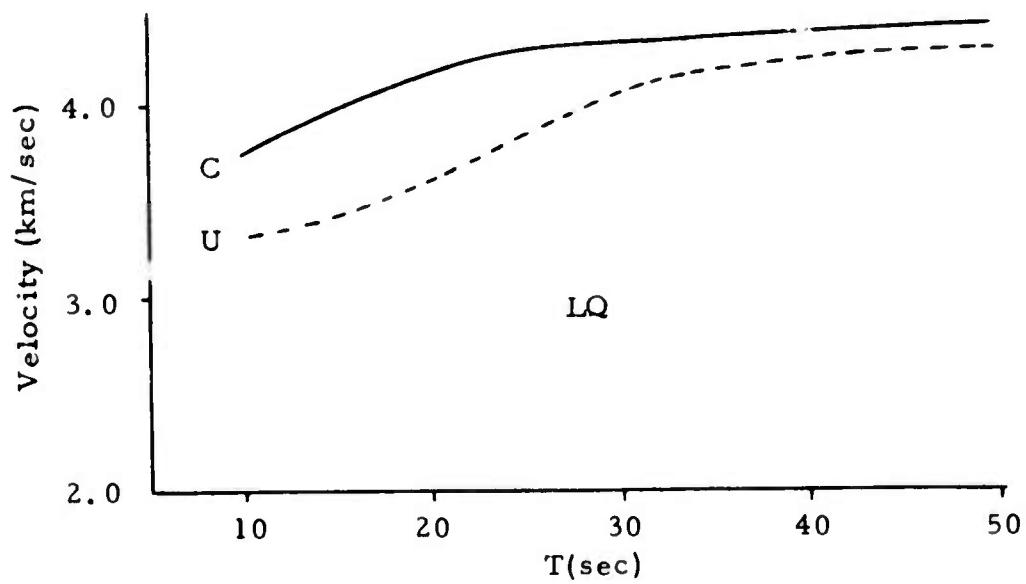
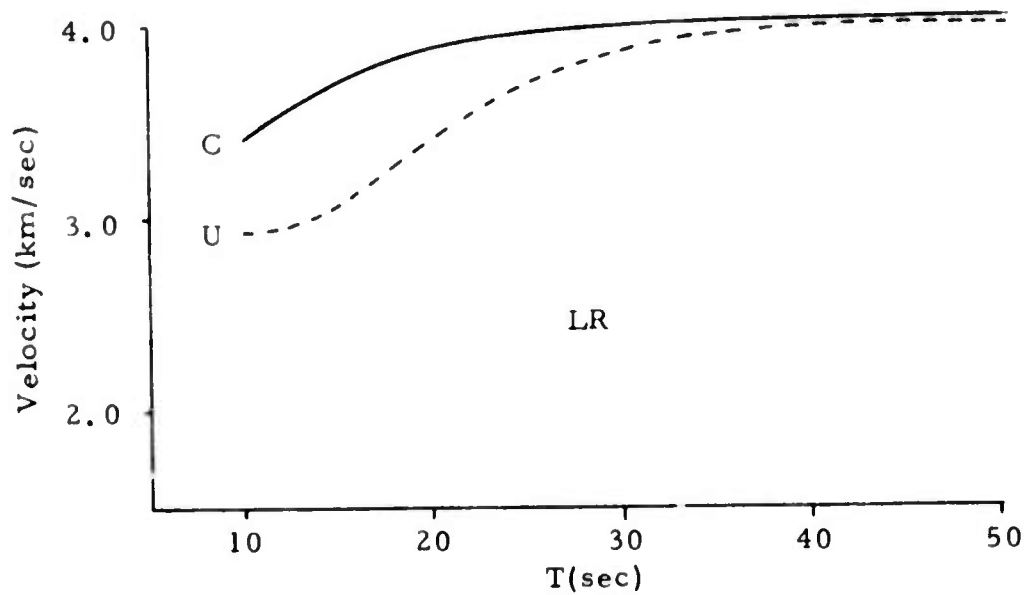


FIGURE A-4
RAYLEIGH AND LOVE WAVE DISPERSION
FOR BEAR VALLEY STRUCTURE
(SOUTHWEST SIDE OF FAULT)

APPENDIX B

SPECTRAL RESPONSE OF THE BEAR VALLEY STRUCTURE

Theoretical spectra were generated for each event using the Bear Valley structures as described in Appendix A. Of particular interest were changes in spectral shape and level. For the Bear Valley event of 22 June 1973, Figures B-1a and B-1b give the Rayleigh and Love wave amplitude spectra as a function of depth for the northeast structure, while Figures B-2a and B-2b give similar spectra for the southwest structure. Figures B-3a and B-3b show the Rayleigh and Love wave radiation patterns at 20 and 30 seconds period for the northeast structure, and Figures B-4a and B-4b give the patterns for the southwest structure.

For the central California event of 28 November 1974, Figures B-5a and B-5b give the Rayleigh and Love wave amplitude spectra as a function of depth for the northeast structure, while Figures B-6a and B-6b give similar spectra for the southwest structure. Figures B-7a and B-7b show the Rayleigh and Love wave radiation patterns at 20 and 30 seconds period for the northeast structure, and Figures B-8a and B-8b give the patterns for the southwest structure.

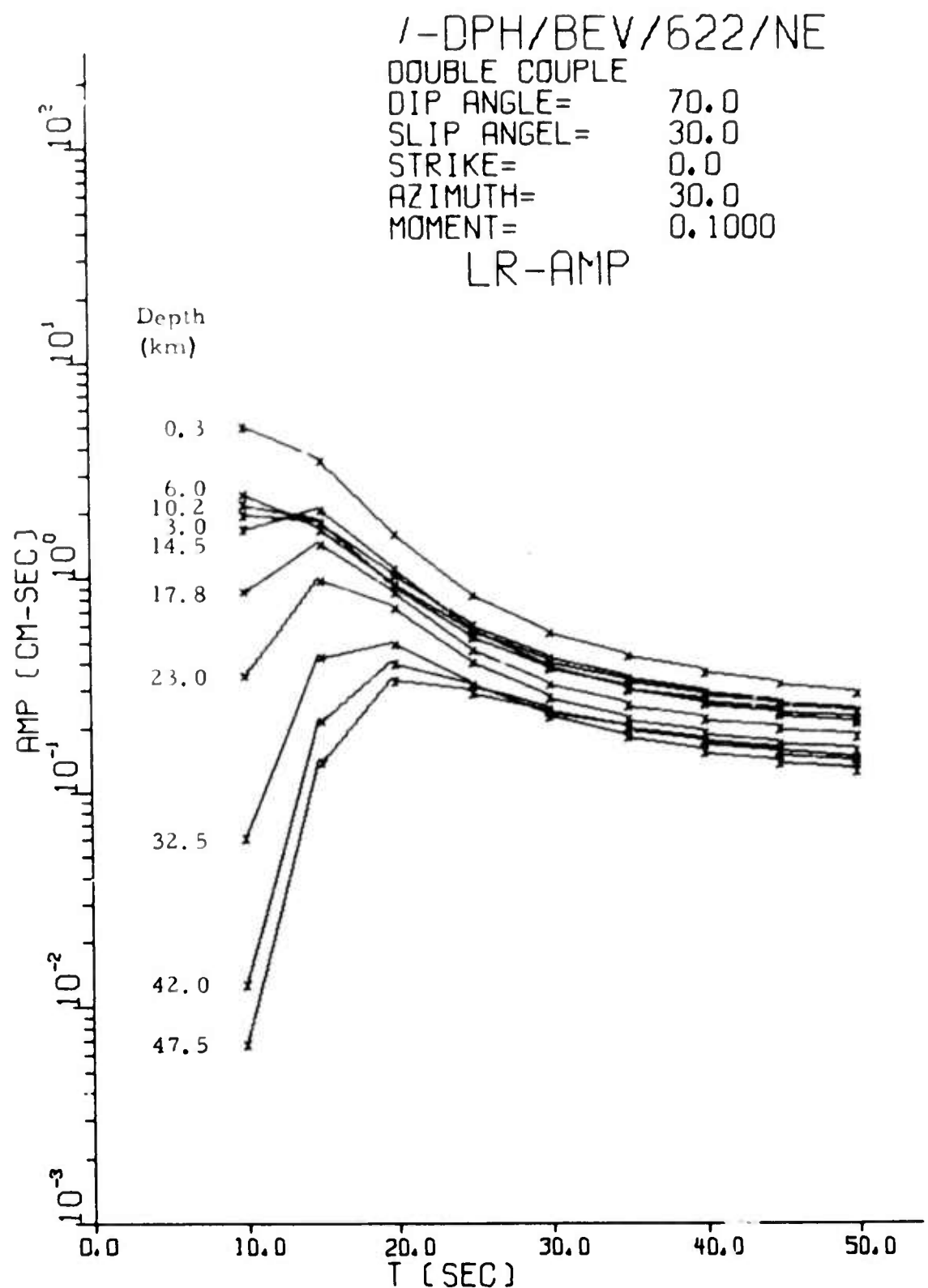


FIGURE B-1a

FUNDAMENTAL MODE RAYLEIGH WAVE SPECTRA USING THE
 SOURCE MECHANISM OF THE 22 JUNE 1973 BEAR VALLEY
 EVENT IN THE NORTHEAST STRUCTURE

V-DPH/BEV/622/NE

DOUBLE COUPLE

DIP ANGLE= 70.0

SLIP ANGLE= 30.0

STRIK = 0.0

AZIMUTH= 30.0

MOMENT= 0.1000

LQ-AMP

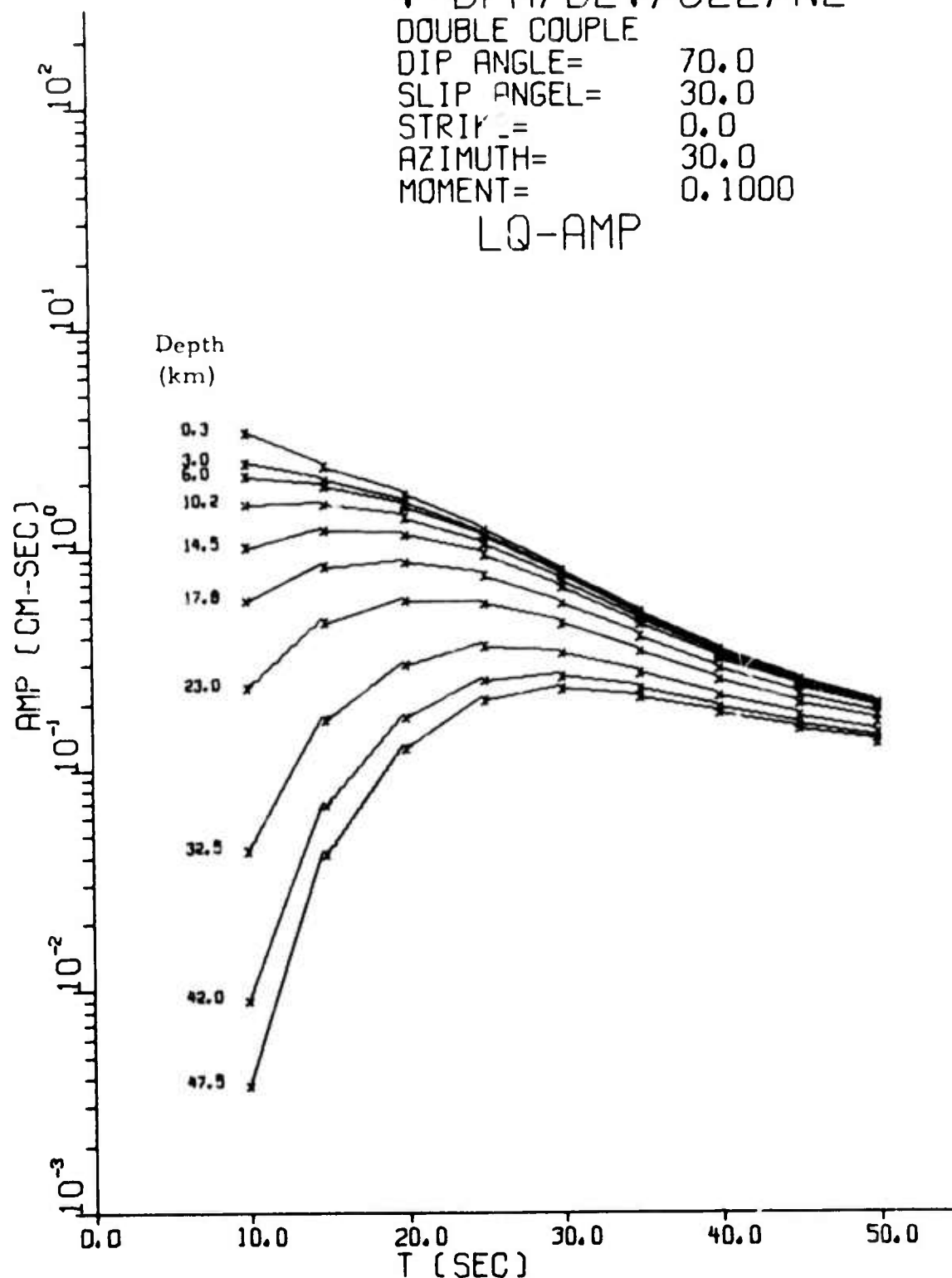


FIGURE B-'b

FUNDAMENTAL MODE LOVE WAVE SPECTRA USING THE SOURCE
MECHANISM OF THE 22 JUNE 1973 BEAR VALLEY EVENT
IN THE NORTHEAST STRUCTURE

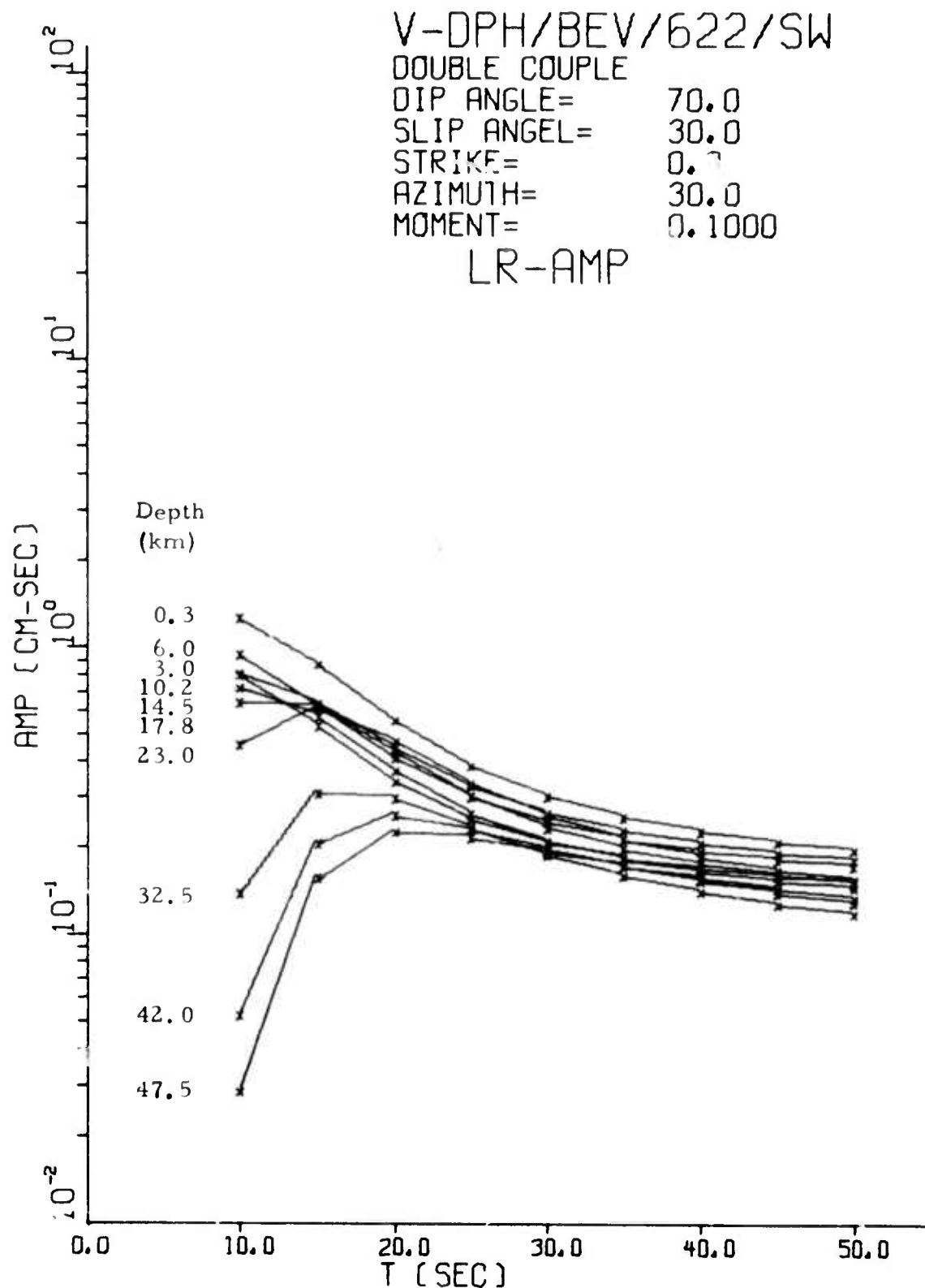


FIGURE B-2a

FUNDAMENTAL MODE RAYLEIGH WAVE SPECTRA USING THE
 SOURCE MECHANISM OF THE 22 JUNE 1973 BEAR VALLEY
 EVENT IN THE SOUTHWEST STRUCTURE

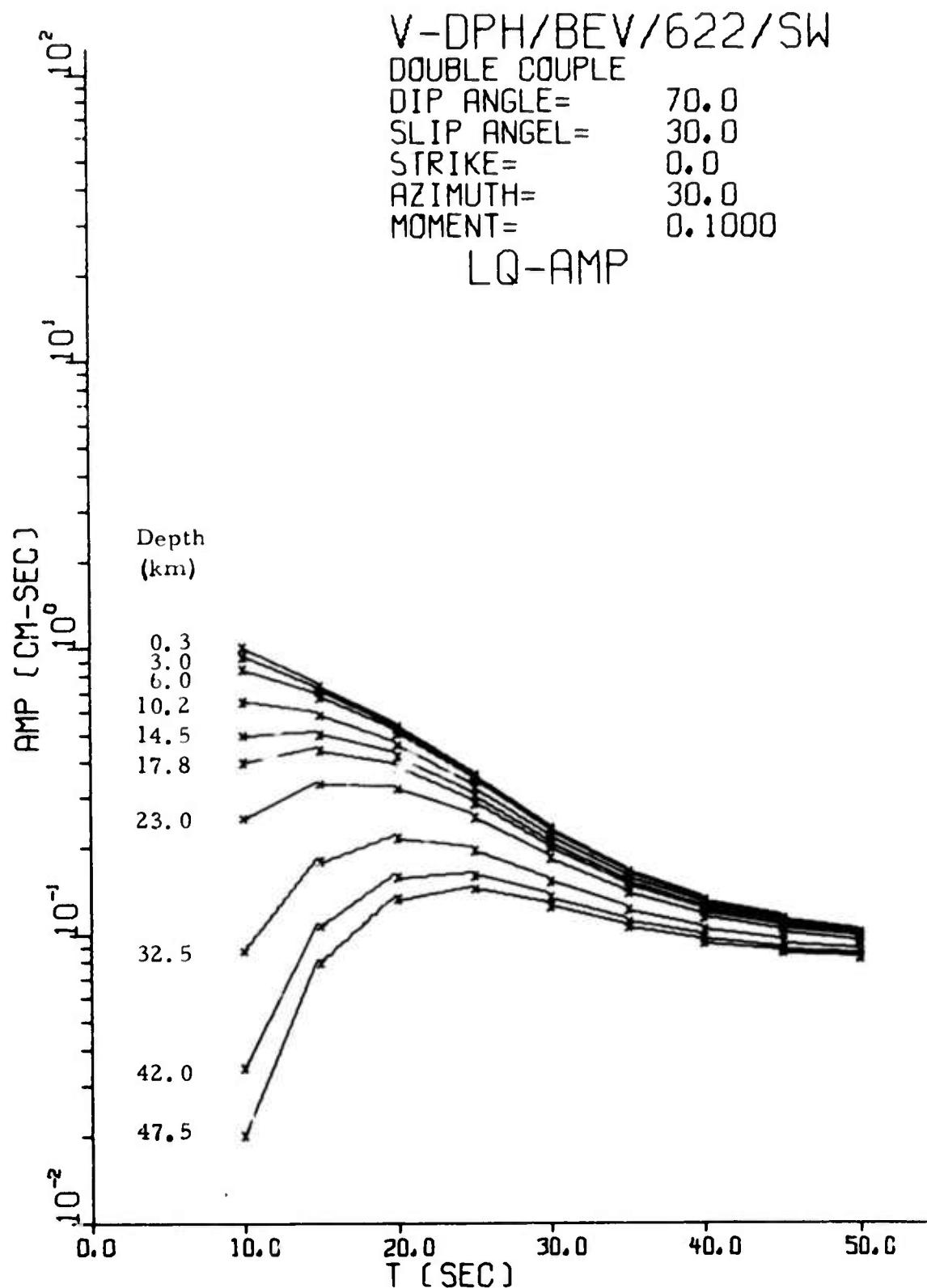


FIGURE B-2b

FUNDAMENTAL MODE LOVE WAVE SPECTRA USING THE SOURCE
 MECHANISM OF THE 22 JUNE 1973 BEAR VALLEY EVENT
 IN THE SOUTHWEST STRUCTURE

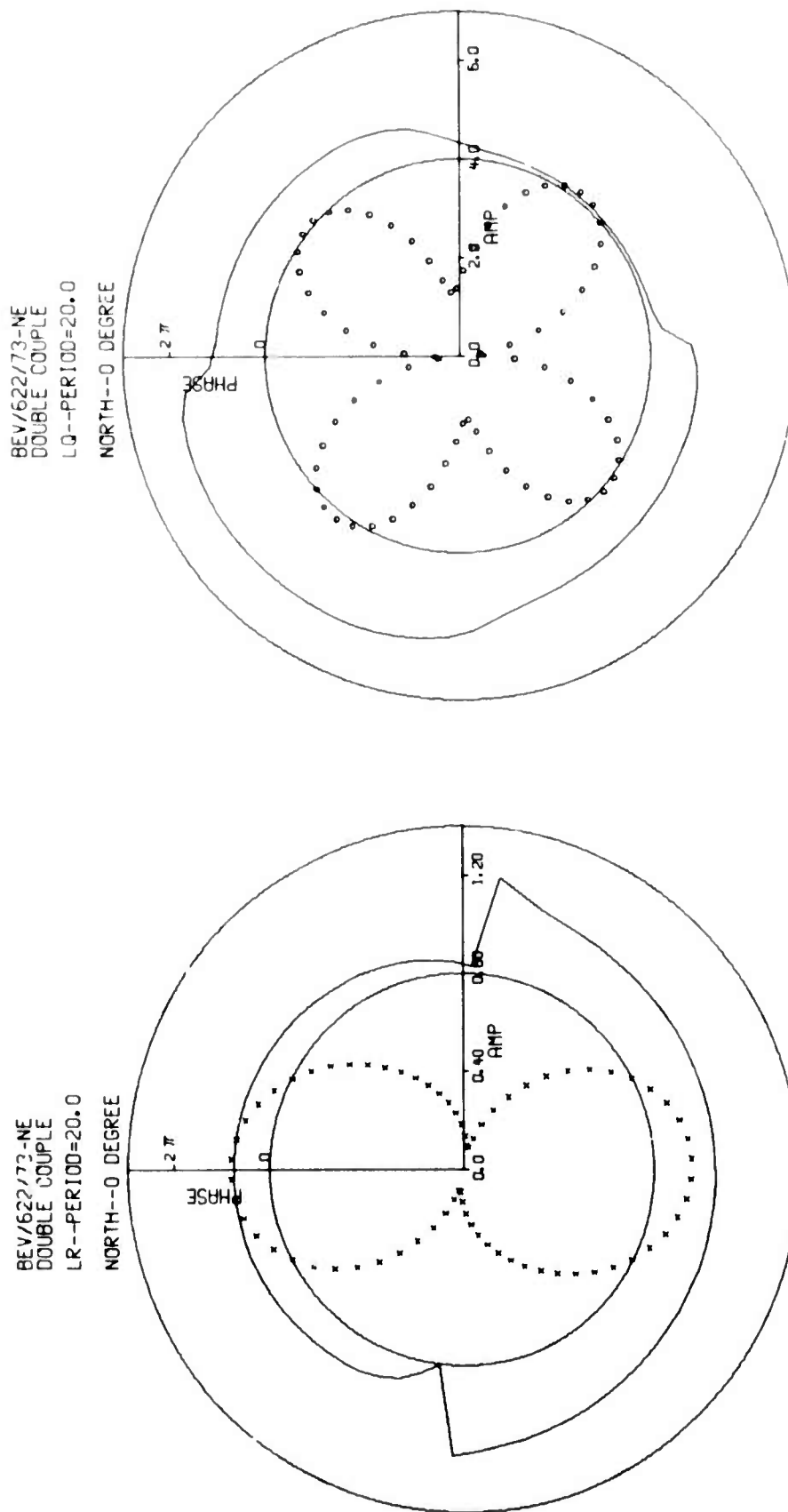


FIGURE B-3a

FUNDAMENTAL MODE RAYLEIGH AND LOVE WAVE RADIATION
(T = 20 SECONDS) USING THE SOURCE MECHANISM OF THE
22 JUNE 1973 BEAR VALLEY EVENT IN THE
NORTHEAST STRUCTURE

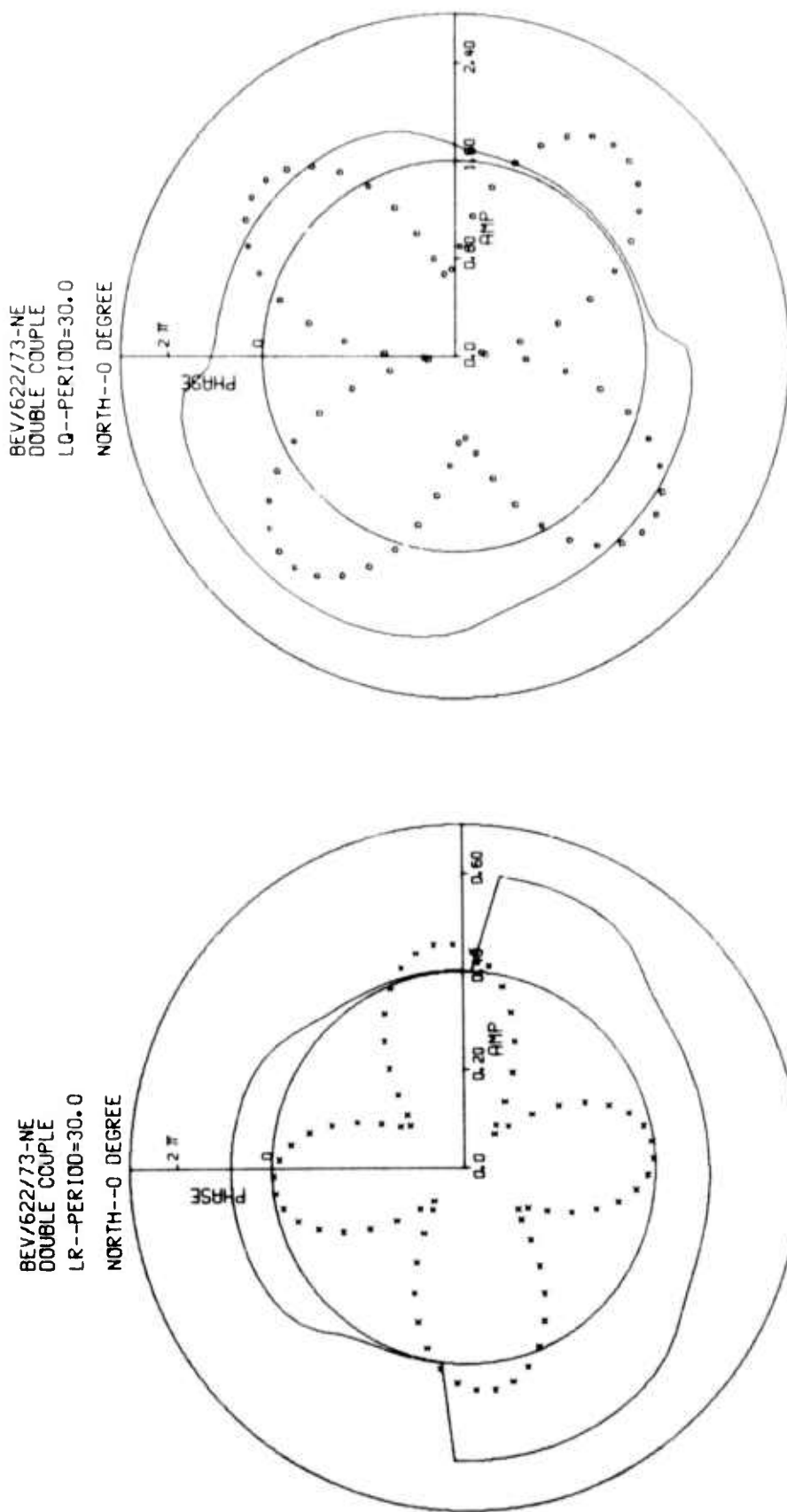
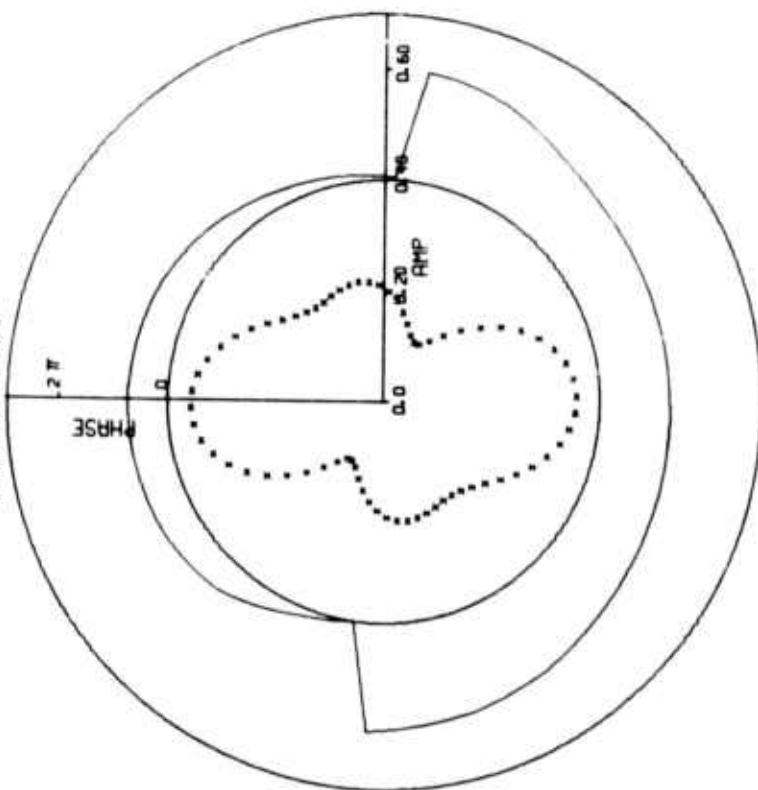


FIGURE B-3b

FUNDAMENTAL MODE RAYLEIGH AND LOVE WAVE RADIATION
(T = 30 SECONDS) USING THE SOURCE MECHANISM OF THE
22 JUNE 1973 BEAR VALLEY EVENT IN THE
NORTHEAST STRUCTURE

BEV/622/73-SW
DOUBLE COUPLE
LR--PERIOD=20.0
NORTH--0 DEGREE



BEV/622/73-SW
DOUBLE COUPLE
LQ--PERIOD=20.0
NORTH--0 DEGREE

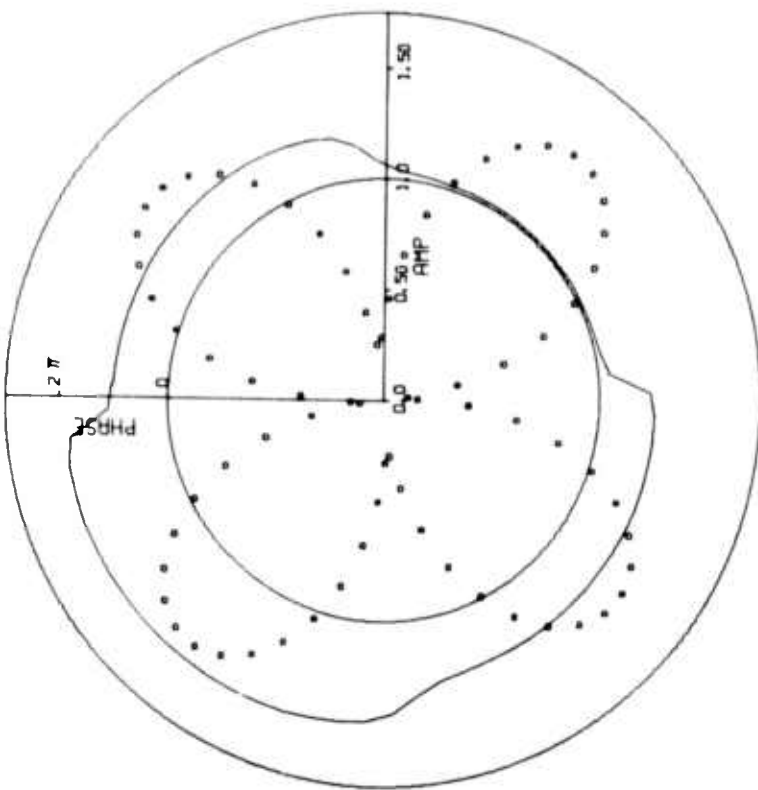


FIGURE B-4a
FUNDAMENTAL MODE RAYLEIGH AND LOVE WAVE RADIATION
(T = 20 SECONDS) USING THE SOURCE MECHANISM OF THE
22 JUNE 1973 BEAR VALLEY EVENT IN THE
SOUTHWEST STRUCTURE

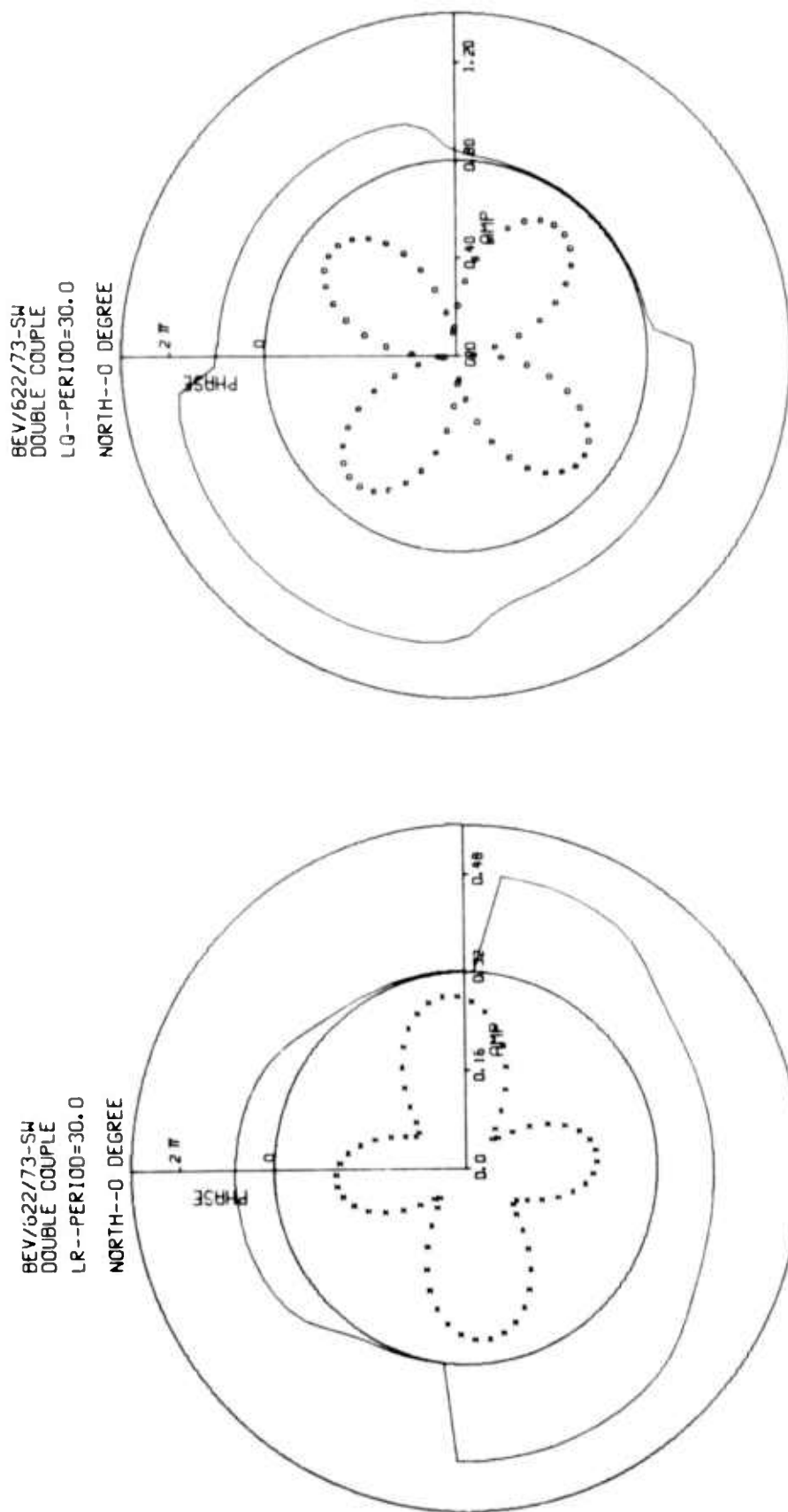


FIGURE B-4b

FUNDAMENTAL MODE RAYLEIGH AND LOVE WAVE RADIATION
(T = 30 SECONDS) USING THE SOURCE MECHANISM OF THE
22 JUNE 1973 BEAR VALLEY EVENT IN THE
SOUTHWEST STRUCTURE

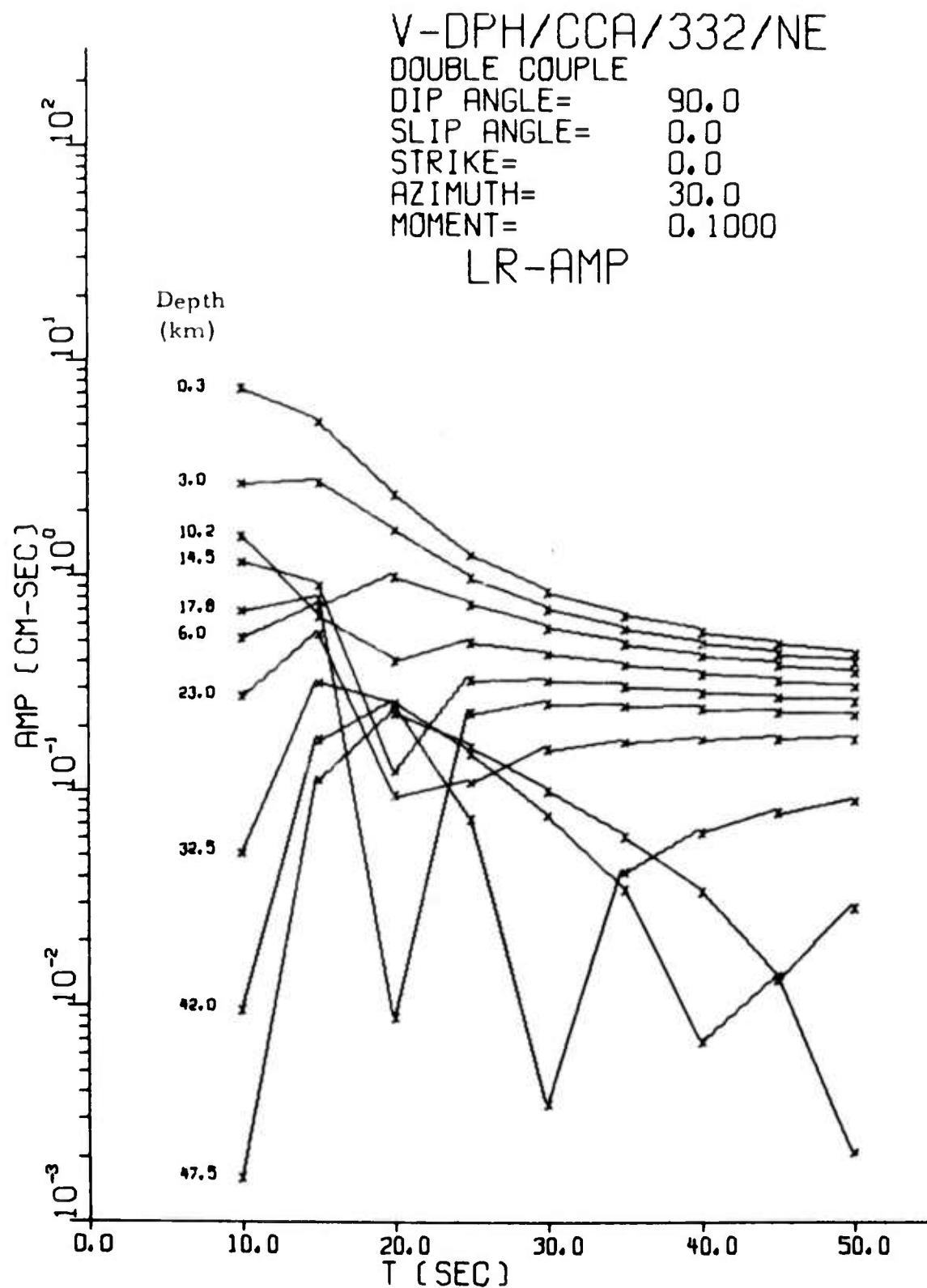


FIGURE B-5a

FUNDAMENTAL MODE RAYLEIGH WAVE SPECTRA USING THE
 SOURCE MECHANISM OF THE 28 NOVEMBER 1974 CENTRAL
 CALIFORNIA EVENT IN THE NORTHEAST STRUCTURE

V-DPH/CCA/332/NE

DOUBLE COUPLE

DIP ANGLE= 90.0

SLIP ANGLE= 0.0

STRIKE= 0.0

AZIMUTH= 30.0

MOMENT= 0.1000

LQ-AMP

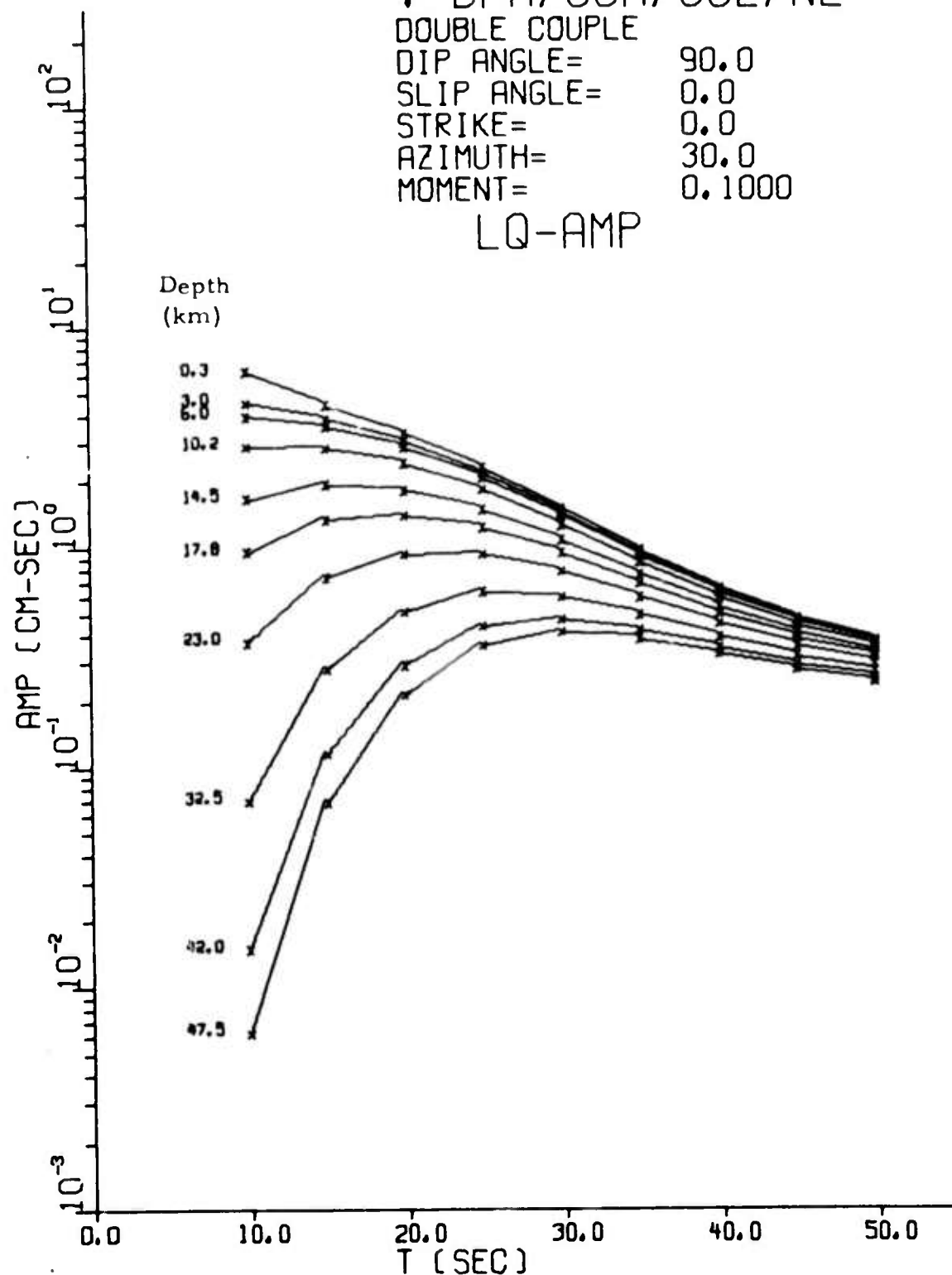


FIGURE B-5b

FUNDAMENTAL MODE LOVE WAVE SPECTRA USING THE SOURCE MECHANISM OF THE 28 NOVEMBER 1974 CENTRAL CALIFORNIA EVENT IN THE NORTHEAST STRUCTURE

V-DPH/CCA/332/SW

DOUBLE COUPLE

DIP ANGLE= 90.0

SLIP ANGLE= 0.0

STRIKE= 0.0

AZIMUTH= 30.0

MOMENT= 0.1000

LR-AMP

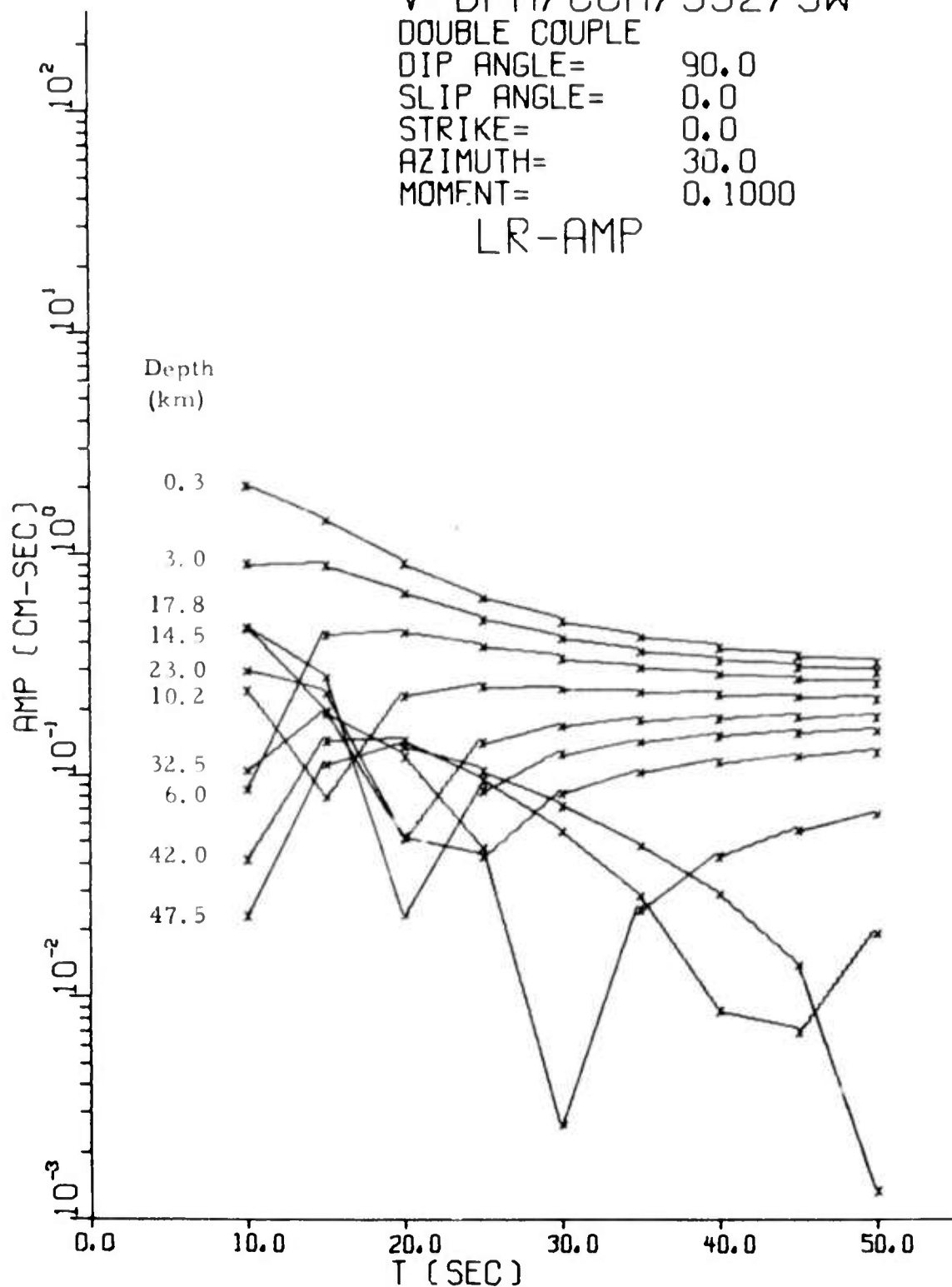


FIGURE B-6a

FUNDAMENTAL MODE RAYLEIGH WAVE SPECTRA USING THE
SOURCE MECHANISM OF THE 28 NOVEMBER 1974 CENTRAL
CALIFORNIA EVENT IN THE SOUTHWEST STRUCTURE

V-DPH/CCA/332/SW

DOUBLE COUPLE

DIP ANGLE= 90.0

SLIP ANGLE= 0.0

STRIKE= 0.0

AZIMUTH= 30.0

MOMENT= 0.1000

LQ-AMP

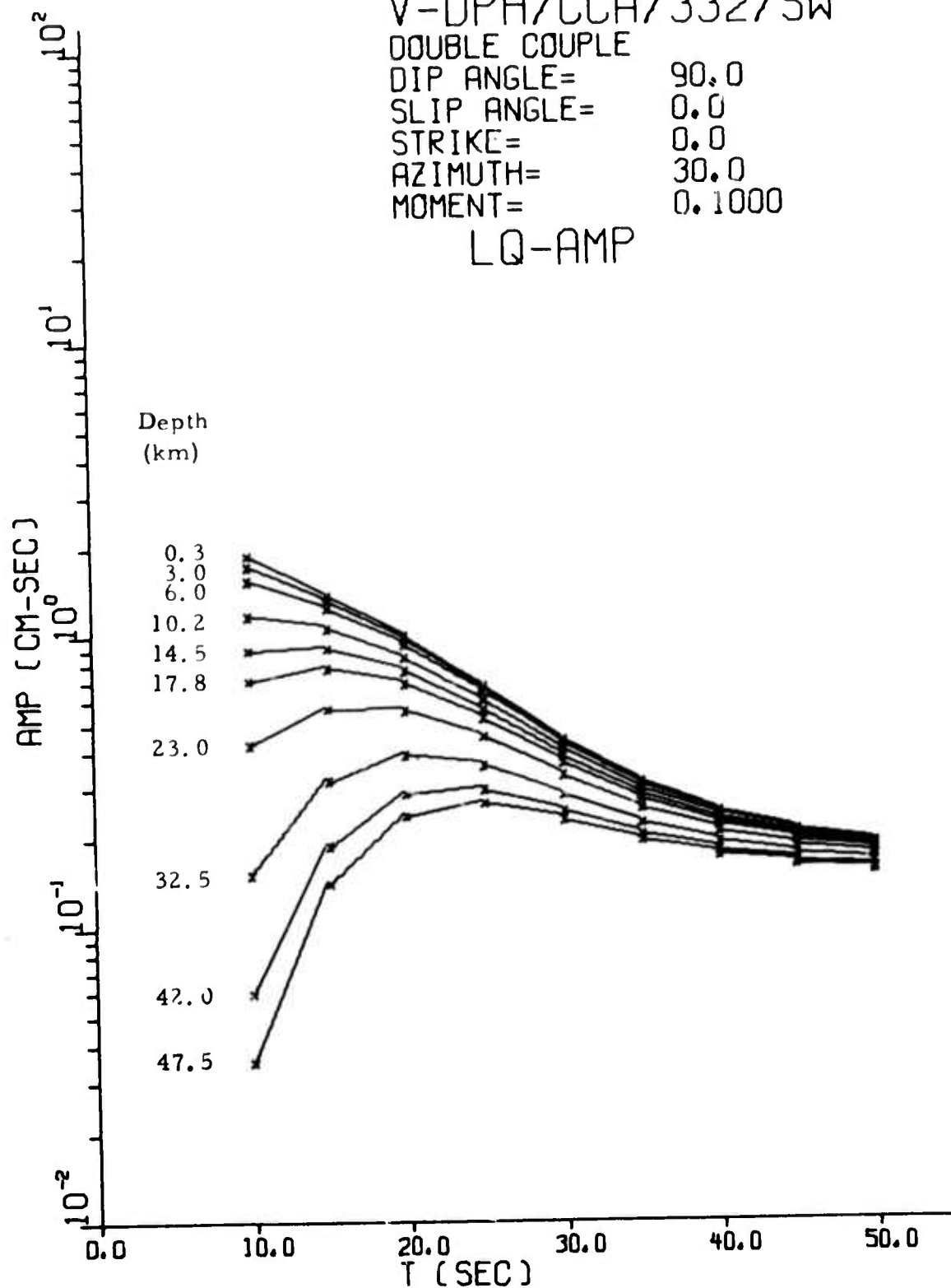


FIGURE B-6b

FUNDAMENTAL MODE LOVE WAVE SPECTRA USING THE SOURCE MECHANISM OF THE 28 NOVEMBER 1974 CENTRAL CALIFORNIA EVENT IN THE SOUTHWEST STRUCTURE

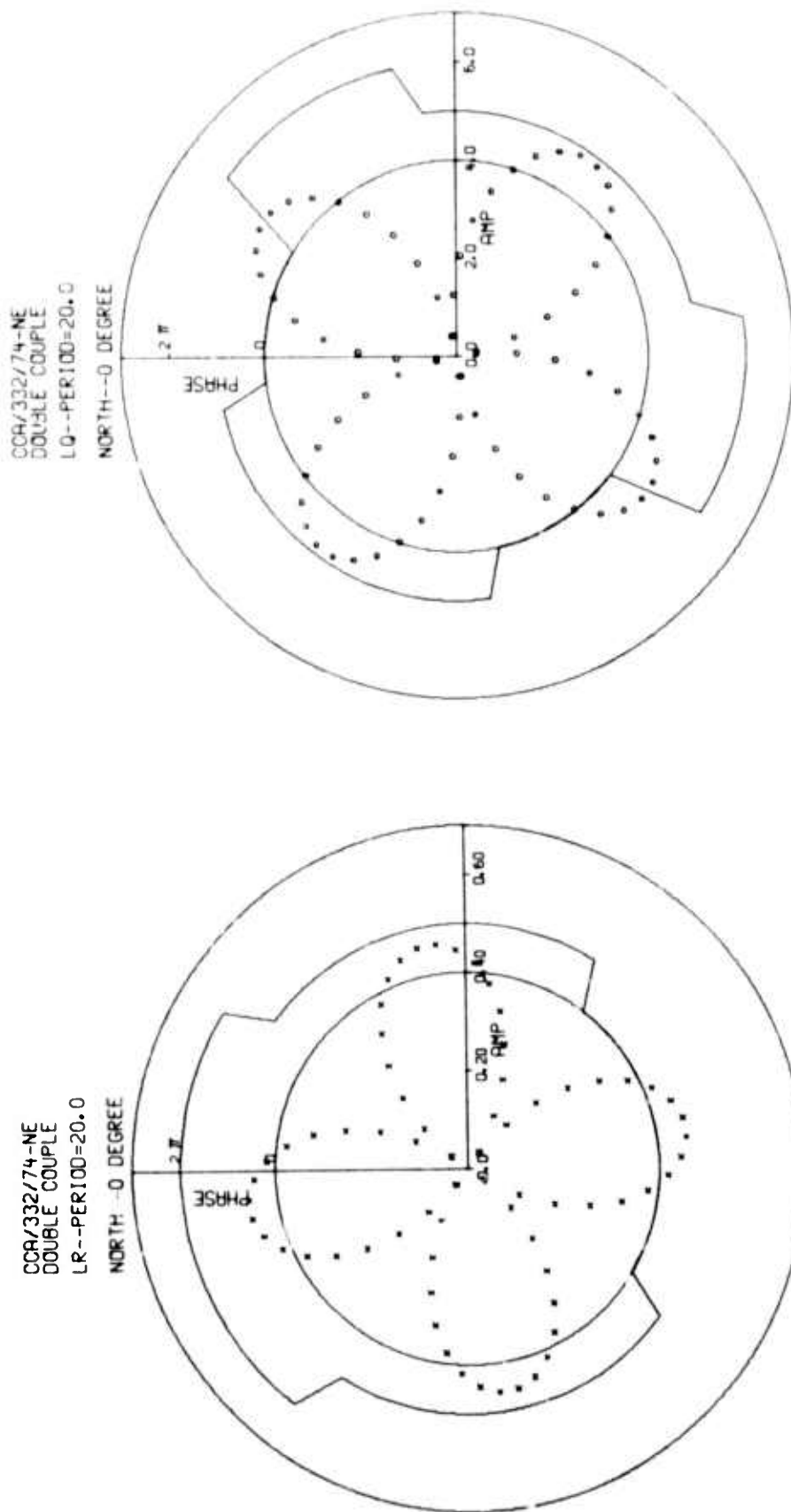


FIGURE B-7a

FUNDAMENTAL MODE RAYLEIGH AND LOVE WAVE RADIATION
(T = 20 SECONDS) USING THE SOURCE MECHANISM OF THE
28 NOVEMBER 1974 CENTRAL CALIFORNIA EVENT
IN THE NORTHEAST STRUCTURE

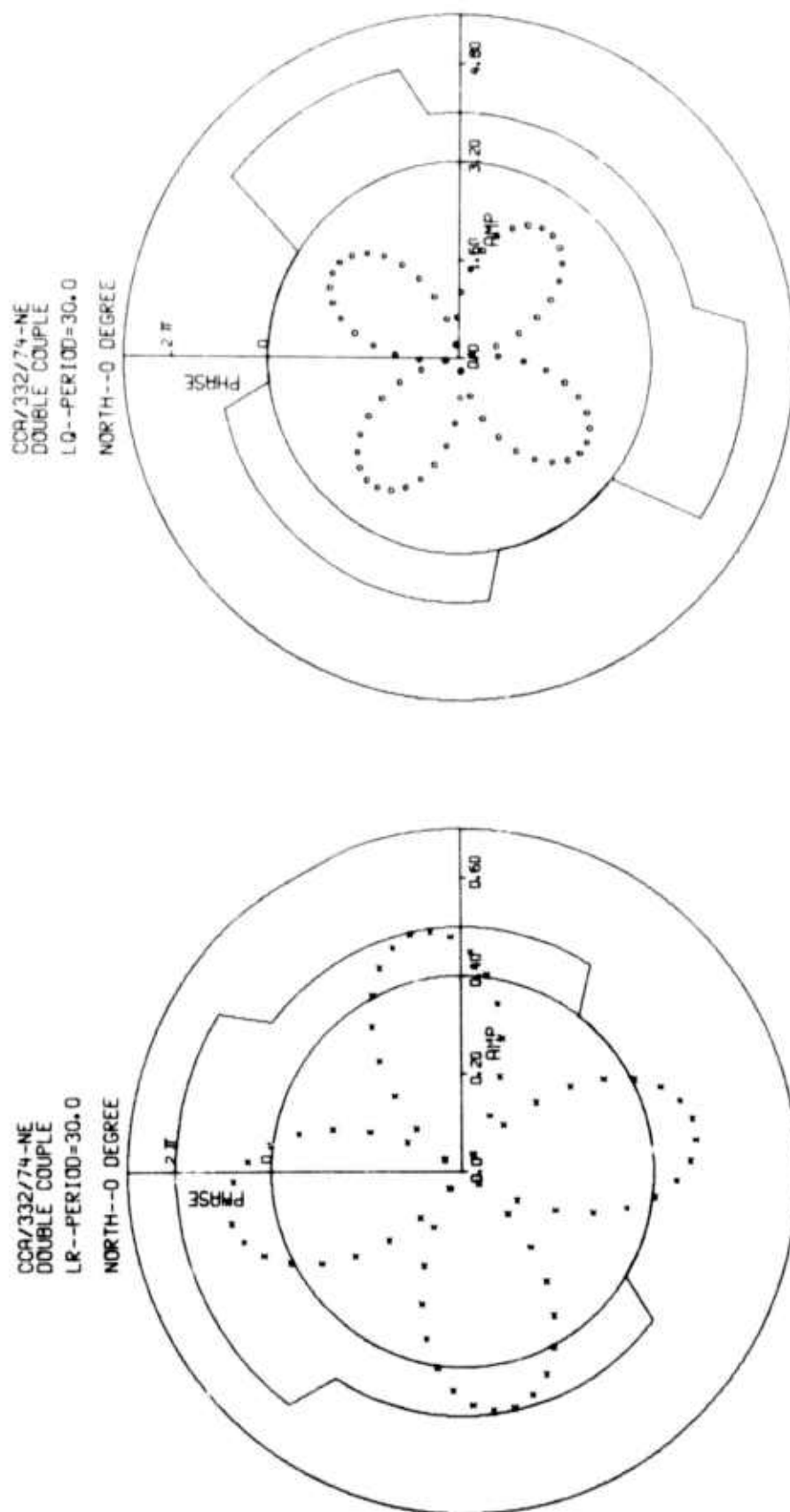


FIGURE B-7b

FUNDAMENTAL MODE RAYLEIGH AND LOVE WAVE RADIATION
(T = 30 SECONDS) USING THE SOURCE MECHANISM OF THE
28 NOVEMBER 1974 CENTRAL CALIFORNIA EVENT
IN THE NORTHEAST STRUCTURE

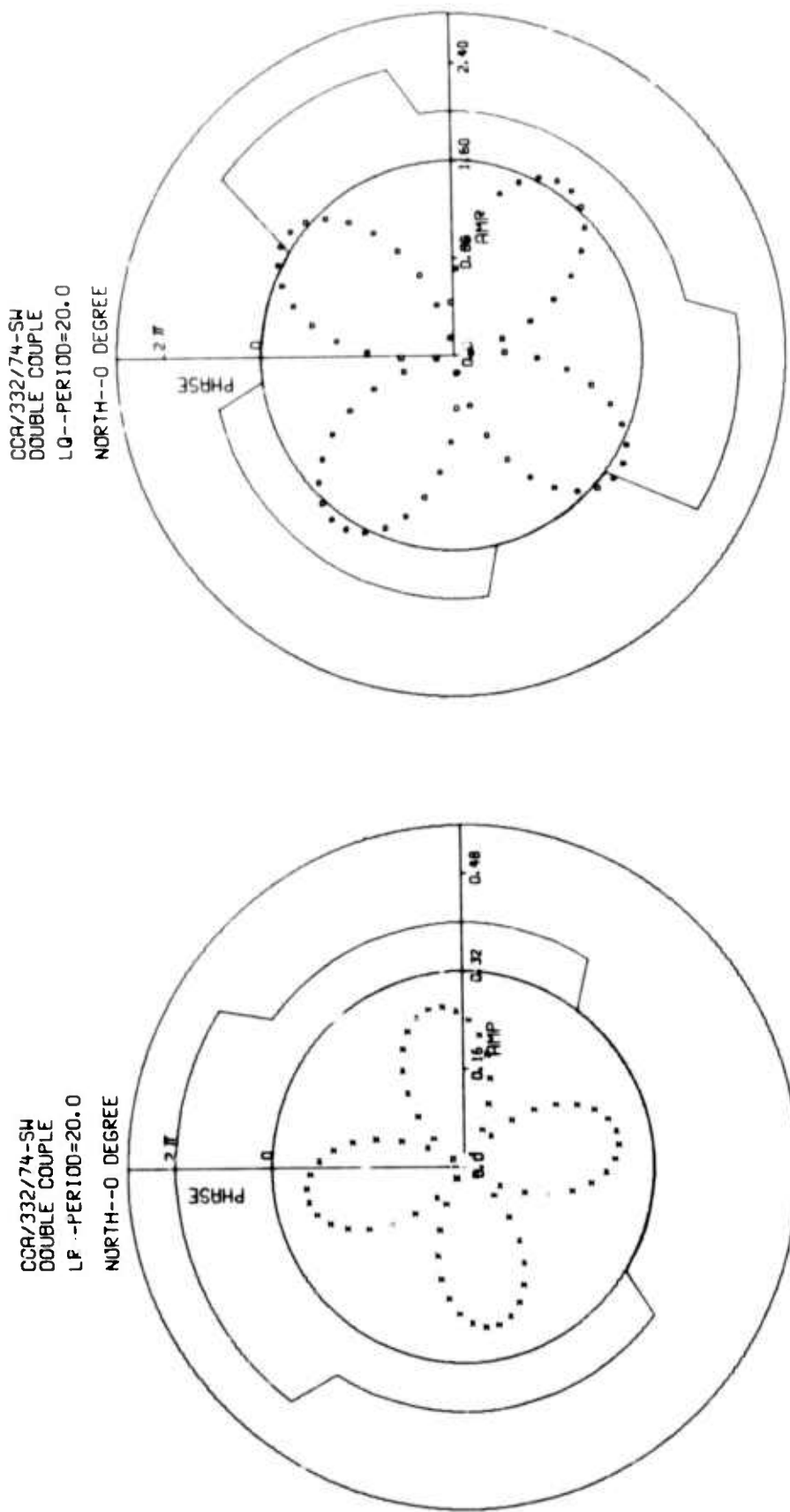


FIGURE B-8a

FUNDAMENTAL MODE RAYLEIGH AND LOVE WAVE RADIATION
(T = 20 SECONDS) USING THE SOURCE MECHANISM OF THE
28 NOVEMBER 1974 CENTRAL CALIFORNIA EVENT
IN THE SOUTHWEST STRUCTURE

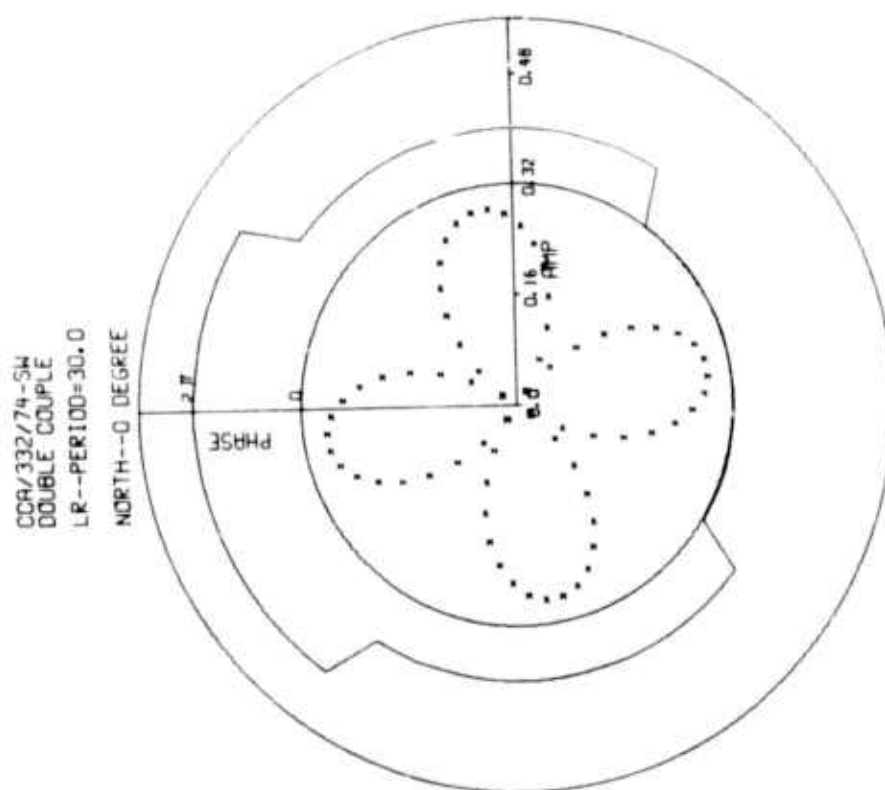
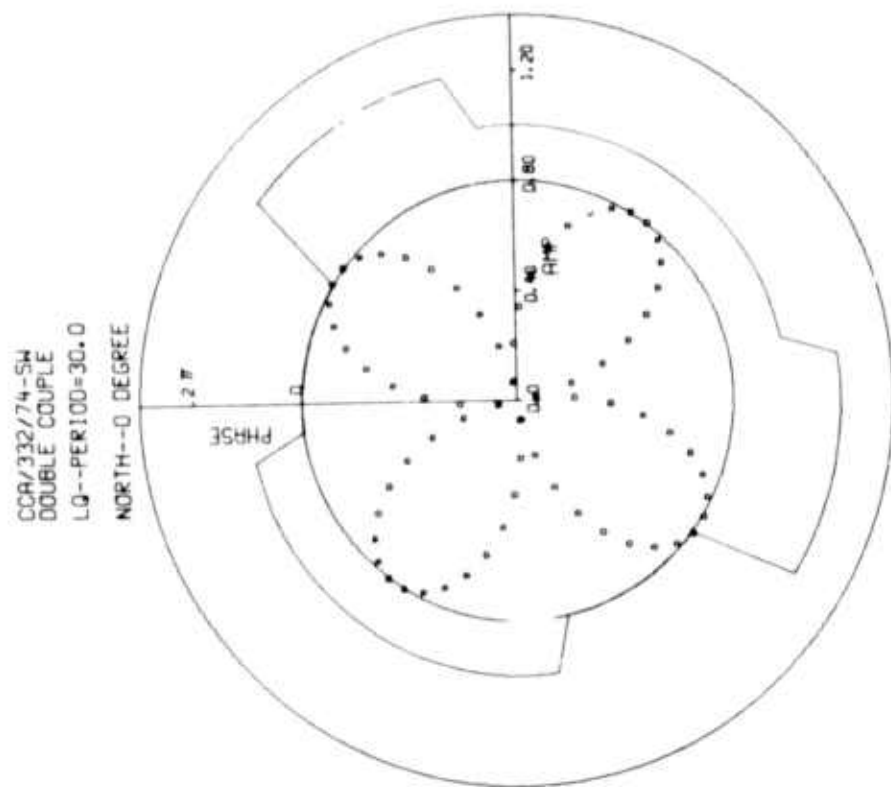


FIGURE B-8b

FUNDAMENTAL MODE RAYLEIGH AND LOVE WAVE RADIATION
(T = 30 SECONDS) USING THE SOURCE MECHANISM OF THE
28 NOVEMBER 1974 CENTRAL CALIFORNIA EVENT
IN THE SOUTHWEST STRUCTURE

APPENDIX C

THEORETICAL FIRST HIGHER MODE SURFACE WAVE SPECTRA

As in previous work (Turnbull, et al., 1975), theoretical first higher mode Rayleigh and Love wave spectra were generated using the Harkrider (1964) formulation of a double couple source in a layered half space. Our objective is to identify any special spectral characteristics (such as shape or amplitude level) that would be useful in determining source depth or structure in the source region.

Figures C-1a through C-1d display the variation of dip, slip, and strike for first higher mode Rayleigh and Love waves over the period range of 3 to 15 seconds and for three representative source depths in a Gutenberg-Bullen earth model. Using the Hamilton-Healy earth model, the effect of dip angle variation is displayed over the same period range and for three source depths in Figure C-2. Finally, in Figure C-3, higher mode surface wave spectra over the period range of 15 to 40 seconds with dip angle variation is shown for three source depths in a Gutenberg-Bullen earth model.

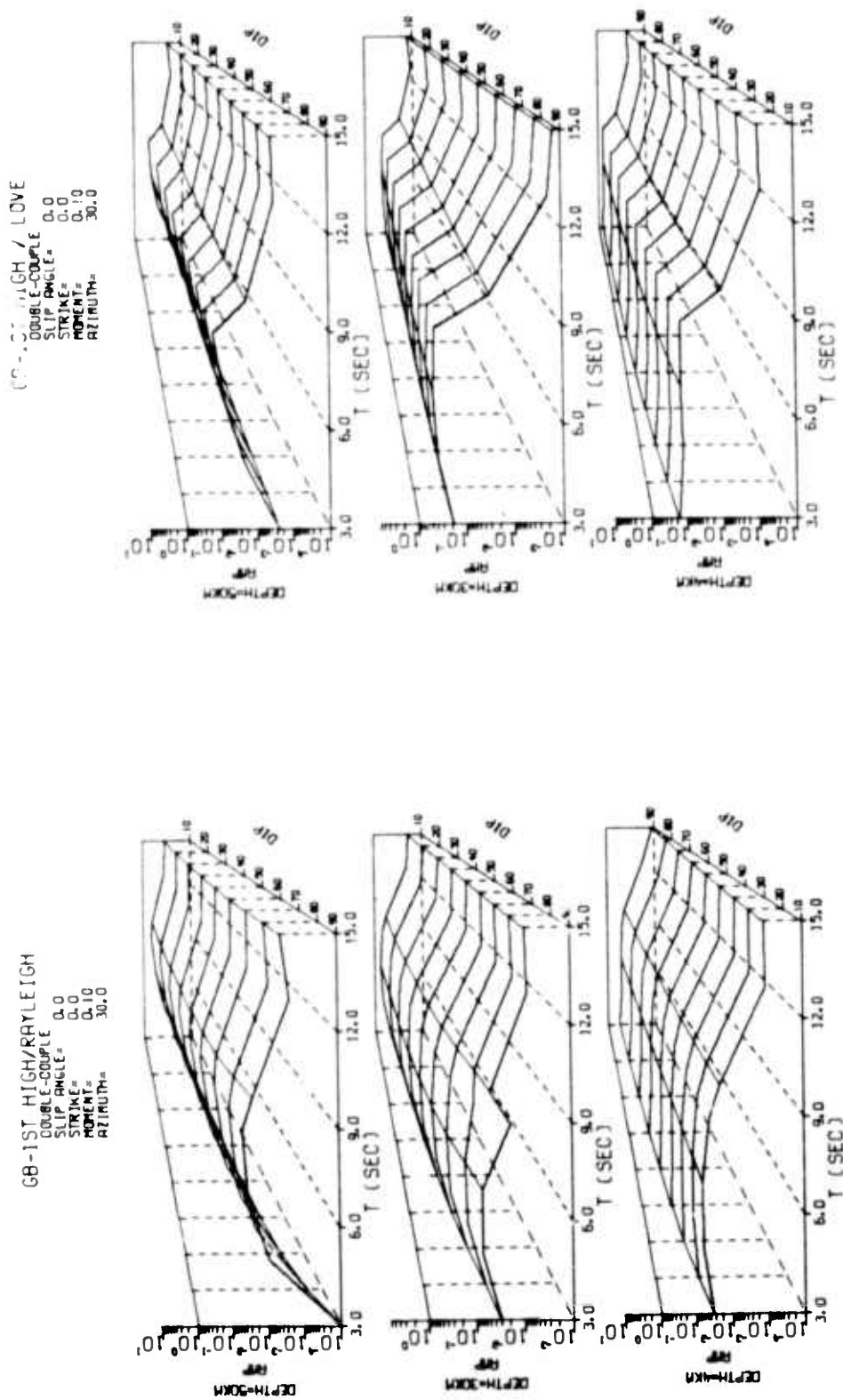


FIGURE C-1a

THEORETICAL FIRST HIGHER MODE RAYLEIGH AND LOVE WAVE SPECTRA
FOR THREE SOURCE DEPTHS IN A GUTENBERG-BULLEN EARTH MODEL:
Period Range 3 to 15 Seconds, Dip (δ) = Variable, Slip (λ) = 0° , Strike (θ) = 0°

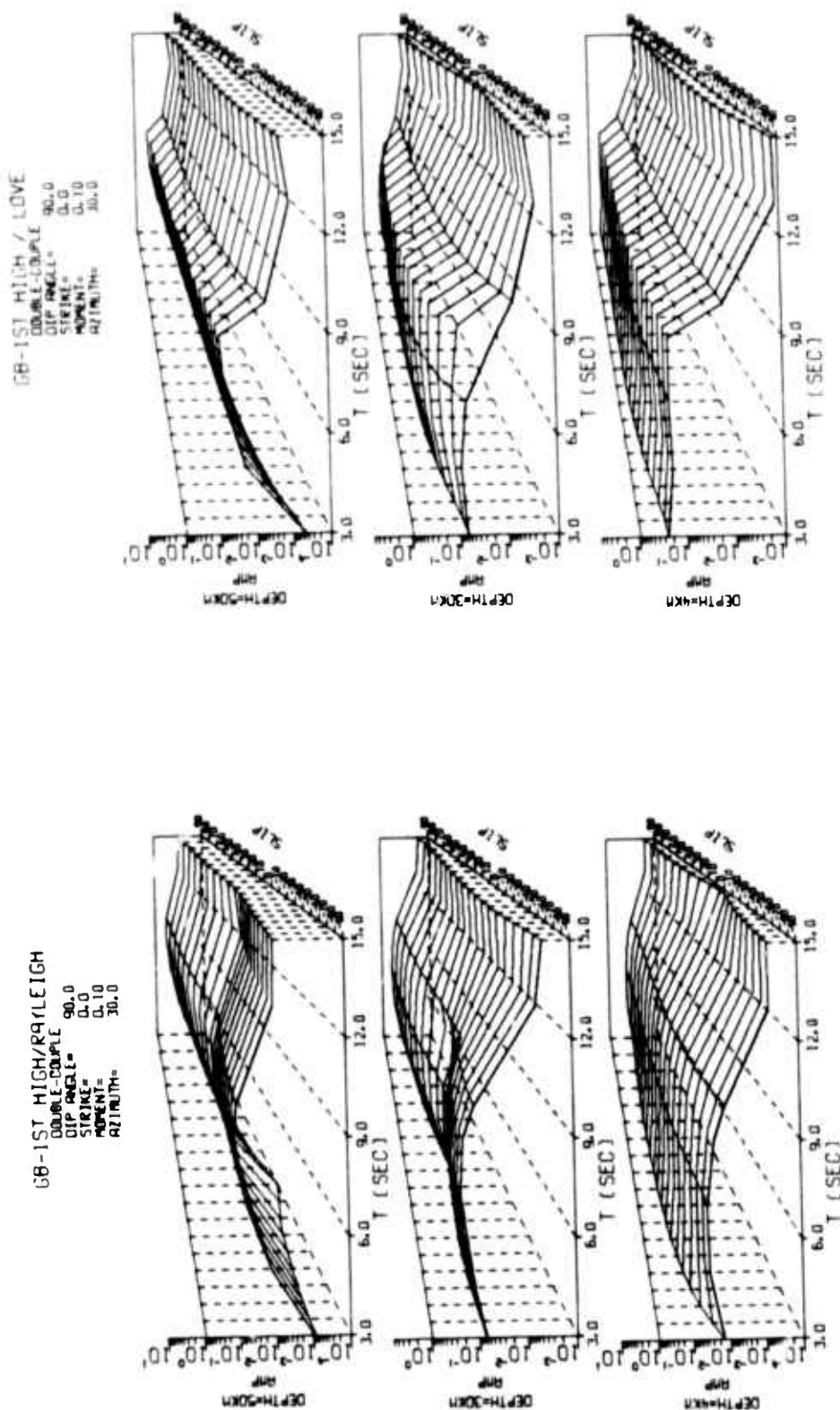


FIGURE C-1b

THEORETICAL FIRST HIGHER MODE RAYLEIGH AND LOVE WAVE SPECTRA
FOR THREE SOURCE DEPTHS IN A GUTENBERG-BULLEN EARTH MODEL:
Period Range 3 to 15 Seconds, Dip (δ) = 90°, Slip (λ) = Variable, Strike (θ) = 0°

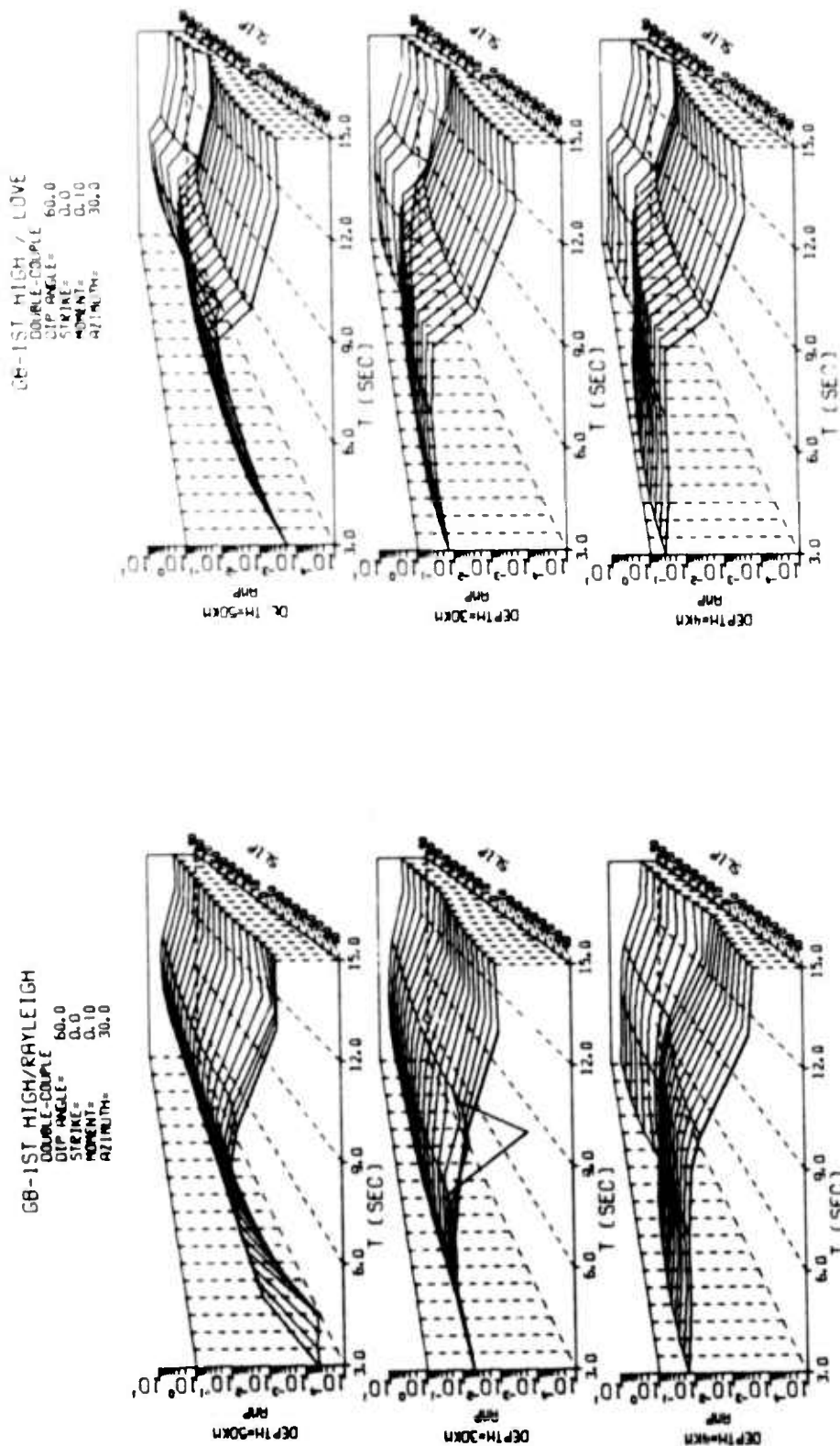


FIGURE C-1c

THEORETICAL FIRST HIGHER MODE RAYLEIGH AND LOVE WAVE SPECTRA
FOR THREE SOURCE DEPTHS IN A GUTENBERG-BULLEN EARTH MODEL L:
Period Range 3 to 15 Seconds, Dip (δ) = 60°, Slip (λ) = Variable, Strike (θ) = 0°

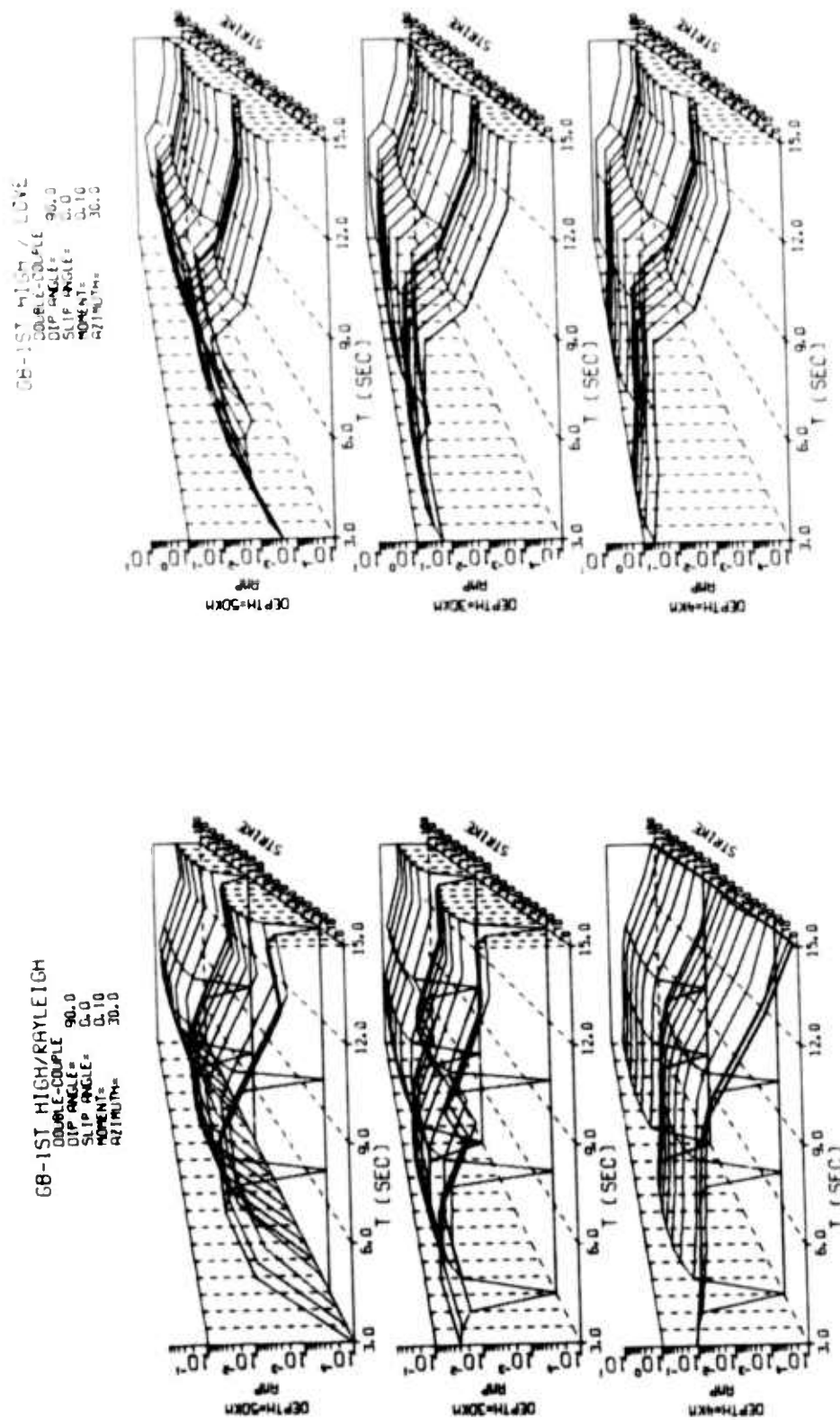


FIGURE C-1d

THEORETICAL FIRST HIGHER MODE RAYLEIGH AND LOVE WAVE SPECTRA
 FOR THREE SOURCE DEPTHS IN A GUTENBERG-BULLEN EARTH MODEL:
 Period Range 3 to 15 Seconds, Dip (δ) = 90°, Slip (λ) = 0°, Strike (θ) = Variable

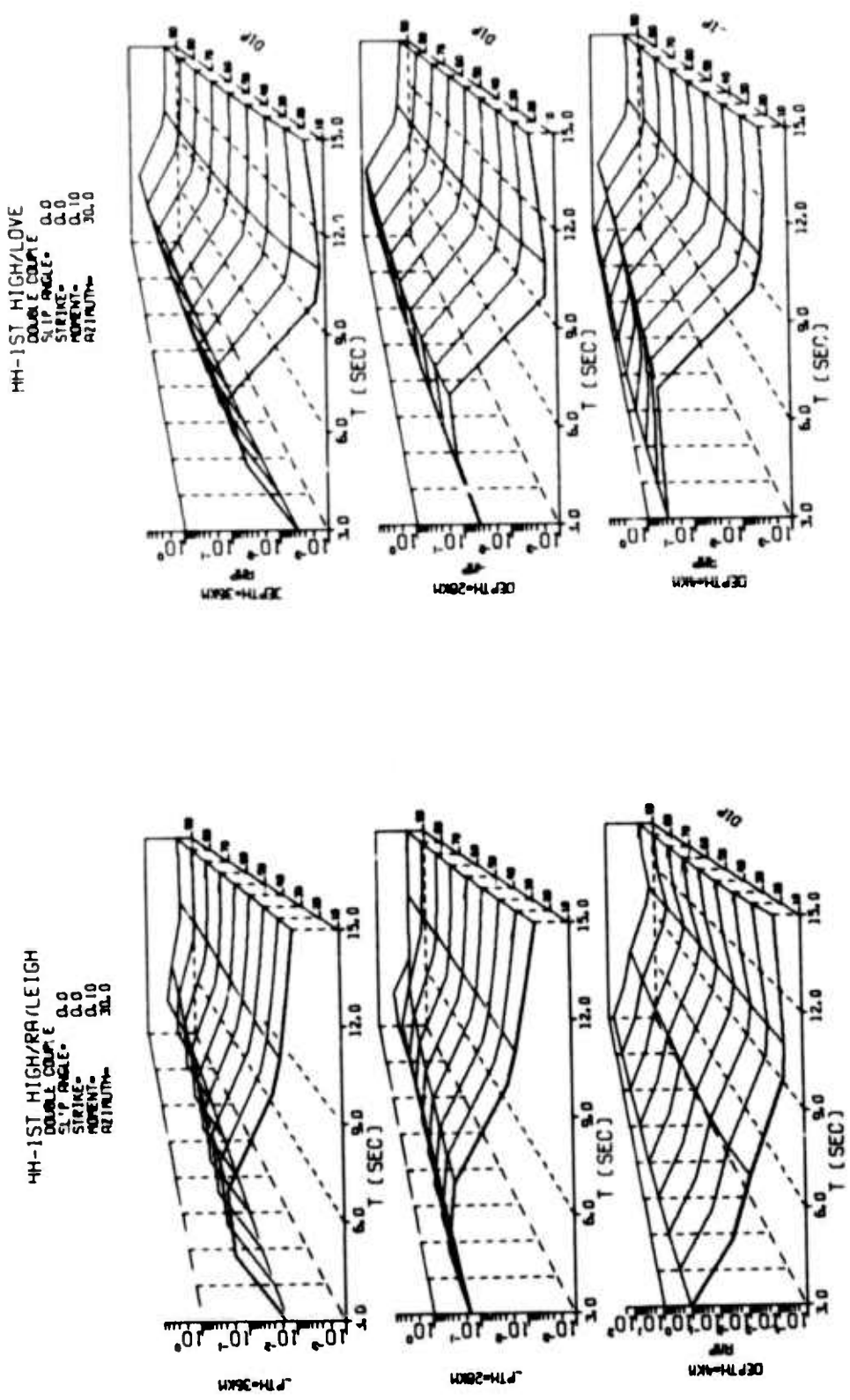


FIGURE C-2

THEORETICAL FIRST HIGHER MODE RAYLEIGH AND LOVE WAVE SPECTRA
FOR THREE SOURCE DEPTHS IN A HAMILTON-HEALY EARTH MODEL:
Period Range 3 to 15 Seconds, Dip (δ) = Variable, Slip (λ) = 0° , Strike (θ) = 0°

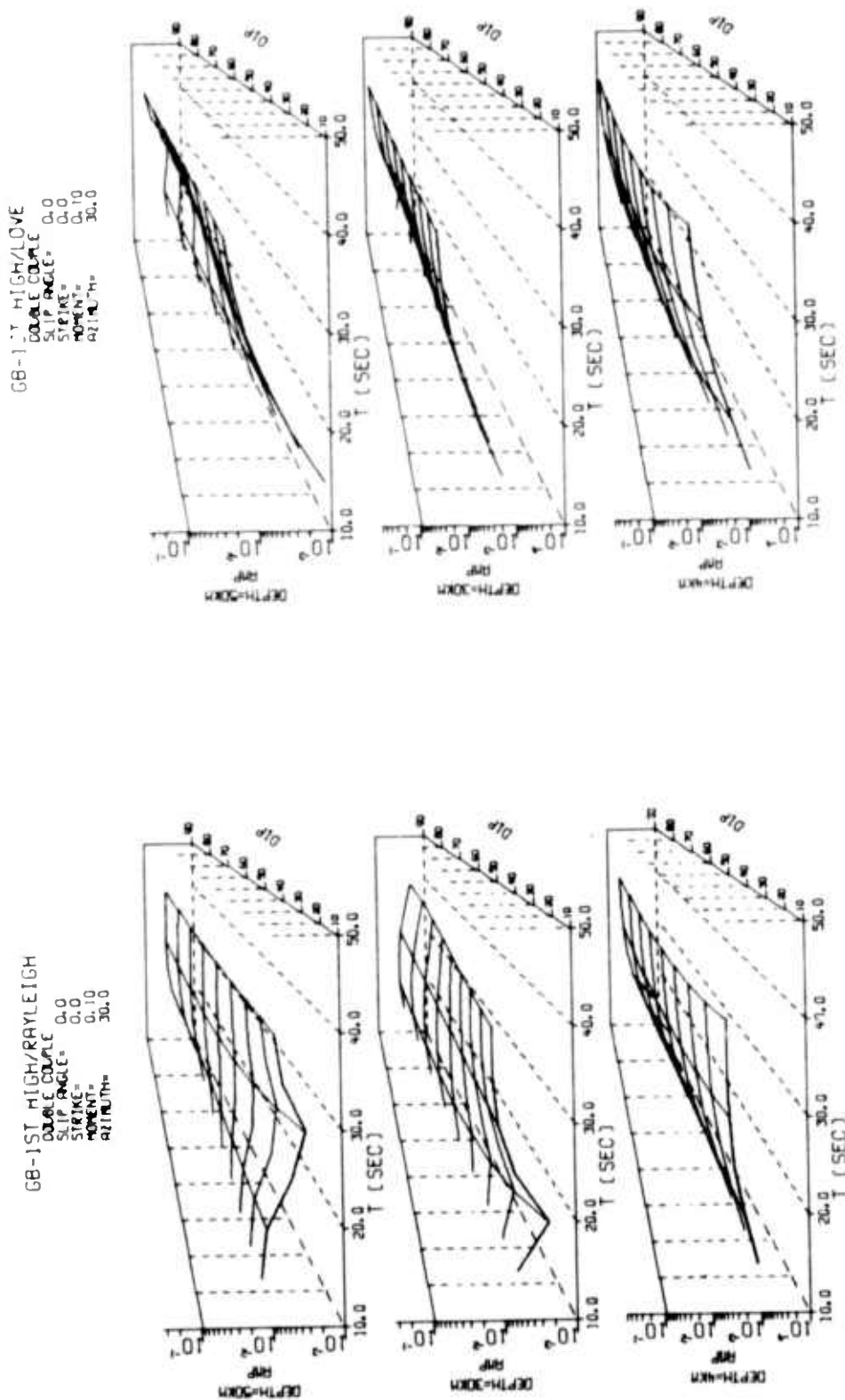


FIGURE C-3

THEORETICAL FIRST HIGHER MODE RAYLEIGH AND LOVE WAVE SPECTRA
FOR THREE SOURCE DEPTHS IN A GUTENBERG-BULLEN EARTH MODEL:
Period Range 15 to 40 Seconds, Dip (δ) = Variable, Slip (λ) = 0° , Strike (θ) = 0°

UNCLASSIFIED

SECURITY CLASSIFICATION OF THIS PAGE (When Data Entered)

17. REPORT DOCUMENTATION PAGE		READ INSTRUCTIONS BEFORE COMPLETING FORM	
1. AFOSR NUMBER TR-76-1063	2. GOVT ACCESSION NO.	3. RECIPIENT'S CATALOG NUMBER	
4. TITLE (and Subtitle) SOURCE STUDIES IN THE NEAR- AND FAR-FIELD		5. TYPE OF REPORT & PERIOD COVERED Semi-Annual Technical	
7. AUTHOR(s) Lawrence S. Turnbull, David Sun, James C. Battis, and Frode Ringdal		6. PERFORMING ORG. REPORT NUMBER ALEX(02)-TR-75-02-PART-A	
9. PERFORMING ORGANIZATION NAME AND ADDRESS Texas Instruments Incorporated Equipment Group - Dallas, Texas 75222		8. CONTRACT OR GRANT NUMBER(s) F44620-73-C-0055 ARPA 0-1-2-7827	
11. CONTROLLING OFFICE NAME AND ADDRESS Advanced Research Projects Agency Nuclear Monitoring Research Office Arlington, Virginia 22209		10. PROGRAM ELEMENT, PROJECT, TASK AREA & WORK UNIT NUMBERS ARPA Program Code No. F10	
14. MONITORING AGENCY NAME & ADDRESS (if different from Controlling Office) Air Force Office of Scientific Research/AF Bolling Air Force Base, Bldg. 410 Washington, D. C. 20332		12. REPORT DATE 30 November 1975	
16. DISTRIBUTION STATEMENT (of this Report) APPROVED FOR PUBLIC RELEASE, DISTRIBUTION UNLIMITED		13. NUMBER OF PAGES 104	
17. DISTRIBUTION STATEMENT (of the abstract entered in Block 20, if different from Report) Recent - annual technical rept. no. 5 (pt. 1) 1 Nov - 31 Nov 75		15. SECURITY CLASS. (of this report) UNCLASSIFIED	
18. SUPPLEMENTARY NOTES TECH, OTHER			
19. KEY WORDS (Continue on reverse side if necessary and identify by block number) Seismology Near-Field Spectra Far-Field Spectra Higher Mode Spectra Maximum Likelihood Method Earthquake Swarm $M_s - m_b$ Discriminant			
20. ABSTRACT (Continue on reverse side if necessary and identify by block number) Several continuing investigations of the seismic source using near- and far-field data are discussed. We completed our analysis of near-field acceleration data recorded at Bear Valley, California, by examining two small events which occurred on 7 February 1974 and 6 July 1974. The February event, using only spectral analysis, was found to have a moment of 3×10^{21} dyne-cm with an equivalent circular dislocation radius of 0.18 km ² . Both spectral and time domain waveform fitting techniques were			

DD FORM 1473
1 JAN 73EDITION OF 1 NOV 65 IS OBSOLETE
G&K/M

UNCLASSIFIED 405 076

20. continued

applied to the July event. The solutions using each method were in reasonable agreement, with a seismic moment in the range of 2 to 4×10^{21} dyne-cm over an equivalent dislocation radius of about 0.1 to 0.3 km². 10 July 21st 1974
2
96 km

Using far-field surface wave data, two central California area earthquakes (22 June 1973 and 28 November 1974) were re-examined using two new earth models which were determined by McEvilly (1975) for the northeast and southwest side of the San Andreas fault. Several far-field solutions for the source mechanism were obtained by using various combinations of stations and earth models, including use of both structures at once for the first time. However, for the central California event of 28 November 1974, the mechanism which agreed closely with that obtained by other means used only those stations on the west side of the fault, with the southwest structure used in the spectral fit. ←

Theoretical first higher mode surface wave spectra were generated for a double couple source in a layered half space. Both Gutenberg-Bullen and Hamilton-Healy earth models were used. As with fundamental mode spectra, 'holes' were found almost exclusively for vertical strike-slip faults. Higher mode spectral levels in the 3 to 9 second period range were found to be comparable with 15 to 50 second period fundamental mode spectra. Also, from the excitation of the earth models, greater amplitude higher mode signals from shallow events should occur from high velocity crustal source regions.

Preliminary results have been obtained for five large events which were a part of the Sinkiang, China earthquake swarm of August 1974. Both simple spectral and spectral ratio fitting methods were employed. The far-field solutions showed a consistent trend for these five events of shallow focal depth.

Finally, we concluded our examination of the scatter of the earthquake population in the $M_s - m_b$ discriminant. Focusing on the bodywave magnitude estimate instead of the surface wave magnitude as in previous studies, we applied the maximum likelihood method of Ringdal (1975) in an attempt to improve the accuracy of the PDE bodywave magnitudes. Although the scatter of the population did not change significantly, the slope of the data set decreased approximately 0.25.